

AD-A196 719

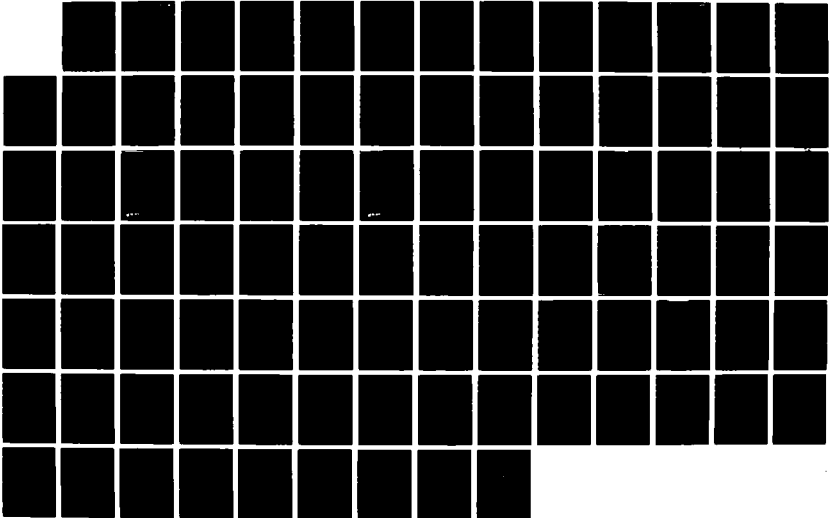
NEW TECHNIQUES IN COMPUTATIONAL AERODYNAMICS(U) BROWN  
UNIV PROVIDENCE RI DIV OF APPLIED MATHEMATICS  
L SIROVICH 06 AUG 87 AFOSR-TR-87-1419 #AFOSR-83-0336

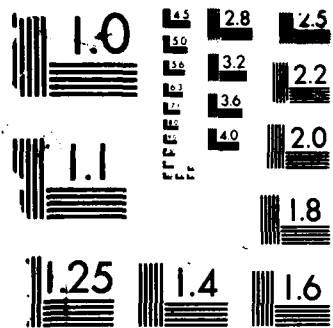
1/1

UNCLASSIFIED

F/G 20/4

ML





MICROCOPY RESOLUTION TEST CHART  
 NATIONAL BUREAU OF STANDARDS-1963-A

RT DOCUMENTATION PAGE

1a. REPORT SECURITY CLASSIFICATION Unclassified		1b. RESTRICTIVE MARKINGS N/A	
2a. SECURITY CLASSIFICATION AUTHORITY N/A		3. DISTRIBUTION/AVAILABILITY OF REPORT Approved for public release, distribution unlimited	
2b. DECLASSIFICATION/DOWNGRADING SCHEDULE N/A			
4. PERFORMING ORGANIZATION REPORT NUMBER(S) --		5. MONITORING ORGANIZATION REPORT NUMBER(S) AFOSR-TR-87-1419	
6a. NAME OF PERFORMING ORGANIZATION BROWN UNIVERSITY	6b. OFFICE SYMBOL (If applicable) --	7a. NAME OF MONITORING ORGANIZATION AFOSR/NA Bld 410 Bolling AFB, DC 20341	
6c. ADDRESS (City, State and ZIP Code) Division of Applied Mathematics 182 George Street Providence, RI 02912		7b. ADDRESS (City, State and ZIP Code) Same as 7a	
8a. NAME OF FUNDING/SPONSORING ORGANIZATION AFOSR	8b. OFFICE SYMBOL (If applicable) AFOSR/NA	9. PROCUREMENT INSTRUMENT IDENTIFICATION NUMBER AFOSR-83-0336	
8c. ADDRESS (City, State and ZIP Code) Aerospace Sciences Air Force Office of Scientific Research Bolling Air Force Base Washington, DC 20332		10. SOURCE OF FUNDING NOS.	
		PROGRAM ELEMENT NO. 61102F	PROJECT NO. 2307
11. TITLE (Include Security Classification) New Techniques In Computational Aerodynamics			
12. PERSONAL AUTHOR(S) Professor Lawrence Sirovich			
13a. TYPE OF REPORT Final Technical	13b. TIME COVERED FROM 6/83 TO 2/87	14. DATE OF REPORT (Yr., Mo., Day) 08/06/87	15. PAGE COUNT 8
16. SUPPLEMENTARY NOTATION Prepared by Professor Lawrence Sirovich			
17. COSATI CODES		18. SUBJECT TERMS (Continue on reverse if necessary and identify by block number) Computational Methods	
FIELD	GROUP SUB. GR.		
19. ABSTRACT (Continue on reverse if necessary and identify by block number) A wide range of problems in gasdynamics have been considered. Advances in subsonic, transonic and supersonic gasdynamics have been made. The emphasis has been made on computational procedures both numerical and algebraic. This work has a strong basis in analytical methods, and a goal has been to produce computational efficient codes which made optimal use of analytically known results.			
20. DISTRIBUTION/AVAILABILITY OF ABSTRACT UNCLASSIFIED/UNLIMITED <input checked="" type="checkbox"/> SAME AS RPT <input type="checkbox"/> DTIC USERS <input type="checkbox"/>		21. ABSTRACT SECURITY CLASSIFICATION Unclassified	
22a. NAME OF RESPONSIBLE INDIVIDUAL Dr. James Wilson		22b. TELEPHONE NUMBER (Include Area Code) (202)767-4935	22c. OFFICE SYMBOL AFOSR/NA

DTIC  
SELECTED  
OCT 23 1987  
S E D

Log Rec'd - 10 Aug 87

Log In  
Final Report  
10 Aug 87  
JW

Final Report

Air Force Grant AFOSR 83-0336

New Techniques in Computational Aerodynamics

Division of Applied Mathematics  
Brown University

**AFOSR-TR- 87 - 1419**

June 1, 1983 to February 28, 1987

Principal Investigator: Lawrence Sirovich, Professor of Applied Mathematics & Director of the Laboratory of Mechanics and Computation.

DTIC  
COPY  
INSPECTED  
6

Accession For	
NTIS GRA&I	<input checked="" type="checkbox"/>
DTIC TAB	<input type="checkbox"/>
Unannounced	<input type="checkbox"/>
Justification	
By _____	
Distribution/ _____	
Availability Codes	
Dist	Avail and/or Special
<b>A-1</b>	

## 1. Objectives

The basic goal of our research effort has been the development of computational methods and tools which optimally exploit the analytical procedures natural to aerodynamic theory. This has resulted in a variety of procedures of non-standard form for treating a wide range of problems in gas dynamics. We believe that our research effort has made significant advances in subsonic, transonic and supersonic gas dynamics.

Specific objectives of the program have been; the use of natural coordinates, e.g. streamlines, characteristics, "potential" lines and so forth in the formatting of compressible computer codes; solution of general inverse or design problems in aerodynamics; use of machine algebra to format codes and deal with non-standard problems; the development of a method of parametric differentiation to extend generally existing codes (in addition to ours) to continuous ranges of validity in parameter space (i.e. Mach number, thickness ratio, camber and more general parameters specifying a body shape.)

All of the stated objectives in the original three year proposal have been accomplished. In addition, as described in the following section, we have also achieved a number of extensions and additional results not anticipated in the original proposal.

## 2. Research Narrative

Our research effort began with a method for treating two-dimensional supersonic flows past airfoils. This is based on transformation to streamline and principal characteristic coordinates, and results in a rapidly convergent and accurate solution. Both body-fit and shock-fit coordinates are generated by this method. The codes produced by our method are perhaps the most efficient now in existence. A typical calculation takes a small fraction of a second on a mainframe. [reference 1]

This method was next extended to the inverse or design problem for two-dimensional supersonic flows. Through analytical procedures the inverse problem was transformed to a direct problem of different type. The result is a speedy accurate procedure for determining shape from a given pressure distribution. [reference 2]

A method based on streamlines, characteristics and Riemann functions has also been introduced for supersonic flow over axisymmetric bodies. Starting from a simple approximation, an iterative procedure is developed which converges rapidly to the exact solution. The scheme is both body-fit and shock-fit. As a result, the procedure is computationally efficient, inherently accurate, and requires relatively few points to calculate the entire flow field. Both the direct and inverse design problems are treated. For a thin axisymmetric body traveling at low supersonic Mach number, our results show the presence of a pressure minimum on the body, a phenomenon which seems to have gone unnoticed. [reference 3]

The method described for the axisymmetric case, has been adapted to the treatment of non-axisymmetric bodies. In particular, we consider flow in azimuthal planes and develop a procedure based on *near characteristics* and projected streamlines. The *cross-talk* between azimuthal phases defines the basis of an iteration procedure which is rapidly convergent. As is the case for axisymmetric flow relatively few computational points are required. Both the direct and indirect flow problems have been treated. [reference 4]

We have treated subsonic gas dynamics in the tangent gas approximation. Using a highly

analytic basis a very fast and accurate method of solution has been developed for the numerical solution of subsonic problem. Comparison of tangent gas and exact flows show that the former is extremely accurate except at locations that are critical. Tangent gas solutions when used as the first step in the iterative solution of the exact flow field are shown to give substantial reduction in computation time. [reference 5]

The inverse problem in the tangent gas approximation has also been considered, and an exact method for designing airfoils developed. Constraints on the speed distribution are easily implemented. A simple numerical algorithm which is fast and accurate has been obtained. Comparison of designed airfoils using the tangent gas method with exact Euler results is found to be excellent for subcritical flows. [reference 6]

The methods used in the treatment of the tangent gas have been extended to the full two-dimensional potential equations. A powerful combined analytical and numerical procedure now permits the treatment of both the direct and inverse problem for subsonic and transonic problems. This method, which still needs further implementation, may have a significant impact on the way that transonic airfoils are designed in the future. [references 7 and 8]

The flow of an inviscid, irrotational and compressible perfect gas in the upper half plane is used as a model to investigate the transonic controversy. The solution of the complete potential equation for the velocity potential  $\phi(x,y)$ , with boundary condition:  $\phi + c \phi_y = U \sin x$  on  $y=0$ , is developed as a regular perturbation series. 36 terms of the series are determined by computer. The effective boundary condition is varied with the choice of  $c$ ; and for each of the velocity series, its nature and the location of the singularity nearest to the origin are investigated using the ratio method of Domb and Sykes and Pade approximants. The result of the analysis shows that the phenomenon of shockless transonic flow is dependent on the imposed boundary condition-which for this example is the constant  $c$ . The relationship of series convergence to local sonic conditions shows no obvious pattern. Cases for which convergence lies below, above or is at critically were found. Moreover, the connection of divergence to the appearance of shocks is also not apparent. For one class of flows divergent series could be resummed to yield

shockless conditions for all Mach numbers. Significant use of the machine algebra code, Macsyma, was used in this study. [reference 9]

We have also treated steady, inviscid supersonic flow over three dimensional wing-like bodies numerically as a coupled set of two-dimensional characteristic problems. Shock fitting is used in a boundary fit coordinate system and the calculation is second order accurate. The difference equations are solved iteratively and the use of an accurate approximation step results in rapid convergence. A variety of different iteration methods are considered and compared. Incorporation of a flexible data structure in the program allows for an efficient use of memory and allows a wide range of wing geometries to be handled. Results for tapered, delta and swept wings at several Mach numbers are compared with two-dimensional theory. The technique is applied to both the direct and inverse problems. Derivations are carried out in a general manner allowing extensions of the method. [reference 10]

We have developed a method using parametric differentiation which can significantly extend any numerical study. In brief flow past a body is in general specified by a variety of parameters such as thickness, angle of attack, camber, Mach number as well as others. A particular flow is, therefore, characterized by a single point in the corresponding parameter space. Conversely, the numerical calculation of a particular flow field yields information at just one point of the parameter space. However, the nature of a continuous range of nearby flow fields is of fundamental significance in the design and performance of aircraft. To treat this generally, one can consider the variational equations (which are linear) obtained by differentiating the exact equations with respect to each of the relevant parameters. The resulting matrix of derivatives of flow quantities is referred to as the Jacobi matrix. The subsequent procedure is in principle now straightforward. One integrates the nonlinear governing equations -- which results in the determination of just one point in parameter space -- and simultaneously the variational equations governing the Jacobi matrix. The last is then used to describe the neighborhood of the already determined point of the parameter space. Since the variational equations are linear the additional computational time required for their integration is modest.

Frequently, when calculating the flow about a body, one is interested in how the flow will change if the base configuration is altered. For example, one may want to know what will happen at a slightly different angle of attack, wing loading, camber or thickness. To answer such questions each parameter change is traditionally considered as a separated case and flow simulation code is repeatedly run. It could be argued, quite effectively, that in many instances this is not an efficient use of resources. Why undertake an entirely new calculation of the flow when we know the results at a nearby state? The method which we have developed allows efficient generation of solutions in the neighborhood of a base solution.

Thus far we have applied the Jacobi matrix technique to five problems. The direct calculation of inviscid supersonic flow about; two dimensional airfoils of varying thickness, angle of attack and camber; axisymmetric bodies of varying thickness and taper: and the design (inverse) calculation of inviscid supersonic flow past; airfoils described by a given family of pressure distributions; axisymmetric bodies described by a given family of pressure distributions. Also to subsonic potential flow about two dimensional airfoils by modifying FLO36. Results of these calculations show that Jacobi method allows for the efficient and accurate generation of parametric solutions in the neighborhood of a known solution. [references 11 and 12]

### 3. References

1. Lewis, T. & L. Sirovich, Approximate and exact numerical computation of supersonic flow over an airfoil. *Jour. Flu. Mech.* 112, 265 (1981).
2. Lewis, T. & L. Sirovich, The inverse problem for supersonic airfoils, *AIAA Jour.* 22, 295 (1984).
3. Fong, J. & L. Sirovich, Supersonic flow over axisymmetric bodies, *AIAA Jour.* 24, 5, May 1986, pp. 852.
4. Fong, J. & L. Sirovich, Supersonic flow over non-axisymmetric bodies
5. Daripa, P. & L. Sirovich, Exact and approximate gas dynamics using the tangent gas. *Jour. Comp. Phys.* 62, 2, February 1986.
6. Daripa, P. & L. Sirovich, An inverse method for subcritical flows. *Jour. Comp. Phys.* 63, 2, April 1986.
7. Daripa, P. Exact Inverse method for subsonic flows, *Quar. Applied Math.* (to appear).
8. Daripa, P., A fast approach for designing airfoils from given pressure data, *AIAA* (to appear).
9. Kwok, Y. & L. Sirovich, The transonic controversy, *SIAM J. Applied Math.*, 47, 2, April 1987.
10. Pratt, M., Analysis of near characteristic methods in the study of steady 3-D compressible flows. (Ph.D. dissertation, May 1988).
11. Sharp, T. & L. Sirovich, Parametric differentiation and the integration of the gas dynamic Equations, (submitted for publication).
12. Sharp, T., The Jacobi matrix method in computational fluid dynamics, (Ph.D. dissertation, May 1988).

4. Ph.D.'s Supported by the Grant.

J. Fong, (May 1986) "Supersonic Flow over Axisymmetric and Asymmetric Bodies".

P. Daripa, (May 1985) "Direct and Inverse Problems in Gas Dynamics".

Y. Kwok, (May 1986) "Transonic Controversy and Regular Perturbation Methods for Sub Critical Flows".

T. Sharp, (May 1988) "The Jacobi Matrix Method in Computational Fluid Dynamics".

M. Pratt, (May 1988) "Analysis of Near Characteristic Methods in the Study of Steady 3-D Compressible Flows".



**Approximate and exact numerical computation of  
supersonic flow over an airfoil**

**By TIMOTHY S. LEWIS AND LAWRENCE SIROVICH**

## Approximate and exact numerical computation of supersonic flow over an airfoil

By TIMOTHY S. LEWIS AND LAWRENCE SIROVICH

Division of Applied Mathematics,  
Brown University, Providence, Rhode Island 02912

(Received 24 January 1980)

An approximate solution is developed for two-dimensional, steady, inviscid supersonic flow over an airfoil. This approximation produces accurate results for a wide range of Mach numbers and airfoil thicknesses. It is used as the starting point for a rapidly convergent iterative numerical solution of the exact equations. A co-ordinate system consisting of the principal characteristics and streamlines is employed. Examples computed for a symmetric airfoil reveal several interesting features in the tail shock and the flow behind the airfoil.

### 1. Introduction

In this paper we consider the computation of inviscid supersonic flow over a two-dimensional airfoil. While the final step in our investigation is numerical, we attempt to incorporate as much as possible our analytical and physical knowledge of such flows. The approach is well suited both for numerical integration and for the interpretation of the resulting flow phenomena. A preliminary version of this approach for the case of one-dimensional unsteady flow has already been reported (Sirovich & Chong 1980; Chong & Sirovich 1980). In the present investigation several new or little-known effects concerning the tail shock and flow behind a two-dimensional airfoil emerge. These are discussed in § 6.

There are two main nonlinear approximations for this problem. Small-amplitude theory gives solutions valid provided the airfoil thickness is not too great and the Mach number is not too high. Under these conditions the leading shock wave is fairly weak and the solution is approximately given by a simple wave involving only the characteristics emanating from the airfoil (Friedrichs 1948; Lighthill 1960). Variations in the entropy and in the Riemann invariant which is carried along the down-running characteristics are only of third order in the shock strength, so the resulting approximation is valid to second order. A correction in the tail shock region is necessary to obtain a second-order solution there (Caughey 1969).

The second type of approximation, shock expansion theory, originated by Epstein (1931), employs the fact that even for flows with strong shocks, for which the assumptions of small perturbation theory do not hold, the effect of the down-running characteristics remains small. This leads to an analytic solution at the airfoil, which has been generalized by several authors (Eggers, Syvertson & Kraus 1953; Meyer 1957) to provide approximate solutions for the entire flow field. In another approach, Jones

(1963) has derived by a perturbation method an approximate solution between simple wave theory and generalized shock expansion theory.

In § 4 we derive an approximate solution which is closely related to these, but which applies its assumptions more consistently and is somewhat more accurate. This approximation includes both shock expansion theory and the second-order theories of Friedrichs and Caughey. The derivation and the numerical computation of the solution are facilitated by the use of the principal characteristics and the streamlines as co-ordinates (§ 3). Adamson (1968) has used a similar co-ordinate system in another context. For a problem in which the down-running characteristics are also important (e.g. flow in a nozzle), this approach is less appropriate.

The approximate solution is used as the starting point for an iterative numerical computation of the exact solution (§ 5). The high accuracy of the approximation leads to the exact solution after only a few iterations. This procedure is different from most numerical methods for hyperbolic problems. Typical methods apply one of a variety of differencing schemes (for a comparison of several such schemes see Taylor, Ndefo & Masson 1972) to the equations in their standard form and compute the solution by 'marching' along in the downstream direction. One disadvantage of these methods is that at low Mach numbers short step sizes are required for stability. The method of characteristics (Liepmann & Roshko 1957, ch. 12) can also be used for this problem, although it is considered in general to be somewhat unwieldy for machine computation. The BVLR method (Babenko *et al.* 1966; Holt 1977) is a finite-difference method which is partly based upon the method of characteristics. The transformation of co-ordinates employed here also results in a method which is closely related to the method of characteristics.

Special account must be taken of the appearance of shock waves in this type of problem. In finite-difference methods this can be done through shock-capturing difference schemes, or through explicit shock fitting (e.g. Salas 1976). In the present method the shock waves can be naturally incorporated in the new co-ordinate system as fixed boundaries of the flow field.

## 2. Formulation of problem

We consider uniform flow of Mach number  $M_0 > 1$  incident upon a two-dimensional airfoil (see figure 1). It is assumed that there are attached shocks at the leading and trailing edges, and that the flow remains supersonic everywhere. The flow fields above and below the airfoil can be computed independently, up to the appearance of the tail shocks. The tail shock and the flow behind it for the case of a symmetric airfoil are treated in appendix B.

The co-ordinates  $x$  and  $y$  are scaled by the airfoil length; the pressure  $p$  and the density  $\rho$  by their upstream values  $p_0$  and  $\rho_0$ ; the velocity  $(u, v) = (q \cos \theta, q \sin \theta)$  and the speed of sound  $a$  by the upstream speed of sound  $a_0$ ; and the entropy  $s$ , which is set to zero upstream, by the gas constant  $R$ . We consider a perfect gas with constant specific heats  $c_v = R/(\gamma - 1)$  and  $c_p = \gamma c_v$ , for which the equation of state is

$$p = \rho^\gamma \exp[(\gamma - 1)s]$$

and the speed of sound is given by  $a^2 = p/\rho$ . The calculations here were done for  $\gamma = 1.4$ . Modifications for the case of a gas with a general equation of state are outlined in appendix A.

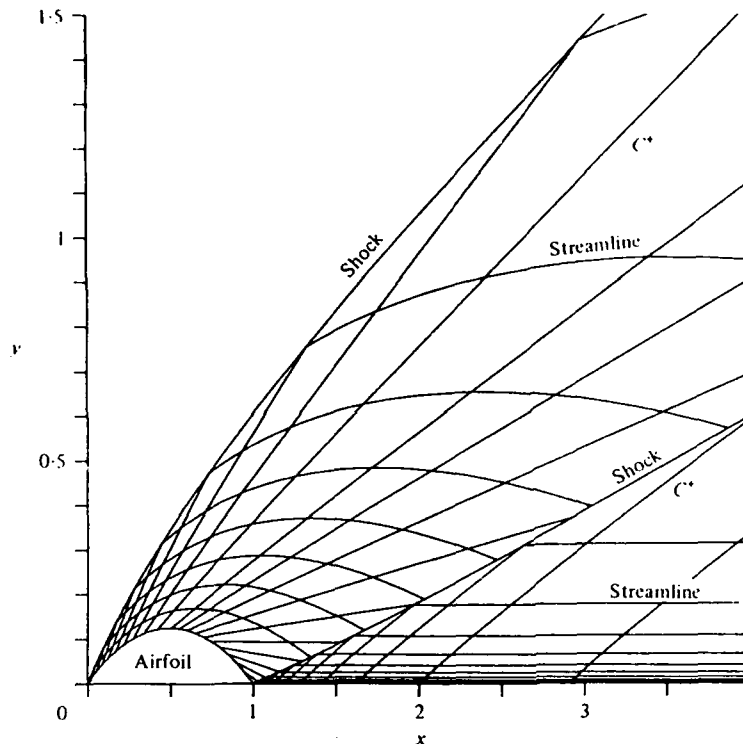


FIGURE 1. Supersonic flow over a symmetric 25% thick circular arc airfoil at upstream Mach number  $M_0 = 2.5$ .

The equations of inviscid two-dimensional steady flow are conveniently written with the entropy  $s$ , the flow angle  $\theta$ , and the Mach angle  $\mu = \sin^{-1}(1/M)$  (where  $M = q/a$  is the local Mach number) as dependent variables. All other physical quantities can be obtained from these and Bernoulli's equation

$$a^2 + \frac{\gamma-1}{2} q^2 = 1 + \frac{\gamma-1}{2} M_0^2. \quad (1)$$

The equations of motion in characteristic form are (Meyer 1960, p. 273)

$$ds = 0 \quad \text{on streamlines} \quad \frac{dy}{dx} = \tan \theta; \quad (2)$$

$$d(\theta \pm P(\mu)) = \pm \frac{\sin 2\mu}{2\gamma} ds \quad \text{on } C^\pm \quad \frac{dy}{dx} = \tan(\theta \pm \mu); \quad (3)$$

where  $P(\mu)$  is given by

$$P(\mu) = \lambda^{\frac{1}{2}} \tan^{-1}(\lambda^{\frac{1}{2}} \tan \mu) - \mu, \quad \lambda = (\gamma+1)/(\gamma-1).$$

The streamlines and the  $C^+$  characteristics are shown in figure 1. The quantities  $r^\pm = \theta \pm P(\mu)$  are called the Riemann invariants.

If the airfoil surface is specified as  $y = f(x)$ , the appropriate boundary condition there is

$$\tan \theta = f'(x) \quad \text{on } y = f(x). \quad (4)$$

The jumps in  $\theta$ ,  $\mu$  and  $s$  across a shock are governed by the Rankine-Hugoniot conditions (Liepmann & Roshko 1957, p. 85). All three quantities can be written as explicit functions of  $M_0$ ,  $\gamma$  and the shock angle,  $\eta$ .

### 3. New co-ordinate system

As mentioned in the introduction, in a problem with weak shock waves deviations in  $s$  and  $r^-$  from their upstream values are third-order quantities. This is shown in figure 2, where  $\Delta s$  and  $\Delta r^-$  are plotted on a logarithmic scale against the deflection angle  $\theta$ , for several Mach numbers. As  $\theta \rightarrow 0$ , the curves approach straight lines of slope 3. While  $\Delta s$  and  $\Delta r^-$  are both third-order quantities, for a given Mach number the jump in  $r^-$  is always significantly smaller than that in  $s$ . This suggests that for weak to moderate strength shock waves the flow field can be considered primarily an interaction between a simple wave and an entropy variation, with  $r^-$  playing only a small role.

This leads us to introduce a co-ordinate system  $(\alpha, \beta)$  consisting of the streamlines,  $\alpha = \text{constant}$ , and the principal ( $C^+$ ) characteristics,  $\beta = \text{constant}$ . Taking  $\alpha$  and  $\beta$  as the independent variables,  $x$  and  $y$  must satisfy

$$y_\beta = x_\beta \tan \theta, \quad y_x = x_x \tan(\theta + \mu). \quad (5)$$

The entropy equation (2) becomes

$$s_\beta = 0, \quad (6)$$

or  $s = s(\alpha)$ . Equations (3+) and (3-) become

$$(\theta + P(\mu))_\alpha = \frac{\sin 2\mu}{2\gamma} s'(\alpha) \quad (7)$$

and

$$\left(\frac{\partial}{\partial \alpha} + w \frac{\partial}{\partial \beta}\right) (\theta - P(\mu)) = -\frac{\sin 2\mu}{2\gamma} s'(\alpha), \quad (8)$$

where

$$w = -\frac{2}{1 - \tan \theta \tan \mu} \left(\frac{x_\alpha}{x_\beta}\right). \quad (9)$$

Using (7), equation (8) can be simplified to

$$(\theta - P(\mu))_\beta = (1 - \tan \theta \tan \mu) \frac{x_\beta}{x_\alpha} \theta_x. \quad (10)$$

Equations (5)–(7) and (10) are five equations in five unknowns:  $\theta$ ,  $\mu$ ,  $s$ ,  $x$  and  $y$ .

The boundary and shock conditions in the  $\alpha\beta$  plane can be simplified by normalizing  $\alpha$  and  $\beta$  appropriately. We let the airfoil surface be the streamline  $\alpha = 0$ , and normalize  $\beta$  by setting  $\beta = x$  at  $\alpha = 0$ . The boundary condition (4) then becomes

$$x(0, \beta) = \beta, \quad y(0, \beta) = f(\beta), \quad \theta(0, \beta) = \tan^{-1} f'(\beta). \quad (11)$$

One convenient way of normalizing  $\alpha$  is to take the front shock angle  $\eta(\alpha)$  to be given by

$$\tan \eta(\alpha) = (1 - \alpha) \tan \eta(0) + \alpha \tan \mu_0, \quad (12)$$

where  $\eta(0)$  is known from solving the shock conditions at the leading edge, and  $\mu_0$  is the upstream Mach angle, which the shock approaches far away from the airfoil.

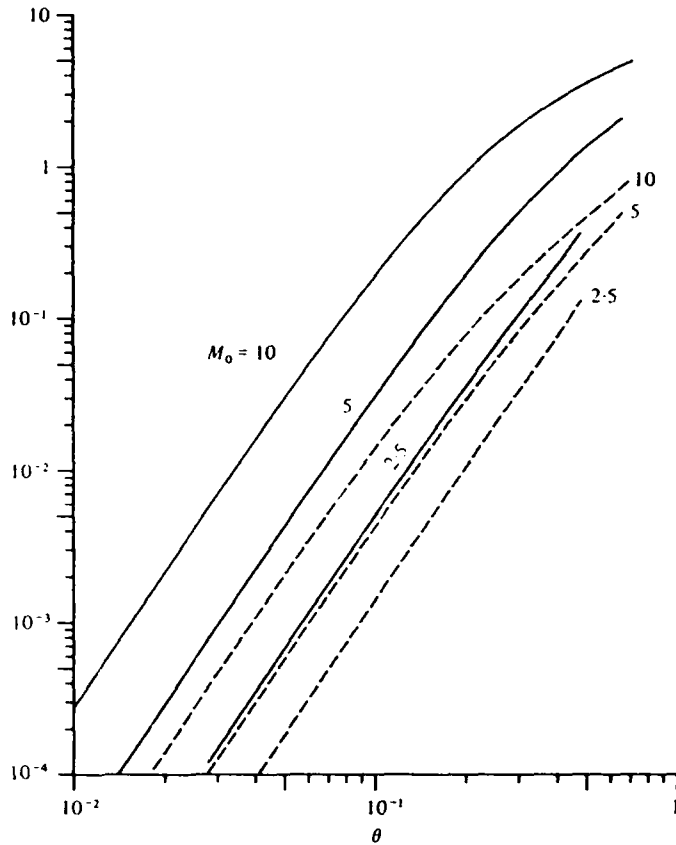


FIGURE 2. Jumps in entropy  $s$  and Riemann invariant  $r^-$  across a shock wave as functions of deflection angle  $\theta$ , at various Mach numbers: —,  $\Delta s$ ; ---,  $\Delta r^-$ .

Hence  $\alpha = 1$  corresponds to  $x, y \rightarrow \infty$ . If  $\eta$  is not a strictly decreasing function, a different normalization must be used. The flow field in the upper half-plane is mapped into a finite region in the  $\alpha\beta$  plane, as shown in figure 3. The principal characteristics become vertical lines, and the streamlines become horizontal lines. The front shock maps into some curve  $\beta(\alpha)$ , and the left- and right-hand sides of the tail shock into two separate curves  $\beta_2(\alpha)$  and  $\beta_3(\alpha)$ . The discussion of the tail shock is left to appendix B. With the shock angle  $\eta(\alpha)$  a given function, the shock conditions can be immediately solved for  $\theta(\alpha, \beta(\alpha))$ ,  $\mu(\alpha, \beta(\alpha))$ , and  $s(\alpha)$ . The shock  $\beta(\alpha)$  itself will in general depend on the rest of the solution, however.

It is possible to eliminate  $y$  from the equations by setting  $y_{\alpha\beta} = y_{\beta\alpha}$  in (5). Using (10), this gives

$$0 = x_{\alpha\beta}/x_\alpha + (\mu + P(\mu))_\beta \cot \mu + (\theta + \mu)_\beta \tan(\theta + \mu), \quad (13)$$

which can be integrated to

$$x(\alpha, \beta) = x(0, \beta) + \int_0^\alpha A(\alpha) a^{-\lambda} \cos(\theta + \mu) d\alpha, \quad (14)$$

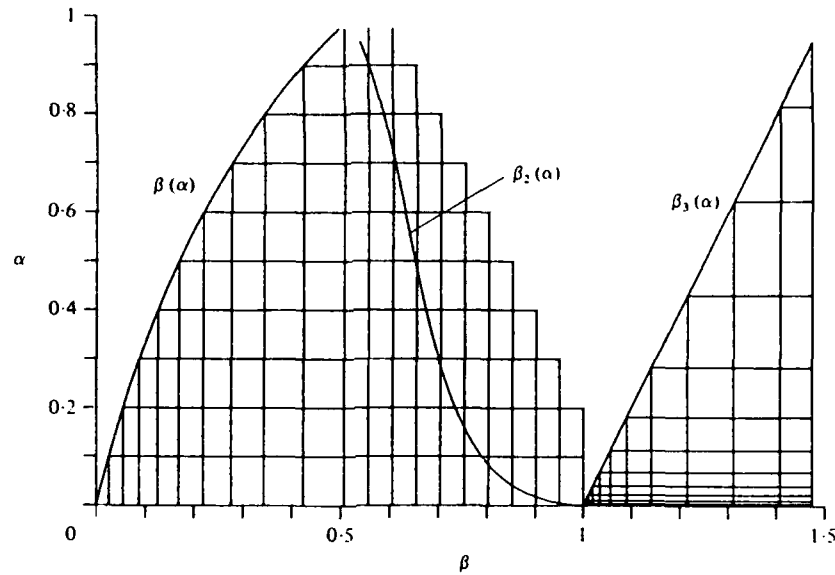


FIGURE 3. Flow field corresponding to figure 1 in  $\alpha\beta$  plane. Streamlines map into horizontal lines,  $\alpha = \text{const.}$ , and  $C^+$  characteristics into vertical lines,  $\beta = \text{const.}$  Front shock maps into  $\beta(\alpha)$ , and left and right sides of tail shock into  $\beta_2(\alpha)$  and  $\beta_3(\alpha)$ , respectively.

where  $A(\alpha)$  is an arbitrary function to be determined later, and we recall

$$\lambda = (\gamma + 1)/(\gamma - 1).$$

Similarly, from (5) we get

$$y(\alpha, \beta) = y(0, \beta) + \int_0^\alpha A(\alpha) a^{-\lambda} \sin(\theta + \mu) d\alpha. \quad (15)$$

At  $\beta = \beta(\alpha)$  the condition

$$\tan \eta = \frac{dy}{dx} = \frac{x_\alpha + y_\beta \beta'(\alpha)}{y_\alpha + x_\beta \beta'(\alpha)} \quad (16)$$

must be satisfied. Elimination of  $y$  using (5) and substitution of (14) for  $x$  produces a linear integral equation for  $A(\alpha)$ :

$$A(\alpha) Q(\alpha, \beta(\alpha)) + b(\alpha) \left[ 1 + \int_0^\alpha A(\hat{\alpha}) Q_\beta(\hat{\alpha}, \beta(\alpha)) d\hat{\alpha} \right] = 0, \quad (17)$$

where  $Q = a^{-\lambda} \cos(\theta + \mu)$ , and

$$b(\alpha) = \beta'(\alpha) \frac{\tan \eta - \tan \theta}{\tan \eta - \tan(\theta + \mu)} \Big|_{\beta = \beta(\alpha)}.$$

If the solution for  $\theta$ ,  $\mu$  and  $s$  is known in the  $\alpha\beta$  plane, this equation can be solved for  $A(\alpha)$ , and the transformation back to the physical plane computed with (14) and (15). In general, however, the solution in the  $\alpha\beta$  plane depends on  $x$ , through (10).

Up to this point the equations in  $\alpha\beta$  co-ordinates have been derived without approximation, and hence are equivalent to the original set (2) and (3).

#### 4. Approximate solutions

If the third-order changes in  $s$  and  $r^-$  are neglected, that is, it is assumed that  $s = 0$  and  $r^- = -P(\mu_0)$  everywhere, the solution of (2) and (3) is a simple wave, in which all quantities are constant on the principal ( $C^+$ ) characteristics, which in turn are straight lines:

$$\theta = \tan^{-1} f'(\beta), \quad \mu = P^{-1}(\theta + P(\mu_0)), \quad s = 0 \quad \text{on } C^+;$$

$$y = f(\beta) + (x - \beta) \tan(\theta + \mu).$$

This approximation is due to Friedrichs (1948). (Friedrichs further simplified the problem by neglecting terms of third and higher order throughout the calculation.)

Because simple wave theory takes  $s$  and  $r^-$  constant at their upstream values, it can be expected to be least accurate near the airfoil, where the shock is strongest and the deviation from upstream conditions is the greatest. An improved approximation in this region can be obtained using shock expansion theory, in which  $s$  and  $r^-$  are assumed to be constant at their values just behind the shock at the leading edge, say  $s = s_0$  and  $r^- = r_0^-$ . This leads to a slightly modified version of the simple wave solution:

$$\theta = \tan^{-1} f'(\beta), \quad \mu = P^{-1}(\theta - r_0^-), \quad s = s_0.$$

This approximation produces a very accurate solution at the airfoil, even for flows with strong shocks, in which  $s$  and  $r^-$  are not at all constant globally. Hayes & Probstein (1966) explain that the down-running waves, which can be considered reflections of the outgoing simple wave by the bow shock, are fairly weak and are nearly cancelled by reflections from the entropy (or vorticity) layers. Mahony (1955) gives a similar explanation. The shock expansion solution rapidly loses accuracy as the distance from the airfoil increases. This is in contrast to simple wave theory, which is more accurate at infinity.

The only assumption in the shock expansion solution at the airfoil is that  $r^-$  is constant. Mahony & Skeat (1955) and Meyer (1957) have pointed out that, since any streamline is a potential airfoil,  $r^-$  should be approximately constant along each streamline, that is  $r^- = r^-(\alpha)$ . In the literature this assumption has been employed in various ways. If  $r^- = r^-(\alpha)$ , then by (10)  $\theta = \theta(\beta)$ , i.e.  $\theta$  is constant on  $C^+$  characteristics. This in turn implies that the pressure is constant on  $C^+$  characteristics, as can be seen from the following form of (3+):

$$d\theta + \frac{\sin 2\mu}{2\gamma} \frac{dp}{p} = 0 \quad \text{on } C^+: \quad \frac{dy}{dx} = \tan(\theta + \mu). \quad (18)$$

Taking both  $\theta = \theta(\beta)$  and  $p = p(\beta)$  along with  $r^- = r^-(\alpha)$  overdetermines the problem however, since any one of  $\theta$ ,  $P$  and  $r^-$  can be written as a function of the other two (and  $s$ ). This was noted by Eggers *et al.* (1953). In their generalized shock expansion method it is resolved by averaging results assuming  $r^- = r^-(\alpha)$  and  $\theta = \theta(\beta)$  with those assuming  $r^- = r^-(\alpha)$  and  $p = p(\beta)$  (see Hayes & Probstein 1966, p. 498). Meyer (1957), on the other hand, implicitly drops the assumption  $p = p(\beta)$ , and uses the solution  $r^- = r^-(\alpha)$  and  $\theta = \theta(\beta)$ , which satisfies (10) exactly, but does not satisfy (7).

In the present formulation, it appears to be more consistent to approach the problem in either of two ways: in equation (10) assume either (i) the left-hand side or (ii) the right-hand side is zero. Then solve (10) together with the remaining equation, (7).

In case (i), the solution becomes  $\theta = \theta(\beta)$ ,  $p = p(\beta)$  and  $s = s(\alpha)$ . The function  $\theta(\beta)$  is determined by the boundary condition, and  $p(\beta)$  must be determined by the shock conditions. It then happens that over the rear half of the airfoil,  $\beta > \beta(1)$ ,  $p(\beta)$  cannot be found, since no data is specified on the rear shock. This difficulty does not arise in approach (ii), which is the one we adopt.

This approach can be thought of more simply as arising from the assumption that  $\theta$  is constant on  $C^+$  characteristics, rather than the assumption that  $r^-$  is constant on streamlines. If  $\theta_\alpha = 0$ , then (10) reduces to

$$(\theta - P(\mu))_\beta = 0 \quad \text{or} \quad \theta - P(\mu) = -P_0(\alpha), \quad (19)$$

where  $P_0(\alpha) = P[\mu(\alpha, \beta(\alpha))] - \theta(\alpha, \beta(\alpha))$ . Substitution of  $\theta = P(\mu) - P_0(\alpha)$  in the remaining equation, (7), then gives

$$2P(\mu)_\alpha - P_0'(\alpha) = \frac{\sin 2\mu}{2\gamma} s'(\alpha). \quad (20)$$

$P_0(\alpha)$  and  $s(\alpha)$  are both given explicitly by the shock conditions, so (20) can be regarded as an ordinary differential equation for  $\mu$ , in which  $\beta$  enters only as a parameter. It is nonlinear, but can be readily solved using standard numerical methods. The initial and final values of  $\mu$  along a given  $C^+$  characteristic are both given, by the boundary condition and the shock conditions, respectively, which allows us to solve for the free boundary  $\beta(\alpha)$ . The solution in the  $\alpha\beta$  plane is then completed by computing  $\theta(\alpha, \beta) = P(\mu(\alpha, \beta)) - P_0(\alpha)$ . The solution for  $\theta$ ,  $\mu$  and  $s$  in the  $\alpha\beta$  plane is independent of  $x$  and  $y$ , because (10), the only equation in which  $x$  or  $y$  appears, is neglected. The transformation back to the  $xy$  plane is found by solving (17) for  $A(\alpha)$  (also a simple numerical calculation) and evaluating the integrals (14) and (15). The solution obtained from this approximation will satisfy the boundary condition and all three shock conditions, but will satisfy (10) only approximately.

This approach requires more work (the solution of an ordinary differential equation on each  $C^+$  characteristic) than approach (i) or the generalized shock expansion method, but has been found to be more accurate. Additional support for this choice is lent by the fact that the factor multiplying  $\theta_\alpha$  in (10) is in general quite small. Approach (i) has however been found useful for calculating the flow behind the tail shock, where method (ii) is difficult to employ (see appendix B).

## 5. Numerical method

Our approximate solution does not satisfy (10), or, equivalently, the  $C^-$  equation (8). In this section we present a simple iterative method for correcting the solution so that it will satisfy all the equations and conditions.

The approximate solution is computed on a rectangular grid in the  $\alpha\beta$  plane (as shown in figure 3), which is then used in the numerical method. The front shock  $\beta(\alpha)$  is therefore kept fixed throughout the iterations. This fixes the normalization of  $\alpha$ , so for every iteration beyond the original approximation  $\eta(\alpha)$  is not given by (12) and must be found as part of the solution. This also implies that  $\alpha = 1$  no longer will correspond exactly to  $x, y \rightarrow \infty$ .

Given the approximate solution for  $\theta$ ,  $\mu$ ,  $s$  and  $x$  in the  $\alpha\beta$  plane, a corrected value of  $r^-$  is computed from the  $C^-$  equation (3-), or (8), starting at the shock with the

value given by the shock conditions and numerically integrating downward along the  $C^-$  characteristics:

$$r^- = r_{\text{shock}}^- - \int_{C^-} \frac{\sin 2\mu}{2\gamma} ds. \quad (21)$$

In particular, this determines a new value  $r^-(0, \beta)$  at the airfoil, which determines a new value of  $r^+(0, \beta)$  there, since  $r^+ = 2\theta - r^-$ , and  $\theta(0, \beta)$  is given by the boundary condition. With this as an initial value, a new  $r^+$  is computed everywhere by numerically integrating (3+), or (7), along  $C^+$  characteristics:

$$r^+(\alpha, \beta) = r^+(0, \beta) + \int_0^\alpha \frac{\sin 2\mu}{2\gamma} s'(\alpha) d\alpha. \quad (22)$$

With  $r^+$  and  $r^-$  thus determined, the solution given by

$$\theta = \frac{1}{2}(r^+ + r^-), \quad \mu = P^{-1}\left[\frac{1}{2}(r^+ - r^-)\right],$$

and  $s$  will satisfy the differential equations and the boundary condition. However, the new value of  $r^+(\alpha, \beta(\alpha))$  will not in general satisfy the shock conditions, and hence will imply a different value for the shock angle  $\eta(\alpha)$ . This can be used to determine a new initial value  $r^-(\alpha, \beta(\alpha))$  for integrating (21), and the procedure can be repeated.

The transformation back to the  $xy$  plane is found by numerically solving the integral equation (17) and evaluating the integrals (14) and (15). This must be done at each iteration, since  $x$  and  $y$  enter into the computation of the integral in (21). The  $C^-$  characteristics are oblique to the  $(\alpha, \beta)$  co-ordinate system, so at each point a small section of the  $C^-$  characteristic through that point is extended backwards to intersect a grid line, and a one-step integration is used to compute  $r^-$ . We might, in place of equation (8), have integrated (10), which has the advantage that  $r^-$  is differentiated only with respect to  $\beta$ , so that the integration would be along the co-ordinate lines, as in (22). In practice, however, this has been found unadvantageous. The solution does not converge as quickly, and may not converge at all without modification (see Chong & Sirovich 1980). We attribute this to the fact that small variations in  $r^-$  are naturally propagated along the  $C^-$  characteristics.

This scheme has been implemented using second-order numerical methods (trapezoidal rule, improved Euler method, etc.). Some results are given in the next section.

## 6. Results

Calculations have been performed for several airfoils over a range of Mach numbers. The results presented in figures 1 and 3-7 are for a symmetric circular arc airfoil with thickness ratio 0.25 at upstream Mach number  $M_0 = 4$ . In figures 8-10 results from the additional cases  $M_0 = 2.5$  and 7.5, for the same airfoil, are included as well. These cases were chosen in part for the interesting effects they exhibit.

The iteration scheme converges quite rapidly, based on a comparison of the solutions at successive iterations. In table 1, the maxima (over all grid points) of the differences in the values of  $\theta$ ,  $\mu$  and  $x$  are given for the case  $M_0 = 7.5$  (the most slowly convergent of the three cases). The greatest differences are in  $x$  and usually occur near  $\alpha = 1$ , where  $x \rightarrow \infty$ . The errors in  $x$  are smaller closer to the airfoil. For thinner airfoils or lower Mach numbers, fewer iterations are required for the same accuracy. In the case

Iteration	$\Delta\theta/\theta(0, 0)$	$\Delta\mu/\mu$	$\Delta x/x$
1	0.0595	0.1170	0.3701
2	0.0141	0.0096	0.1221
3	0.0008	0.0007	0.0112
4	0.0002	0.0006	0.0017
5	0.0001	0.0003	0.0009

TABLE 1

of a 10% thick parabolic arc airfoil, for example, even at  $M_0 = 10$  the difference between the approximate and exact solutions is less than one per cent in  $\theta$  and  $\mu$  and six per cent in  $x$ . In such a case there is little reason to go beyond the approximate solution.

The case  $M_0 = 2.5$  is discussed in Holt (1977). Figure 4 contains a comparison of the leading shock when computed by our approximate and exact methods, the BVL method (an exact numerical method), and generalized shock expansion theory (the latter and the BVL solution are taken from Holt 1977, p. 77). In this case, our approximate solution is indistinguishable from the exact solution. The small difference between these and the BVL solution is probably attributable to copying errors.

Figure 5 contains plots of pressure contours in the  $xy$  plane and the value of  $\log p$  on the airfoil surface and on the line of symmetry behind the airfoil. Comparison with figure 1 shows that the contour lines between the lead and tail shocks are nearly identical to  $C^+$  characteristics, i.e. the pressure is approximately constant on  $C^-$  characteristics. This was seen in § 4 to be related to the fact that  $\theta$  is approximately constant on  $C^+$  characteristics, which in turn is related to the fact that  $r^-$  is approximately constant on streamlines. The latter two assumptions are illustrated in figures 6 and 7.

In figure 6, the deflection angle  $\theta$  is plotted versus  $\alpha$  on each of the  $C^+$  characteristics shown in figure 3. In the region behind the tail shock  $\theta$  is very nearly zero ( $|\theta| < 0.005$ ) everywhere. The variation in  $\theta$  along each characteristic is quite small, with the most serious departure occurring on the characteristics originating from the rear part of the airfoil. These characteristics tend to intersect the tail shock fairly close to the airfoil, however. A related phenomenon is that the principal characteristics are nearly straight. This however does not remain true in the region behind the airfoil.

Figure 7 shows the variation of  $r^-$  with  $\beta$  on each streamline of figure 3. Somewhat remarkably the assumption  $r^- = -P_0(\alpha)$  is better at the airfoil than a short distance away. The assumption is less satisfactory behind the tail shock. The rapid downstroke of the  $r^-$  curves also indicates a large value of  $\theta_x$ , although  $\theta$  itself remains quite small.

The entropy jumps created by the lead and tail shocks are given in figure 8 for the three cases  $M_0 = 2.5, 4.0$  and  $7.5$ . The entropy variation along the tail shock has a two-scale appearance, especially at the higher Mach numbers, which shows a very rapid decrease in strength in the initial portion of the shock. The slower variation in entropy follows that induced by the front shock. Looking at figure 1, we see that the streamlines spread apart rapidly as the flow passes the midchord position. The inclination of the flow incident upon the tail shock therefore decreases rapidly, which causes a correspondingly rapid decrease in shock strength.

Another important effect is also at work in this region. The gas, which is compressed

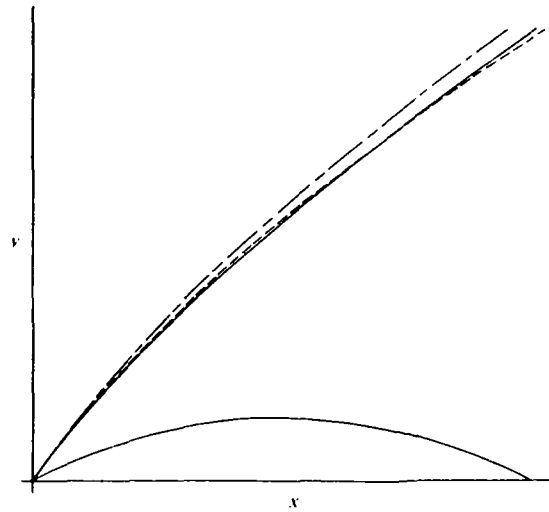


FIGURE 4. Front shock for flow field of figure 1 as computed by: present approximate and exact methods (—), BVLR method (---), generalized shock expansion method (- - -).

at the front shock, in following the profile past the midchord experiences a rapid expansion, which is strong enough that the local Mach number at the trailing edge exceeds the upstream value ( $M = 9.83$  for the  $M_0 = 7.5$  case). This recovery process is largely cut off by the tail shock, however, since the large negative value of  $\theta$  on the after part of the airfoil causes the principal characteristics to have negative slopes, so that waves originating there must intersect the tail shock near the airfoil. As a result the Mach number along the tail shock falls off rapidly, which augments the rapid decrease in strength of the tail shock. For the case  $M_0 = 7.5$  the Mach number along the shock even falls below 7.5.

The pressure field behind the airfoil (figure 5) also contains interesting features. In spite of the very high shock strength at the trailing edge, the pressure jump through the shock does not quite bring  $p$  up to the equilibrium pressure  $p = 1$ . There is a rapid pressure increase immediately behind the trailing edge, in which  $p$  increases above the equilibrium value, reaching a maximum about one chord length out. The return to equilibrium from this point is very gradual. The total variation in pressure behind the tail shock is quite small compared with that along the airfoil surfaces.

Far behind the airfoil  $p \rightarrow 1$  and  $\theta \rightarrow 0$ . It then follows from the equation of state that

$$a^2 = \exp[-(\gamma - 1)s_3(\alpha)/\gamma],$$

where  $s_3(\alpha)$  is given by figure 8. From (1), we can then compute the velocity  $q$  at infinity. This is shown in figure 9 for  $M_0 = 2.5, 4.0$  and  $7.5$ . As a result of the non-uniform entropy, the flow at infinity has a vorticity distribution.

A feature which is difficult to perceive from figure 1 or figure 5 is that the tail shock angle is not monotonic. In figure 10 the variation of the slope of the tail shock is given for the three cases we have discussed. In each case the shock angle decreases on leaving the trailing edge. (This result has been verified independently by J. C. Townsend 1979 (private communication), using a numerical method developed by

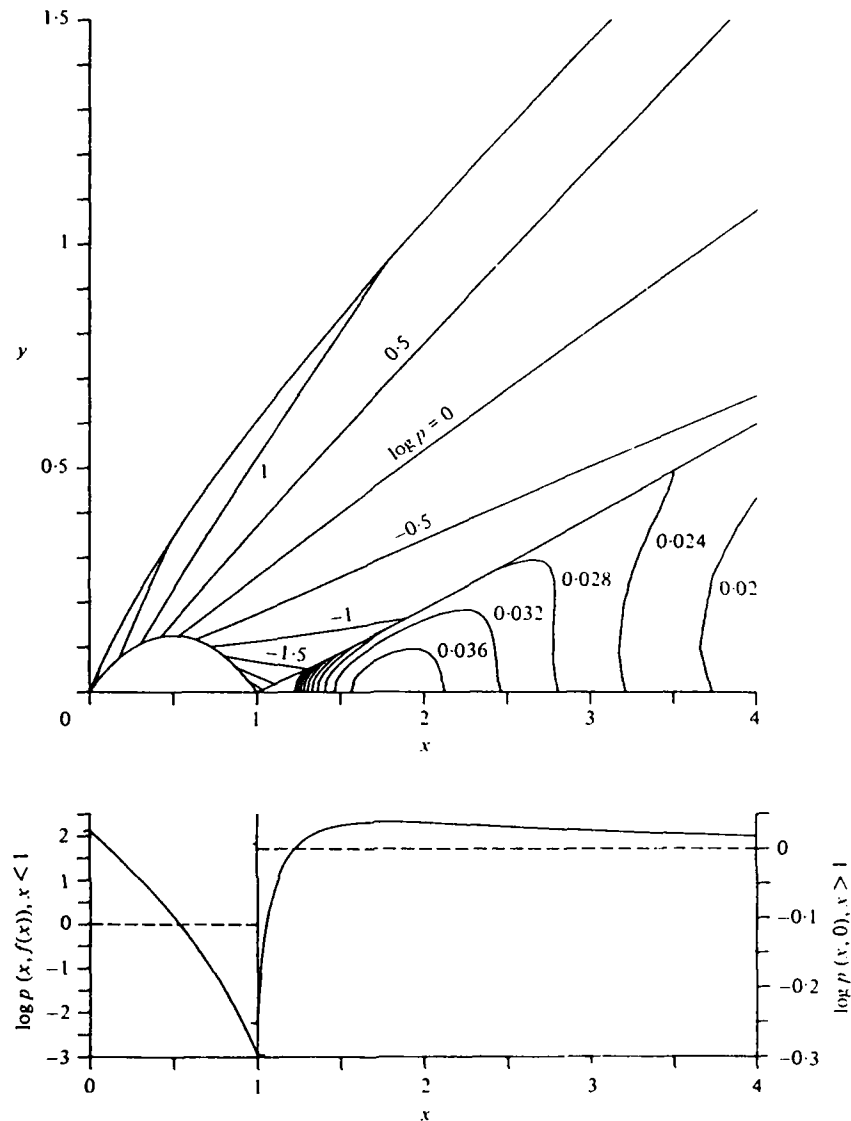


FIGURE 5. Upper graph: pressure contours in flow field of figure 1. Lower graph:  $\log p$  vs.  $x$  at  $\alpha = 0$ . Note different scales for  $0 < x < 1$  and  $x > 1$ .

M. D. Salas.) This is contrary to what is observed for lower Mach numbers or thinner bodies. We have seen that the inclination of the incident flow decreases along the shock. If the Mach number upstream of the shock were constant, this would predict a decrease in shock angle. The Mach number actually decreases along the shock however, which tends to increase the shock angle. At high Mach numbers the shock angle is more dependent on the flow angle than on the Mach number, as can be seen from the fact that the shock polars for different Mach numbers approach a limiting curve as  $M \rightarrow \infty$  (see e.g. Liepmann & Roshko 1957, p. 87). In these cases, near the trailing edge the decreasing flow angle dominates. Farther away from the airfoil, or

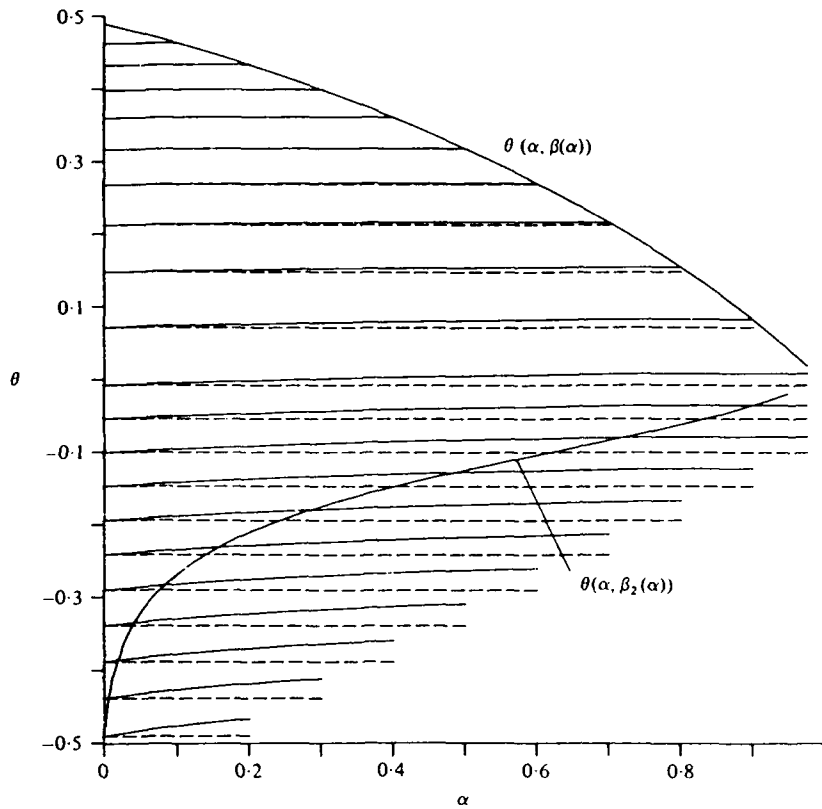


FIGURE 6. Flow angle  $\theta$  vs.  $\alpha$  on each  $C^+$  characteristic of figure 3. Dashed lines are constant values  $\theta = \tan^{-1} f'(\beta)$  for comparison. Values along front shock  $\beta(\alpha)$  and tail shock  $\beta_2(\alpha)$  are also given.

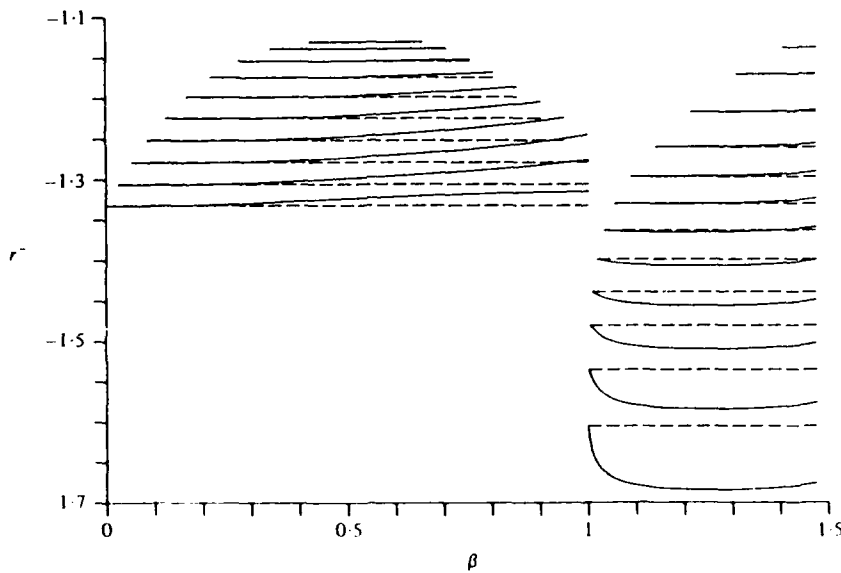


FIGURE 7. Riemann invariant  $\tau^-$  vs.  $\beta$  on each streamline of figure 3. Dashed lines are constant values  $\tau^- = -P_0(\alpha)$  for comparison.

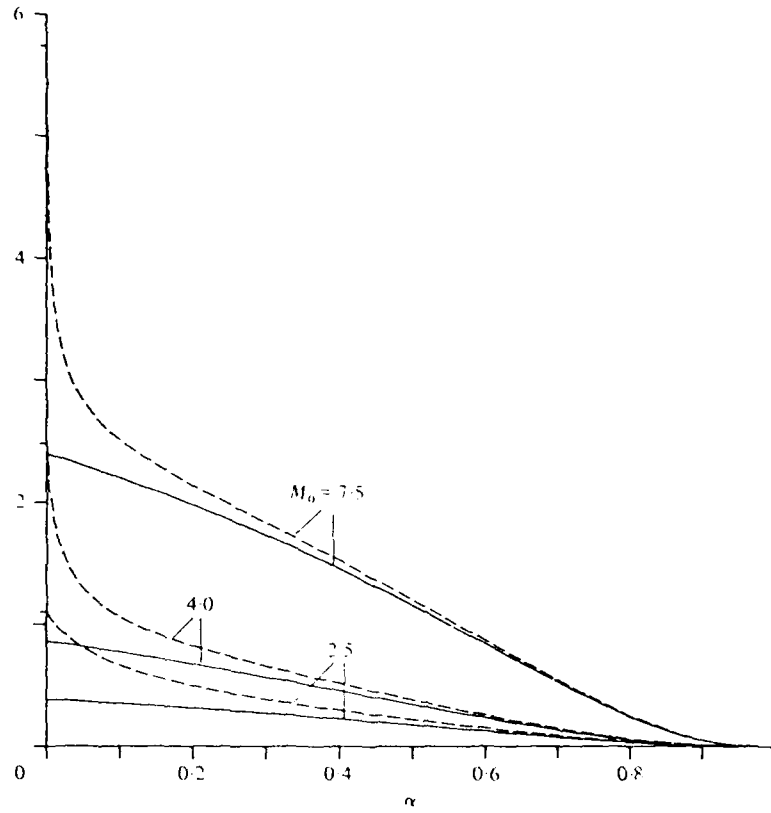


FIGURE 8. Entropy  $s(\alpha)$  (—) in region between front and tail shocks, and  $s_3(\alpha)$  (---) in region behind tail shock, for 25% circular arc airfoil at upstream Mach numbers  $M_0 = 2.5$ ,  $4.0$ , and  $7.5$ .

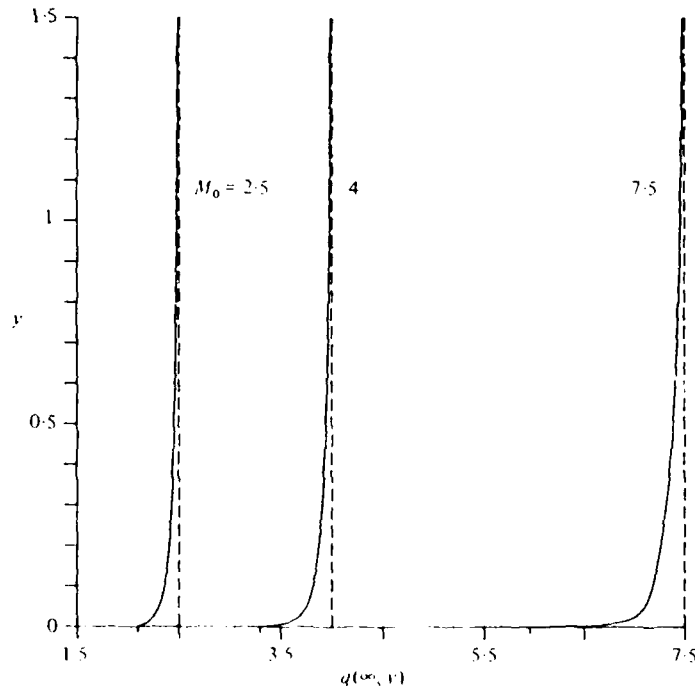


FIGURE 9. Velocity profiles far behind airfoil for  $M_0 = 2.5$ ,  $4.0$  and  $7.5$ . Dashed lines are asymptotic values,  $M_0$ .

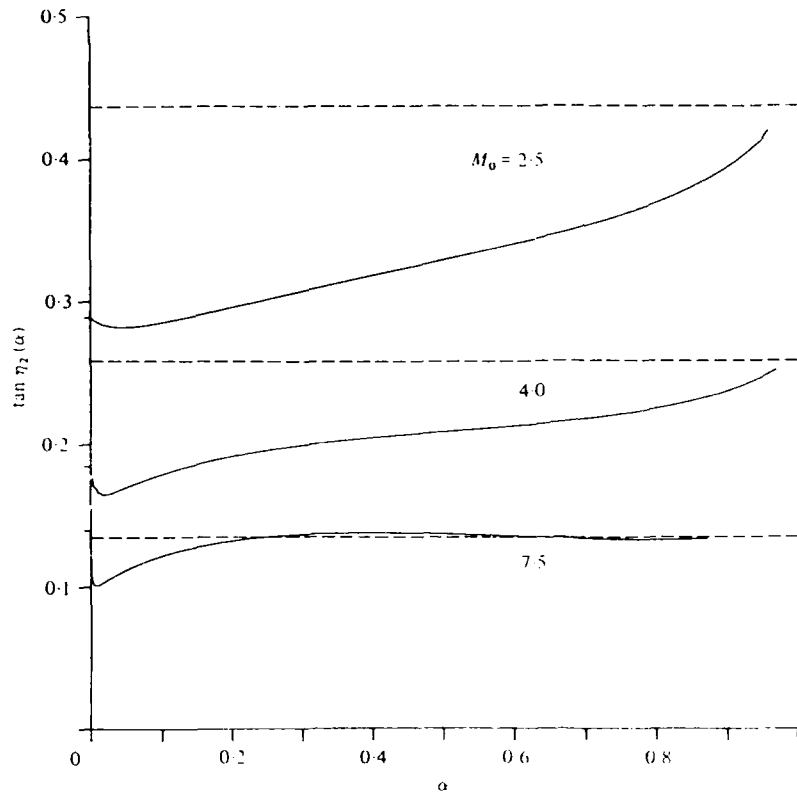


FIGURE 10. Tail shock slope  $\tan \eta_2(\alpha)$  for  $M_0 = 2.5, 4.0$  and  $7.5$ .  
Dashed lines are asymptotic values,  $\tan \mu_0$ .

in problems with lower Mach numbers or thinner airfoils, the effect of decreasing Mach number dominates.

In the case  $M_0 = 7.5$  the shock angle undergoes a second oscillation in which it rises above the Mach angle at infinity,  $\mu_0$ . This is explained by the rapid fall-off of Mach number along the shock, below its value at infinity. A final item of note in figure 10 is that for  $M_0 = 7.5$  the shock angle actually starts off with a value which is greater than  $\mu_0$ . As  $M_0 \rightarrow \infty$  the upstream Mach angle  $\mu_0$  goes to zero, as does the Mach angle at the trailing edge, since the Mach number there also increases. The shock slope at the trailing edge approaches a finite value however, which depends on the airfoil slope at the trailing edge.

## 7. Conclusions

The methods we have presented are useful in computing two-dimensional flow fields about airfoils. The approximate solution is accurate enough for many cases of interest, and the numerical method furnishes a rapid correction to the solution in those cases where it is not. The characteristic-streamline co-ordinate system is useful both for the computation of the approximate solution and the corrections, and is also convenient for displaying and interpreting the results.

The use of the streamlines as one co-ordinate and the iterative nature of the numerical calculation make the method convenient for the incorporation of a boundary-layer correction. In a boundary thickness method, for example, a succession of inviscid calculations are performed with a changing airfoil shape. The changing shape could be easily included in the present iteration method.

In response to a referee's request for comparison with other integration schemes, we asked Dr James C. Townsend of the NASA Langley Research Center to run some speed trials on their CDC Cyber 175 computer comparing our code with a 'marching' method developed there. At the lowest Mach number,  $M_0 = 1.25$ , our scheme runs about seven times faster than the marching method, while at the highest Mach number,  $M_0 = 10$ , our scheme was slightly slower. The present method is most efficient at low Mach numbers where the approximate solution is most accurate and the fewest iterations are required. This is in contrast to the marching method, where low Mach number necessitates a short step size for stability, and hence longer computation times. While these trials give some idea of relative speed they cannot be considered definitive.

This work was supported by the National Aeronautics and Space Administration under NASA Grant no. NSG 1617. The authors would like to thank Dr James C. Townsend for carrying out a number of computations which were very useful in the course of this research.

#### Appendix A. Case of an arbitrary gas

For an arbitrary gas, the equations of motion in characteristic form can be written (Hayes & Probstein 1966, p. 484)

$$ds = 0 \quad \text{on} \quad dy/dx = \tan \theta, \quad (\text{A } 1)$$

$$d\theta \pm \Phi dp = 0 \quad \text{on} \quad dy/dx = \tan(\theta \pm \mu), \quad (\text{A } 2)$$

where  $\Phi = p_0/(\rho_0 a_0^2 \rho q^2 \tan \mu)$ . We can consider  $\Phi$  to be a function of  $p$  and  $s$ . By introducing the variables

$$\omega(p, s) = \int \Phi(p, s) dp \quad \text{and} \quad \Omega(p, s) = \partial \omega(p, s) / \partial s,$$

which are defined so that  $d\omega = \Phi dp + \Omega ds$ , (A 2) can be written as

$$d\theta \pm d\omega = \pm \Omega ds \quad \text{on} \quad dy/dx = \tan(\theta \pm \mu). \quad (\text{A } 3)$$

If  $\omega$  and  $\Omega$  are now regarded as functions of  $\mu$  and  $s$ , (A 1) and (A 3) are three equations in three unknowns:  $\theta$ ,  $\mu$  and  $s$ . Equations (3) are a special case of (A 3) in which  $\omega = P(\mu)$  and  $\Omega = (\sin 2\mu)/2\gamma$ .

The transformation to  $\alpha\beta$  co-ordinates goes through for the most part as before. Equations (6) (8) in the general case become

$$s_\mu = 0, \quad (\theta + \omega)_x = \Omega s'(x),$$

$$\left( \frac{\partial}{\partial x} + w \frac{\partial}{\partial \beta} \right) (\theta - \omega) = -\Omega s'(x),$$

where  $w$  is still given by (9). The counterpart of (13) is

$$0 = \frac{x_\alpha \beta}{x_\alpha} + (\mu + \omega)_\beta \cot \mu + (\theta + \mu)_\beta \tan(\theta + \mu).$$

This equation can in principle be solved in the same manner as (13), but, depending on the form of  $\omega$ , we may not have an explicit integral like (14).

The assumption  $\theta_\alpha = 0$  in the general case implies  $(\theta - \omega)_\beta = 0$  or  $\theta - \omega = -\omega_0(\alpha)$ . The resulting approximation can be expected to be valid at least in cases in which the behaviour of the gas does not differ too greatly from that of a perfect gas with constant specific heats and  $\gamma = 1.4$ . In particular, it has been shown (see Hayes & Probstein 1966, §7.2) that shock expansion theory tends to lose accuracy if  $\gamma$  is allowed to approach 1.

### Appendix B. Tail shock for a symmetric airfoil

In general, the solutions above and below the airfoil can be computed independently, up to the appearance of the tail shocks. The flows from the top and bottom interact behind the airfoil, which complicates the computation of the tail shocks and the flow behind them. The upper and lower regions behind the airfoil are separated by a contact discontinuity, or slipstream, across which  $\theta$  and  $p$  are continuous, but the other variables jump. In the case of an airfoil symmetric with respect to the  $x$  axis the slipstream coincides with the  $x$  axis, and can be considered a rigid boundary. The problem is still quite different from the front shock problem, because the flow upstream of the tail shock is not uniform.

The transformation to  $\alpha\beta$  co-ordinates behind the tail shock can be chosen differently than that ahead of it. In particular, it is more proper to regard the  $C^-$  characteristics as the principal characteristics, since the  $C^+$  waves are only produced as reflections of the  $C^-$  waves, which originate at the tail shock. The approximate solution is somewhat more accurate if the  $C^-$  characteristics are used. On the other hand, for numerical work it is better to take the  $C^+$  characteristics as the  $\beta$  co-ordinates, because this has the effect of putting more points near the trailing edge, where a rapid variation in the solution occurs. We keep  $\alpha$  constant on streamlines as they cross the shock, and normalize  $\beta$  behind the tail shock so that the infinite region behind the tail shock is mapped into a finite region in the  $\alpha\beta$  plane. In the calculations presented here, this was done by setting  $\beta_3(\alpha) = 1 + \frac{1}{2}\alpha$ , producing the triangular region shown in figure 3.

The approximate solution used for the flow over the airfoil cannot be conveniently employed for the flow behind the tail shock, because the non-uniform flow to its left makes it impossible to calculate  $P_0(\alpha)$  and  $s(\alpha)$  *a priori* for use in (20). Therefore the simpler of the approximations given in §4 is used:  $\theta = \theta_3(\beta)$ ,  $p = p_3(\beta)$ , and  $s = s_3(\alpha)$ . All the characteristics intersect the  $x$  axis, where  $\theta = 0$ , so  $\theta_3(\beta) = 0$ , and hence in this approximation  $\theta = 0$  everywhere. This turns out to be quite accurate (see §6). Given that  $\theta = 0$  behind the tail shock, it is possible to solve the shock conditions for the tail shock angle  $\eta_2(\alpha)$ , in terms of the solution upstream of the tail shock, which we assume has been previously computed. This also determines  $p_3(\beta)$  and  $s_3(\alpha)$ , and gives an ordinary differential equation to solve for the tail shock  $\beta_2(\alpha)$ . It is possible to derive expressions for  $x$  and  $y$  similar to (14) and (15) for the region behind the tail shock, which will involve a new function  $A_3(\alpha)$ . An explicit solution for  $A_3(\alpha)$  can be found in this case, involving the computed tail shock trajectory.

The iteration scheme proceeds essentially as before. Given  $r^-(\alpha, \beta_3(\alpha))$  from the shock conditions, we integrate (21) along  $C^-$  characteristics down to the slipstream

$\alpha = 0$ . Then we reset  $r^+(0, \beta) = -r^-(0, \beta)$ , and integrate (22) upwards to  $\beta_3(\alpha)$ . The new  $r^+$  and  $r^-$  define a new  $\theta(\alpha, \beta_3(\alpha))$ , which is used to solve for a new shock  $\beta_3(\alpha)$  and new functions  $\eta_2(\alpha)$ ,  $s_3(\alpha)$ , and  $r^-(\alpha, \beta_3(\alpha))$ , with which we start the next iteration.

## REFERENCES

- ADAMSON, T. C. 1968 *J. Fluid Mech.* **34**, 735.  
 BABENKO, K. I., VOSKRESENSKIY, G. P., LYUBIMOV, A. N. & RUSANOV, V. V. 1966 Three-dimensional flow of ideal gas past smooth bodies. *N.A.S.A. Tech. Transl.* F-380.  
 CAUGHEY, D. A. 1969 Second-order wave structure in supersonic flows. *N.A.S.A. CR-1438*.  
 CHONG, T. H. & SIROVICH, L. 1980 *Phys. Fluids* **23**, 1296.  
 EGGERS, A. J., SYVERTSON, C. A. & KRAUS, S. 1953 *N.A.C.A. Rep.* no. 1123.  
 EPSTEIN, P. S. 1931 *Proc. Nat. Acad. Sci.* **17**, 532.  
 FRIEDRICHS, K. O. 1948 *Comm. Pure Appl. Math.* **1**, 211.  
 HAYES, W. D. & PROBSTEIN, R. F. 1966 *Hypersonic Flow Theory*, vol. I. Academic.  
 HOLT, M. 1977 *Numerical Methods in Fluid Dynamics*. Springer.  
 JONES, J. G. 1963 *J. Fluid Mech.* **17**, 506.  
 LIEPMANN, H. W. & ROSHKO, A. 1957 *Elements of Gasdynamics*. Wiley.  
 LICHTHILL, M. J. 1960 *Higher Approximations in Aerodynamic Theory*. Princeton University Press.  
 MAHONY, J. J. 1955 *J. Aero. Sci.* **22**, 673.  
 MAHONY, J. J. & SKEAT, P. R. 1955 *Austr. Aero. Res. Lab., Aero. Note* 147.  
 MEYER, R. E. 1957 *Q. Appl. Math.* **14**, 433.  
 MEYER, R. E. 1960 Theory of characteristics in inviscid gas dynamics, *Handbuch der Physik*, vol. IX. Springer.  
 SALAS, M. D. 1976 *A.I.A.A. J.* **14**, 583.  
 SIROVICH, L. & CHONG, T. H. 1980 *Phys. Fluids* **23**, 1291.  
 TAYLOR, T. D., NDEFO, E. & MASSON, B. S. 1972 *J. Comp. Phys.* **9**, 99.

# The Inverse Problem for Supersonic Airfoils

T. S. Lewis and L. Sirovich



Reprinted from

Volume 22, Number 2 February 1984, Page 295

AMERICAN INSTITUTE OF AERONAUTICS AND ASTRONAUTICS • 1633 BROADWAY • NEW YORK, N. Y. 10019

# Technical Notes

TECHNICAL NOTES are short manuscripts describing new developments or important results of a preliminary nature. These Notes cannot exceed 6 manuscript pages and 3 figures; a page of text may be substituted for a figure and vice versa. After informal review by the editors, they may be published within a few months of the date of receipt. Style requirements are the same as for regular contributions (see inside back cover).

## The Inverse Problem for Supersonic Airfoils

Timothy S. Lewis\* and Lawrence Sirovich†  
Brown University, Providence, Rhode Island

### Introduction

THE inverse or design problem for the case of two-dimensional supersonic airfoil shapes is considered. In view of the hyperbolic structure of the underlying equations, the calculation is simpler than the corresponding subsonic problem. In a recent paper,<sup>1</sup> the authors developed a numerical procedure for treating the direct problem, the calculation of supersonic flowfields past given profiles. This procedure makes use of streamlines as one of the coordinates. As a result, it is especially suited to the inverse problem. Since the adaptation of the method to the present problem is very similar to the original formulation, we will give only a brief outline of the procedure in this Note. For purposes of comparison, we also present two approximate solutions of the problem, one a simple treatment based on linearized analysis and the other based on shock expansion theory. The latter proves to be highly accurate and fails only in extreme cases.

### Outline of the Method

Consider two-dimensional supersonic flow, which we describe by the flow deflection angle  $\theta$ , the Mach angle  $\mu = \sin^{-1}(1/M)$ , and  $s$ , the entropy divided by the gas constant  $R$ .

The equations of motion in characteristic form are<sup>2</sup>

$$dr' \pm \frac{\sin 2\mu}{2\gamma} ds \text{ on } C^{\pm}; \quad \frac{dv}{dx} = \tan(\theta \pm \mu) \quad (1)$$

$$dv = \theta \text{ on streamlines}; \quad \frac{dy}{dx} = \tan\theta \quad (2)$$

and where  $r' = \theta + P(\mu)$  and  $P(\mu)$ , the Prandtl angle, is defined by

$$P(\mu) = \lambda \tan^{-1}(\lambda \tan\mu) + \mu, \quad \lambda = (\gamma + 1)/(\gamma - 1) \quad (3)$$

We introduce a coordinate system made up of the streamlines ( $\alpha = \text{const}$ ) and the  $C^{\pm}$  characteristics ( $\beta = \text{const}$ ). The equations then become

$$s = \theta \quad (4)$$

$$r' = \frac{\sin 2\mu}{2\gamma} s \quad (5)$$

$$r' + wr' = -\frac{\sin 2\mu}{2\gamma} s, \quad w = \frac{2}{1 - \tan\theta \tan\mu} \quad (6)$$

In this formulation, the coordinates  $(x, y)$  in the physical plane become dependent variables and are governed by the equations

$$x_{\alpha} = x_0 \tan\theta, \quad x_{\beta} = x_0 \tan(\theta + \mu) \quad (7)$$

Equations (4-7) are to be augmented by the shock relations, which are not repeated here, and by the given airfoil pressure distribution  $p = p_0(x)$ .

The transformation from the physical to the  $(\alpha, \beta)$  plane leaves open two arbitrary functions. One of these is fixed by setting

$$v(0, \beta) = \beta \quad (8)$$

on the streamline  $\alpha = 0$ , which we take to be the as yet unknown airfoil. As a second condition, we require that the shock angle  $\eta$  vary linearly with  $\alpha$ ,

$$\eta(\alpha) = \eta(0) + [\mu_0 - \eta(0)]\alpha, \quad 0 \leq \alpha \leq 1 \quad (9)$$

The method of solution is iterative and begins with an approximate solution. This approximation is allied to shock expansion theory.<sup>3,4</sup> Figure 1 contains a sketch of the plane of integration. The curve  $\alpha(\beta)$  represents the as yet unknown shock trajectory. As indicated in Fig. 1, a uniform  $\alpha$  mesh is chosen, which with  $\alpha(\beta)$  generates the  $\beta$  mesh over the first portion of the figure. The determination of the solution starts with the replacement of Eq. (6) by the approximation

$$r' = \theta - P(\mu) = -P_0(\alpha) \quad (10)$$

where  $-P_0(\alpha)$  is the value determined at the shock. If Eq. (10) is substituted into Eq. (5), we obtain

$$2 \frac{\partial}{\partial \alpha} P(\mu) = P_0'(\alpha) + \frac{\sin 2\mu}{2\gamma} s'(\alpha) \quad (11)$$

where  $s(\alpha)$  is also determined from the shock relations.

For each given value of  $\beta$ , this is an ordinary differential equation for  $\mu$ , which can be solved numerically. Initial and final values  $\mu[\alpha(\beta), \beta]$  and  $\mu(0, \beta)$  are both known, which allows us to determine the shock  $\alpha(\beta)$ . The values  $\mu[\alpha(\beta), \beta]$  come from the shock conditions and the values  $\mu(0, \beta)$  from the following relation between  $\mu, s$ , and the normalized pressure  $p$ :

$$\sin^2 \mu = \frac{\gamma - 1}{2} \frac{\exp\left\{\frac{\gamma - 1}{\gamma}(s + \ln p)\right\}}{1 + \frac{\gamma - 1}{2} M_0^2 - \exp\left\{\frac{\gamma - 1}{\gamma}(s + \ln p)\right\}} \quad (12)$$

Since  $s(0)$  is known and  $p(0, \beta) = p_0(\beta)$  is given, this determines  $\mu(0, \beta)$ .

On the portion of  $\alpha = 0$  not lying under the front shock, we choose a uniform  $\beta$  mesh. We use Eq. (12) to determine  $\mu(0, \beta)$  and integrate Eq. (11) up from  $\alpha = 0$  to finish the determination of  $\mu(\alpha, \beta)$ . Equation (10) is used to determine  $\theta(\alpha, \beta)$ . The approximate solution is then known everywhere

Received July 8, 1982; revision received March 22, 1983. Copyright American Institute of Aeronautics and Astronautics, Inc., 1983. All rights reserved.

\*Visiting Assistant Professor, Division of Applied Mathematics (presently with KOD Research Laboratory, Eastman Kodak Co., Rochester, N.Y.)

†Professor, Division of Applied Mathematics

in the  $(\alpha, \beta)$  plane. Finally, Eqs. (7) are integrated to find the transformation to the physical plane everywhere. In particular, the body shape  $f(x)$  is given by

$$f(x) = f(0) + \int_0^x \tan \theta(0, \beta) d\beta \quad (13)$$

which completes the computation of the approximate solution.

The iteration procedure starts with the neglected Eqs. (6), which were replaced in the approximate solution by Eq. (10). We numerically integrate Eqs. (6) downstream along the  $C^+$  characteristics, starting at the shock. This produces new values of  $r^*$   $(\alpha, \beta)$  everywhere. From  $r^*$   $(0, \beta)$  we can determine

$$r^* (0, \beta) = r^* (0, \beta) + 2P[\mu(0, \beta)] \quad (14)$$

since  $\mu(0, \beta)$  is given by Eq. (12). Equation (5) is then integrated up from the body along the  $C^+$  characteristics to give  $r^*$   $(\alpha, \beta)$  everywhere. We can then obtain improved values of  $\theta$  and  $\mu$  everywhere from

$$\theta = 1/2(r^* - r^*), \quad \mu = P^{-1}[1/2(r^* - r^*)] \quad (15)$$

A new shock angle  $\eta(\alpha)$  is determined from the shock relations, and a new transformation to the physical plane is

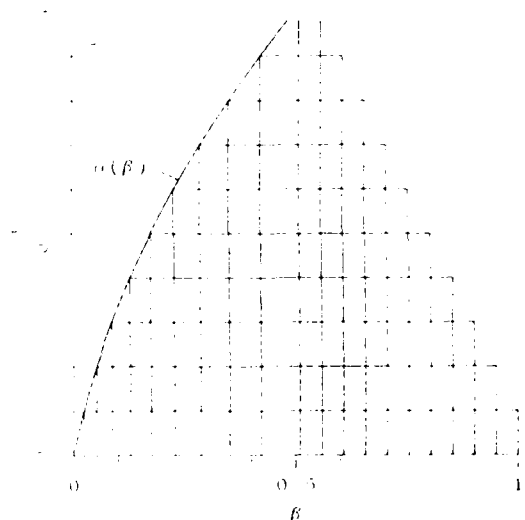


Fig. 1 Plane of integration: lines  $\alpha = \text{const}$  represent streamlines, lines  $\beta = \text{const}$  represent  $C^+$  characteristics, and curve  $\alpha(\beta)$  represents the bow shock.

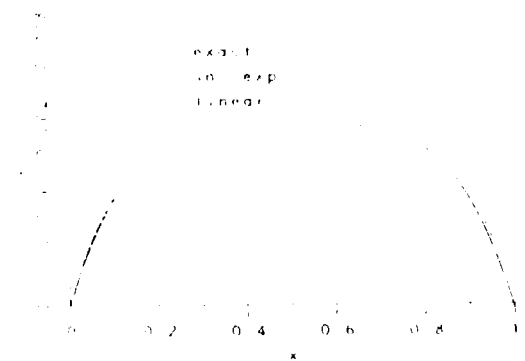


Fig. 2 Airfoil shapes computed for  $M_\infty = 1.2$  and airfoil pressure distribution  $(c_p)_a(x) = 0.05(1 - 2x)^2$ .

obtained from Eqs. (13) and (7). The iteration is then repeated until a convergence criterion is met.

**Approximate Calculations**

**Linearized Approximation**

Perhaps the simplest calculation for  $f(x)$  given the pressure distribution  $p_a(x)$  follows from linearized theory.<sup>1</sup> In our normalization, linearized theory

$$f'(x) = \frac{\sqrt{M_\infty^2 - 1}}{\gamma M_\infty^2} [p_a(x) - 1]$$

or

$$f(x) = f(0) + \frac{\sqrt{M_\infty^2 - 1}}{\gamma M_\infty^2} \left( \int_0^x p_a(\xi) d\xi - x \right) \quad (16)$$

**Shock Expansion Approximation**

One may also base an approximate calculation of  $f(x)$  on shock expansion theory.<sup>1</sup> We recall that if  $\theta_a(x)$  and  $\mu_a(x)$  denote values on the airfoil, then in this approximation it is assumed that

$$\theta_a(x) = P[\mu_a(x)] - P_a \quad (17)$$

where  $P_a$  is the value at the leading edge behind the shock. Equation (12) determines  $\mu_a(x)$  from the given pressure  $p_a(x)$  and the entropy at the leading edge  $s_a$ , and then  $f(x)$  follows from

$$f(x) = f(0) + \int_0^x \tan[P(\mu_a(\xi)) - P_a] d\xi \quad (18)$$

As an examination shows,  $f(x)$  calculated in this way agrees with the first approximation in the iterative solution outlined in the previous section.

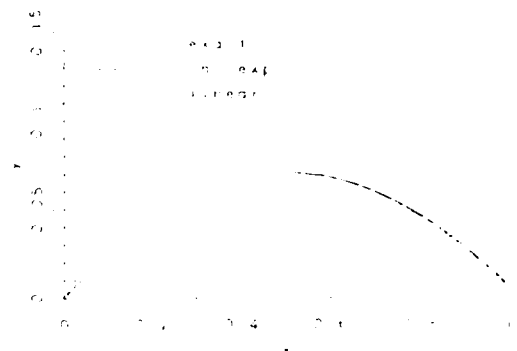


Fig. 3 Airfoil shapes computed for  $M_\infty = 2.5$  and airfoil pressure distribution  $(c_p)_a(x) = 1 - 2x$ .

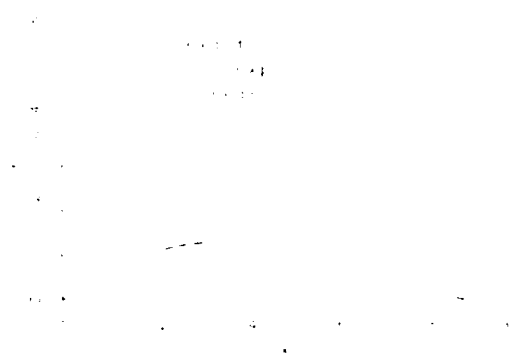


Fig. 4 Airfoil shapes computed for  $M_\infty = 5$  and airfoil pressure distribution  $(c_p)_a(x) = 3(1 - 2x)$ .

### Results

Sample calculations are shown in Figs. 2-4. In each the results obtained from linearized theory, shock expansion theory, and the exact numerical calculation are compared.

Figure 2 contains the results for a low Mach number ( $M_0 = 1.2$ ) and small pressure jump. As should be expected, all of the results are in close agreement. For Fig. 3, the Mach number is moderate ( $M_0 = 2.5$ ) and the jump in  $\ln \rho$  at the leading edge is unity. In this case, linear theory is poor in predicting an overly thick body. The result based on shock expansion theory, on the other hand, is virtually indistinguishable from the exact case. In the final example (Fig. 4), both the upstream Mach number ( $M_0 = 5$ ) and the pressure jump are relatively large. Linearized theory is now very poor. Shock expansion theory still does quite well for most of the derived airfoil and begins to depart significantly only near the trailing edge.

### Conclusions

A method for the design of two-dimensional supersonic airfoils has been presented, which incorporates available physical and mathematical knowledge of the problem (e.g., shock expansion theory and characteristics), in order to facilitate the numerical computation. A similar approach should prove useful in the more complicated problem of the design of real airfoils in which three-dimensional flow, boundary-layer effects, etc., must be considered. The iterative nature of the present method, in particular, makes it well suited to the inclusion of boundary-layer corrections.

### References

- <sup>1</sup>Lewis, T. S. and Sirovich, L., "Approximate and Exact Numerical Computation of Supersonic Flow over an Airfoil," *Journal of Fluid Mechanics*, Vol. 112, 1981, pp. 265-282.
- <sup>2</sup>Meyer, R. E., "Theory of Characteristics of Inviscid Gas Dynamics," *Handbuch der Physik*, Vol. IX, Springer-Verlag, Berlin, 1960, pp. 225-282.
- <sup>3</sup>Eggers, A. J., Syverston, C. A., and Kraus, S., "A Study of Inviscid Flow about Airfoils at High Supersonic Speeds," NACA Rept. 1123, 1953.
- <sup>4</sup>Hayes, W. D. and Probstein, R. F., *Hypersonic Flow Theory*, Academic Press, New York, 1959, pp. 265-277.

# Direct and Inverse Problem in Supersonic Axisymmetric Flow

J. Fong and L. Sirovich



Reprinted from

Volume 24 Number 5 May 1986 Page 852

AMERICAN INSTITUTE OF AERONAUTICS AND ASTRONAUTICS • 1633 BROADWAY • NEW YORK N Y 10019

## Direct and Inverse Problem in Supersonic Axisymmetric Flow

Jefferson Fong\* and Lawrence Sirovicht  
*Brown University, Providence, Rhode Island*

### Introduction

**SUPERSONIC** inviscid flow can generally be solved by the method of characteristics or by shock-capturing methods.<sup>1,2</sup> The method of characteristics computes the flow along characteristics and uses the Rankine-Hugoniot conditions at the shock. This method has the advantage of accuracy, but is regarded as complex and computationally inefficient, especially in regions of near coalescence of the two sets of characteristics.<sup>1,3</sup> In shock-capturing methods the shock is smeared over several grid points, where oscillations can occur and the scheme loses accuracy. However, due to their directness and computational ease, shock-capturing methods have been preferred in recent years.

In this Note, we develop an efficient method using the characteristics and streamlines of a flow. These are used as coordinates and the flow quantities are expressed in terms of Riemann functions. A scheme is obtained which is significantly more efficient and accurate than shock-capturing methods for flow over axisymmetric bodies. Since streamlines form one of the coordinates, we naturally obtain a body-fit system. It is also a truly shock-fit coordinate system. Not only are the Rankine-Hugoniot conditions used, but the shock lies exactly on grid points also.

The success of the present method in the two-dimensional case rests on the discovery of an accurate and simple approximation.<sup>4</sup> In the axisymmetric case, a similarly accurate and simple approximation has eluded us. The approximation presented herein is simple, but generally not as accurate as that for the two-dimensional case. A better iterative procedure has been developed to compensate for this weakness. As was the case for the two-dimensional flow,<sup>4</sup> our method is well suited for the inverse design problem (i.e., given  $M_\infty > 1$  and the pressure distribution on the body, find the shape of the body and the flow everywhere).

### Formulation

We consider axisymmetric flow with incident Mach number  $M_\infty > 1$  and shock attached at the tip. The characteristic equations can be written in terms of entropy  $s$ , flow angle  $\theta$ , Mach angle  $\mu = \sin^{-1}(1/M)$  ( $M$  = local Mach number), pressure  $p$ , density  $\rho$ , and velocity  $q$  as follows:<sup>5</sup>

$$ds = 0 \text{ on } \frac{dr}{dx} = \tan\theta \tag{1}$$

$$d\theta + \frac{dp}{\rho q^2 \tan\mu} + \frac{\sin\theta \sin\mu}{\sin(\theta + \mu)} \frac{dr}{r} \text{ on } C^+ = \frac{dr}{dx} = \tan(\theta + \mu) \tag{2}$$

At the body  $r = f(x)$  we impose the boundary condition  $\tan\theta = f'(x)$ . Jumps across a shock are given by the Rankine-Hugoniot conditions.<sup>6</sup> If we denote the shock angle

by  $\eta$ , the position of the shock is governed by

$$\frac{dr}{dx} = \tan\eta \tag{3}$$

We introduce new coordinates  $(\alpha, \beta)$  through

$$r_\alpha = x_\beta \tan\theta \tag{4}$$

$$r_\beta = x_\alpha \tan(\theta + \mu) \tag{5}$$

so that constant  $\alpha$  refers to streamlines, and constant  $\beta$  refers to  $C^+$  characteristics. Expressed in these coordinates, Eq. (1) is simply  $s = 0$ , while Eq. (2) becomes

$$\frac{\partial}{\partial \alpha} R = D(\theta, P_{(\alpha, \beta)}) \frac{\sin 2\mu}{2\gamma} s(\alpha) \frac{\tan\theta \tan\mu}{\tan\theta + \tan\mu} \frac{r_\beta}{r} \tag{6}$$

$$DR = D(\theta, P_{(\alpha, \beta)}) \frac{\sin 2\mu}{2\gamma} s(\alpha) \frac{\tan\theta \tan\mu}{\tan\theta + \tan\mu} D \tag{7}$$

where  $P(\mu) = (\lambda) \tan^{-1}[(\lambda) \tan\mu]$ ,  $\mu$  is the Prandtl angle,  $\lambda = (\gamma + 1)/(\gamma - 1)$ , and

$$D = \frac{\partial}{\partial \alpha} \frac{2 \tan\theta}{\tan\theta + \tan\mu} \frac{r_\beta}{r} = \frac{\partial}{\partial \beta}$$

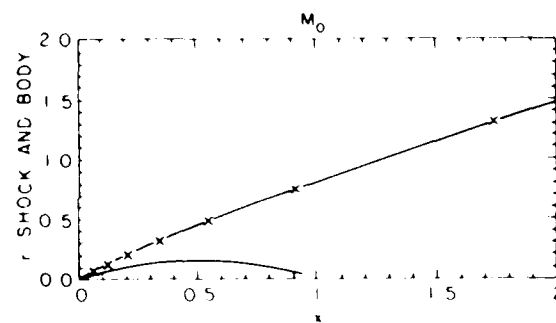


Fig. 1 Body and shock of 30%-thick parabolic body at  $M_\infty = 2$ .

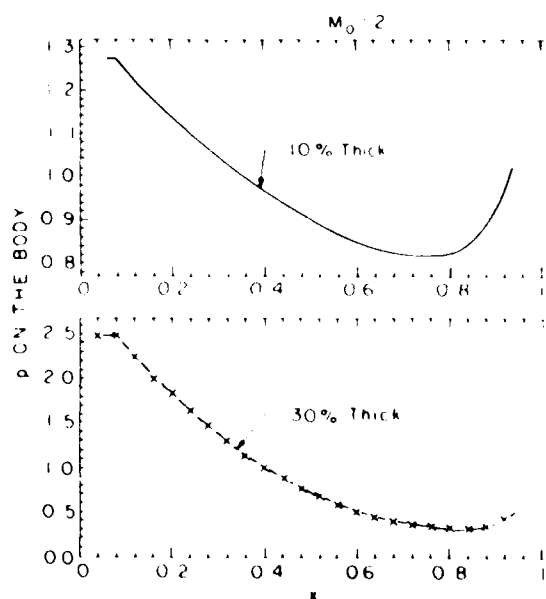


Fig. 2 Pressure distributions on the body for 10% and 30%-thick parabolic bodies at  $M_\infty = 2$ .

Received Feb. 8, 1985; revision received Aug. 15, 1985. Copyright © American Institute of Aeronautics and Astronautics, Inc., 1985. All rights reserved.

\*Research Associate, Division of Applied Mathematics. Presently at Supercomputer Computations Research Institute, Florida State University, Tallahassee, FL.

†Professor, Division of Applied Mathematics.

Here  $\gamma = 1.4$ . An alternate form of Eq. (7) used later is as follows:

$$R_{,\beta} = (1 - \tan\theta \tan\mu) \frac{x_{,\beta}^2}{x_{,\alpha}} \theta_{,\alpha} + \tan\mu \frac{r_{,\beta}}{r} \quad (8)$$

It is important to note that the dynamical equations must be augmented by the coordinate equations (4) and (5). This transformation is still undetermined up to two arbitrary functions. We fix one of these functions by taking  $x(0, \beta) = \beta$  at the body  $\alpha = 0$ . It therefore follows that

$$r(0, \beta) = f(\beta), \quad \theta(0, \beta) = \tan^{-1} f'(\beta) \quad (9)$$

To determine the second arbitrary function we fix the shock by

$$\frac{d\alpha}{d\beta} = 1 \quad (10)$$

The above formulation must be modified slightly in order to treat the inverse design problem. For this problem, pressure is specified on an unknown body. To accommodate this boundary condition, we obtain from Bernoulli's equation and the perfect gas law

$$\mu = \sin^{-1} \left[ \left( \frac{\gamma - 1}{2} \right)^{1/2} \frac{\exp\left\{[(\gamma - 1)/\gamma](s + h/p)\right\}}{1 + [(\gamma - 1)/2] M_0^2 \exp\left\{[(\gamma - 1)/\gamma](s + h/p)\right\}} \right] \quad (11)$$

Since the entropy  $s$  is constant along streamlines and is known behind the tip shock, the right-hand side of Eq. (11) is determined. Therefore, instead of Eq. (9), we have Eqs. (4) and (11) on the body. The flow above the body can be calculated exactly as before. Hence the inverse problem becomes a direct problem by the method presented here.

### Numerical Procedure

Near the tip of the body, the flow is taken to be flow over a cone. For the rest of the flow, we use a marching scheme along each column of  $\beta$ . A good approximation is first obtained at the points on that column. The governing equations are then iterated until an error tolerance is satisfied before we proceed to the next column.

It is worth noting that we are free to choose any mesh size of  $\beta$ , even when the  $C^+$  and  $C^-$  characteristics are nearly parallel. Due to Eq. (10), we are also not forced to take very small mesh sizes in  $\alpha$  either.

### Approximation Solution

Eggers and Savin<sup>10</sup> noted that hypersonic flow over asymmetric bodies can be approximated as locally two

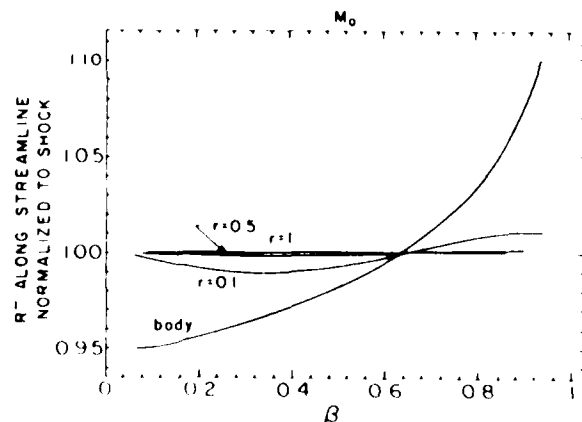


Fig. 3  $R$  along streamlines for a  $10^\circ$ -thick parabolic body at  $M_0 = 2$ .

dimensional and, hence, shock-expansion theory ( $R$  constant along an entire streamline) is valid. Indeed, for hypersonic flow, along  $C^+$  we have  $s'(\alpha)$  large and  $r_{,\alpha}$  small so that Eqs. (7) and (8) are well approximated by two-dimensional theory. At lower Mach numbers, this approximation is no longer valid. However, in our marching scheme, we need only to approximate one grid point away, and to assume that  $R$  changes slowly along a streamline. Combining Eqs. (7) and (9),

$$R_{,\beta} = \frac{\sin 2\mu}{2\gamma} \frac{Q_{,\beta}}{x_{,\alpha}}$$

$$Q_{,\beta} = \frac{\gamma - 1}{\gamma} \ln \left( 1 + \frac{\gamma - 1}{2 \sin^2 \mu} \right)$$

Here  $Q_{,\beta} = 0$  is an approximation consistent with the approximation  $R_{,\beta} = 0$ . These are the two ordinary differential equations which give us the initial guesses in the iteration scheme.

### Results and Discussions

Calculations of flow over bodies of various shapes for a range of Mach numbers have been performed. The average number of iterations (generally between 2 and 4 for an error tolerance of  $10^{-4}$ ) used per point decreases as the total number of points used increases. In view of our special coordinate system, few points are required to describe the entire flowfield. Grid points are spaced appropriately according to the natural variations of the flow. This is demonstrated in Fig. 1 with a  $30^\circ$ -thick parabolic body at  $M_0 = 2$ , where we compare a calculation using 248 points in the whole flowfield to one using 829 points.

Figure 2 shows the pressure distributions on two parabolic bodies. The flow near the tip is conical, hence pressure is constant there. The presence of a pressure minimum on the body should be noted. No such minimum appears in two-dimensional parabolic wings. Consistent with this is the fact that the minimum moves further down along the body as  $M_0$  or the thickness increases, because thicker bodies are more two-dimensional. This should be of some interest since the presence of a pressure minimum in some cases can be an indication of flow separation.

Figure 3 shows the changes of  $R$  (normalized to its value at the shock) along streamline for a  $10^\circ$ -thick body at  $M_0 = 2$ . The streamlines shown lie on the body and at about 0.1, 0.5, and 1 body length away from the axis. As one can see,  $R$  changes monotonically along the body. The approximation  $R$  constant along the whole body is poor, but  $R$  does become nearly constant at less than a body length away.

To test the method for solving the inverse problem, a direct problem was solved, and the resulting pressure distribution on the body was used in the inverse method. The agreement was excellent and the computational time is comparable to the direct problem.

### Conclusion

A streamlines characteristics coordinate system for axisymmetric flow has been presented. In our coordinate system the body lies along one coordinate, and the shock is a straight line with grid points falling exactly on it. Rankine-Hugoniot conditions are used at the shock. Consequently, the scheme is inherently accurate. Relatively few points are required to describe the entire flowfield since grid points are spaced according to the natural variation of the flow. Even in regions of near coalescence of the  $C^+$  and  $C^-$  characteristics, we are not forced to take very small mesh sizes. Starting from a simple initial guess, the scheme converges rapidly to the exact solution. Because so few points and iterations are needed, the method is computationally very efficient. Our body fit coordinate system also allows us to solve the inverse design problem with ease, and due to our

coordinate system the inverse problem becomes a direct problem. Our results for thin bodies at low Mach numbers show there is a pressure minimum on the bodies, which can imply flow separation in some cases.

### References

- <sup>1</sup>Anderson, D., Tannehill, J., and Pletcher, R., *Computational Fluid Mechanics and Heat Transfer*, McGraw-Hill Book Co., New York, 1984, pp. 260-288.
- <sup>2</sup>Richtmyer, R. and Morton, K., *Difference Method for Initial Value Problem*, 2nd Ed., John Wiley & Sons, New York, 1967, pp. 375-383.
- <sup>3</sup>Peyret, R. and Taylor, T., *Computational Methods for Fluid Flow*, Springer-Verlag, New York, 1983, pp. 46-63, 135-138.
- <sup>4</sup>Marconi, F., Salas, M., and Yaeger, I., "Development of a Computer Code for Calculating the Steady Super/Hypersonic Inviscid Flow Around Real Configurations," NASA CR-2675, 1976.
- <sup>5</sup>Moretti, G., Grossman, B., and Marconi, F., "A Complete Numerical Technique for the Calculation of Three-Dimensional Inviscid Supersonic Flows," AIAA Paper 72-192, 1972.
- <sup>6</sup>Lewis, T. and Sirovich, I., "An Approximate and Exact Numerical Computation of Supersonic Flow Over an Airfoil," *Journal of Fluid Mechanics*, Vol. 112, 1981, pp. 265-282.
- <sup>7</sup>Lewis, T. and Sirovich, I., "The Inverse Problem for Supersonic Airfoils," *AIAA Journal*, Vol. 22, 1984, pp. 295-297.
- <sup>8</sup>Hayes, W. and Probstein, R., *Hypersonic Flow Theory*, 2nd Ed., Academic Press, New York, p. 484.
- <sup>9</sup>Liepmann, M. and Roshko, A., *Elements of Gasdynamics*, John Wiley & Sons, New York, 1957, p. 85.
- <sup>10</sup>Eggers, A. and Savin, R., "A Unified Two Dimensional Approach to the Calculation of Three Dimensional Flows, With Application to Bodies of Revolution," NACA Rept. 1249, 1955.

# Supersonic Inviscid Flow— A Three-Dimensional Characteristics Approach

JEFFERSON FONG\*

*Supercomputer Computations Research Institute, Florida State University,  
Tallahassee, Florida 32304-4052*

AND

LAWRENCE SIROVICH†

*Division of Applied Mathematics, Brown University,  
Providence, Rhode Island*

Received September 18, 1985; revised April 25, 1986

Supersonic inviscid flow over nonaxisymmetric bodies is considered. A new version of the method of reference planes is used. In this version, a near characteristics-streamlines coordinate system and a highly efficient numerical integration scheme is developed. The CFL condition is rigorously satisfied on the flow. Several sample calculations are presented. © 1987 Academic Press, Inc.

## 1. INTRODUCTION

The method of characteristics for three-dimensional flows has been developed in a number of ways. Surveys of this method have been given [1, 2, 3], and the leading approaches have been compared [4]. The main advantages of such methods lie in their intrinsic use of characteristics as well as their accurate calculation of shockwaves. Generally these methods, which require consideration of characteristic conoids and bicharacteristics, are regarded as complex and computationally inefficient compared to the more popular finite difference shock capturing and shock fitting methods, e.g., [5, 6, 7].

Another class of schemes allied to the characteristics method but much simpler to apply is generically referred to as reference plane methods [8-12, 1]. Another designation is method of near characteristics, a terminology which reflects the idea that characteristics are employed in an approximate fashion. In this paper we apply

\* Work supported in part by grants from the National Science Foundation (CHE 83 04021) and the U.S. Department of Energy (DE-FC05-85ER25000).

† Work supported by the Air Force Office of Scientific Research (AFOSR 5 28320).

a variant of this approach to the problem of flow past nonaxisymmetric bodies. Our approach is most closely related to that of Sauer [5] and Rakich [12].

For the case treated here, flow past a body is divided into a set of azimuthal planes. In each plane a highly successful two-dimensional characteristics method [13, 14] is applied. The "cross-talk" between such planes created by azimuthal derivatives and velocities then serve as forcing terms in the equations. Unlike earlier treatments that we are familiar with we are able to rigorously consider domains of dependence follow the Courant-Friedrichs-Lewy (CFL) condition. The result is a method which is extremely fast without loss of efficiency or accuracy.

## 2. FORMULATION

Since the form of the governing equations is not standard, we now outline their development. Flow in cylindrical coordinates  $(x, r, \phi)$  is governed by the following equations:

$$\nabla \cdot (\rho \mathbf{u}) = 0, \quad (1)$$

$$v \frac{\partial u}{\partial r} + u \frac{\partial u}{\partial x} = \frac{w}{r} \frac{\partial u}{\partial \phi} - \frac{1}{\rho} \frac{\partial p}{\partial x}, \quad (2)$$

$$v \frac{\partial v}{\partial r} + u \frac{\partial v}{\partial x} = \frac{-w}{r} \frac{\partial v}{\partial \phi} + \frac{w^2}{r} - \frac{1}{\rho} \frac{\partial p}{\partial r}, \quad (3)$$

$$v \frac{\partial w}{\partial r} + u \frac{\partial w}{\partial x} = \frac{w}{r} \frac{\partial w}{\partial \phi} - \frac{vw}{r} - \frac{1}{\rho r} \frac{\partial p}{\partial \phi}. \quad (4)$$

In addition to the continuity (1) and momentum equations (2), (3), (4), we have Bernoulli's relation

$$\frac{u^2 + v^2 + w^2}{2} + \frac{a^2}{\gamma - 1} = \frac{M_0^2}{2} + \frac{1}{\gamma - 1}. \quad (5)$$

The gas is specified by the state equation

$$\frac{p}{\rho} e^{(\gamma - 1)S} = \text{constant}, \quad (6)$$

where the entropy  $S$  satisfies

$$\mathbf{u} \cdot \nabla S = 0, \quad (7)$$

between shocks while (5) is also valid across shocks [15]. We normalize  $u, v, w$ , and the speed of sound  $a$  by the upstream speed of sound  $a_0$ ;  $x, r$  by the body length;  $\rho$  by its upstream value  $\rho_0$ ;  $p$  by  $\gamma p_0$ ; and  $S$  is replaced by  $(S - S_0)/R$ , where  $R$  is the universal gas constant.

We introduce

$$\theta(x, r, \phi) = \tan^{-1} \left( \frac{v}{u} \right), \quad (8)$$

the flow deflection angle in the projected plane,  $\phi = \text{constant}$ . Similarly

$$\mu(x, r, \phi) = \sin^{-1} \left( \frac{1}{M_*} \right) \quad (9)$$

is the projected flow Mach angle, where

$$M_*^2 = \frac{u^2 + v^2}{a^2}. \quad (10)$$

In Appendix A it is shown

$$\begin{aligned} d_{\pm}(\theta \pm P(\mu)) = & \pm \frac{\sin 2\mu}{2} \left( \frac{d_{\pm} S}{\gamma} - \frac{d_{\pm} W}{\gamma - 1} \right) \\ & + \frac{G_1 \mp (\tan \theta \tan \mu + G_2) d_{\pm} r}{\tan \theta \pm \tan \mu} \frac{1}{r}, \end{aligned} \quad (11)$$

where

$$C^{\pm} : d_{\pm} = \frac{\hat{c}}{\hat{c}x} + \tan(\theta \pm \mu) \frac{\hat{c}}{\hat{c}r} \quad (12)$$

denotes differentiation in the  $C^{\pm}$ -directions, i.e., in the near characteristic directions.  $\theta \pm P(\mu)$  are the corresponding "Riemann invariants." The various terms appearing in (11) are defined in Appendix A. In what follows we also use

$$\sigma = \ln p = \frac{\gamma}{\gamma - 1} \ln \left( 1 + \frac{\gamma - 1}{2} M_0^2 \right) / \left( 1 + \frac{\gamma - 1}{2} \frac{1 + \omega^2}{\sin^2 \mu} \right) - S - \ln \gamma, \quad (13)$$

where  $\omega = w/q$ . The second form for  $\sigma$  in (13) follows from (5) and (6). It should be noted that for axisymmetric flow, we have  $\omega = \theta_{\phi} = \sigma_{\phi} = 0$ , and (11) reduces to the appropriate axisymmetric equations.

Next we define new coordinates  $(\alpha, \beta, \zeta)$  such that

$$r_{\alpha} = x_{\alpha} \tan(\theta + \mu), \quad r_{\beta} = x_{\beta} \tan \theta, \quad \zeta = \phi. \quad (14)$$

This mapping is further fixed by the condition at the body

$$x(x = 0, \beta, \zeta) = \beta, \quad (15)$$

and the condition that the shock have unit slope at each constant  $\zeta$  plane, i.e.,

$$\frac{\partial x}{\partial \beta} = 1 \quad (16)$$

at the shock. Under this transformation the  $C'$  form of (11) becomes

$$R'_\zeta = \frac{\sin 2\mu}{2} \left( \frac{S'_z}{\gamma} - \frac{W'_z}{\gamma-1} \right) + \frac{G_1 + (\tan \theta \tan \mu + G_2) r_z}{\tan \theta + \tan \mu} \frac{1}{r}, \quad (17)$$

while the  $C$  form

$$DR = \frac{-\sin 2\mu}{2} \left( \frac{DS}{\gamma} - \frac{DW}{\gamma-1} \right) + \frac{G_1 + \tan \theta \tan \mu + G_2}{\tan \theta + \tan \mu} \frac{Dr}{r}, \quad (18)$$

where differentiation in  $C'$  direction is now given by,

$$D = \frac{\partial}{\partial x} - \frac{2 \tan \theta}{\tan \theta + \tan \mu} \frac{r_z}{r} \frac{\partial}{\partial \beta}$$

As shown in Appendix B the  $\phi$  and  $\zeta$  derivatives are related by

$$\frac{\partial}{\partial \phi} = \frac{(r_z + \tan \theta x_z) x_\beta (\partial / \partial x) + (\tan(\theta + \mu) x_z - r_z) x_\alpha (\partial / \partial \beta)}{(\tan \theta + \tan(\theta + \mu)) x_\alpha x_\beta} + \frac{\partial}{\partial \zeta}. \quad (19)$$

If we combine (17) and (18), then

$$\begin{aligned} R'_\mu = & (1 + \tan \theta \tan \mu) \frac{x_\beta}{x_\alpha} \frac{\sin 2\mu}{2} \left[ \frac{S'_z}{\gamma} - \frac{W'_z}{\gamma-1} + (F(\mu))'_z \right] \\ & + \frac{x_\beta}{r} G_1 + \frac{\sin 2\mu}{2} \left( \frac{W'_\beta}{\gamma-1} - \frac{S'_\beta}{\gamma} \right), \end{aligned} \quad (20)$$

where

$$F(\mu) = -2 \int \frac{P'(\mu)}{\sin 2\mu} d\mu = \frac{1}{\gamma-1} \ln \left( 1 + \frac{\gamma-1}{2 \sin^2 \mu} \right).$$

The entropy equation as shown in Appendix A is now

$$S'_\mu = \frac{\omega}{r \cos \theta} S'_\phi x_\beta, \quad (21)$$

while the  $\phi$  component of the momentum equation is

$$\begin{aligned} \frac{\sin^2 \mu}{\gamma r} \sigma_\phi + \frac{\cos \theta}{x_\beta} \omega_\beta + \frac{\omega}{r} \omega_\phi \\ = \frac{\omega \sin^2 \mu \cos \theta}{\gamma} \frac{\sigma_\mu}{x_\beta} - (1 + \omega^2) \frac{\omega}{r} \sin \theta. \end{aligned} \quad (22)$$

With the use of (13)  $\sigma$  can be eliminated from (22) to give

$$\begin{aligned} \omega_\beta = \omega \tan \mu P_\beta - \frac{x_\beta}{r \cos \theta} (\omega \sin \theta + \tan \mu P_\phi) \\ + \frac{\tan^2 \mu}{1 + \tan^2 \mu} \left[ \frac{x_\beta}{r \cos \theta} \left( \frac{S_\phi}{\gamma} - \frac{W_\phi}{\gamma - 1} \right) + \omega \left( \frac{W_\beta}{\gamma - 1} - \frac{S_\beta}{\gamma} \right) \right] \\ - \frac{x_\beta}{r \cos \theta} \omega (\omega_\phi + \omega^2 \sin \theta). \end{aligned} \quad (23)$$

The dependent variables  $x$ ,  $r$ ,  $\theta$ ,  $\mu$ ,  $\omega$ , and  $S$  are determined by (14), (17), (18) or (20), (21), and (23). On the body  $x$ ,  $r$ ,  $\theta$  are specified by the boundary conditions

$$x(\alpha = 0, \beta, \zeta) = \beta, \quad (24)$$

$$r(\alpha = 0, \beta, \zeta) = f(\beta, \zeta), \quad (25)$$

$$\theta(\alpha = 0, \beta, \zeta) = \tan^{-1} \left( \frac{\partial f}{\partial \beta}(\beta, \zeta) \right). \quad (26)$$

In addition to the shock conditions, we also apply (16) at the shock.

### 3. NUMERICAL PROCEDURES

The following scheme is an extension of the one used in the axisymmetric case [13]. Each azimuthal section ( $\zeta_k = \text{constant}$ ;  $k = 1, 2, \dots$ ) has the  $(\alpha, \beta)$  grid shown in Fig. 1. In the neighborhood of the tip,  $0 \leq \beta \leq \beta_1$ , the flow is taken as flow past a cone, not necessarily circular. For  $\beta > \beta_1$  a marching scheme described next is used.

Regard the flow as determined for all columns up to  $\beta = \beta_n$  for all  $\zeta_k$  sections. We first indicate how the flow is determined at the body of the  $\beta_n$  column, denoted by  $a_1$  in Fig. 1. When integrating in the  $C$  direction as it explicitly appears in (18), we trace this near characteristic back to the  $\beta_{n-1}$  column, the point  $b_1$  in Fig. 1. Flow variables at  $b_1$  are found by a second order accurate interpolation scheme.  $\zeta$  derivatives are taken as the averages of the center differences at  $a_1$  and at  $b_1$ . All other equations are integrated by appropriate elementary grid points differences since they only involve  $\alpha$  and  $\beta$  derivatives. The values of the flow for the entire row  $\zeta_k$ ,  $k = 1, \dots$ , of body points are now iterated until a convergence criterion is met.

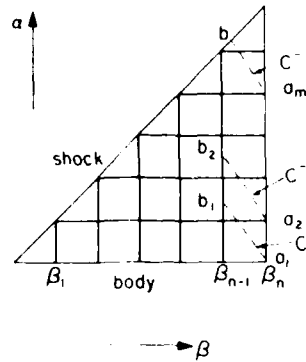


FIG. 1.  $(\alpha, \beta)$  coordinates.

Above the body, instead of the boundary conditions (14) (26) we have (14), (17). Again values for an entire row are iterated together. We proceed in this manner until the point  $a_m$  of Fig. 1 is reached. At this point the  $C^-$  near characteristic strikes the shock before hitting the  $\beta_{n-1}$  column. All remaining rows in  $\beta_n$  are now iterated simultaneously.

To consider stability denote the true Mach angle by  $\bar{\mu}$ . It then follows that

$$\sin^2 \bar{\mu} = \frac{a^2}{q^2 + w^2} = \frac{\sin^2 \mu}{1 + w^2}$$

and hence

$$\bar{\mu} \lesssim \mu.$$

At each constant  $\zeta$  plane, the true domain of dependence for the flow projected onto that plane lies inside the domain of dependence determined by the two near characteristics. As for the  $\zeta$  derivatives, let  $b$  in Fig. 2 be the point to be considered, and let  $\xi_1$  and  $\xi_2$  be the angles (in  $(x, r, \phi)$  space) between  $r_{ab}$  and  $r_n$  and between  $r_{ab}$  and  $r_{bd}$ . We want  $\xi_1 \geq \bar{\mu}$  and  $\xi_2 \geq \bar{\mu}$ . This requirement is easily satisfied unless the aspect ratio (the ratio of the largest to the smallest radius at the cross section) is large, in which case a smaller step size of  $\beta$  is required.

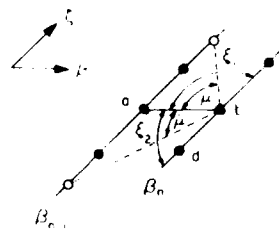


FIG. 2.  $(\beta, \zeta)$  coordinates with corresponding angular value in  $(x, r, \phi)$  space

Some mention of the calculation over a noncircular cone is ordered. Near the tip ( $0 \leq \beta \leq \beta_{1i}$ ) at each section  $\zeta = \zeta_k$ , we approximate the flow as being the flow over a circular cone with half angle  $\theta_k = \tan^{-1}(J'(\beta = \beta_{1i}, \zeta = \zeta_k))$ . We then compute the rest of the flow ( $\beta > \beta_{1i}$ ) by integrating the (nonaxisymmetric) equations using the numerical scheme described above. Note that flow over a noncircular cone is constant along the shock and the body at each section  $\zeta = \zeta_k$ . Hence we compute the flow along the  $\beta$  direction until this constancy condition is met within a prescribed error tolerance.

Since many of the steps in our procedure are iterative, a good first approximation can significantly accelerate convergence. To motivate our choice of a first approximation observe that (17), (18), and (21) differ from axisymmetric flow in the "second order" terms,

$$\omega^2, \quad \omega \frac{\partial}{\partial \phi}, \quad \frac{\partial \omega}{\partial \phi},$$

where as (19) indicates,  $\partial^2 \phi = O(\partial^2 \zeta)$ . Thus if a body can be regarded as locally axisymmetric taking the flow as axisymmetric should be an excellent approximation. In any case locally axisymmetric flow is the first approximation adopted by us.

#### 4. RESULTS AND DISCUSSIONS

For purposes of exposition we have performed calculations of flow over bodies with elliptical cross sections and azimuthal parabolic profiles. Relative few points, planes, and iterations are needed to compute the entire flow field.  $\phi = 0, \pi$  and  $\phi = \pi/2, 3\pi/2$  are planes of symmetry which are not assumed in the calculations, and are used as a check on the correctness of the results. Throughout the entire flow field, all grid points with such symmetry are found to have values in agreement within the same order of magnitude as the prescribed error tolerance.

Figure 3 shows the body and shock along the half planes  $\phi = 0$  and  $\phi = \pi$  for flow at  $M_0 = 2$  over a body with 30% thickness at  $\phi = 0$  and 20% thickness at  $\phi = \pi/2$ . To carry out this calculation we took 32 azimuthal sections each having 164 grid points, 20 on the body. The result of reducing the number of azimuthal planes to 16 is shown by x's and +'s. For calculations with the fine mesh size, the lines for  $\phi = 0$  and  $\phi = \pi$  are indistinguishable in this figure. For calculations with the coarse mesh size, + signifies a point at  $\phi = 0$  and x signifies a point at  $\phi = \pi$ . Each pair of + and x appearing together in the figure have the same values of  $\alpha$  and  $\beta$ , and hence they have the same flow values. Figure 4 shows the body and the shock for the same flow along  $\phi = \pi/4$  and  $\phi = 3\pi/4$ . Again, for calculations with the fine mesh size, the lines for the two half planes are indistinguishable. For calculations with the coarse mesh size, + signifies a point at  $\phi = \pi/4$ , and x signifies a point at  $\phi = 3\pi/4$ .

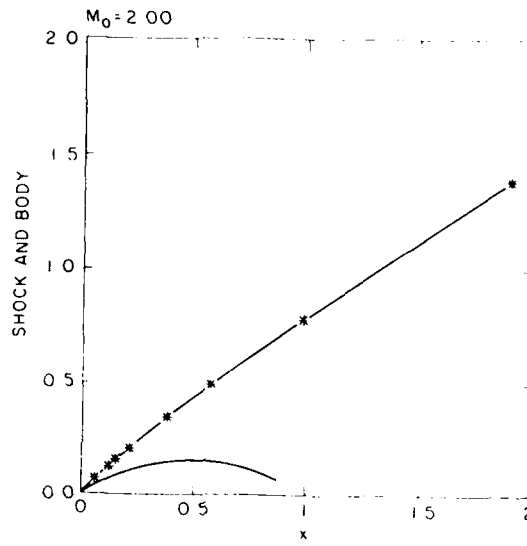


FIG. 3. Body and shock at  $\phi = 0(+)$  and at  $\phi = \pi(x)$ .

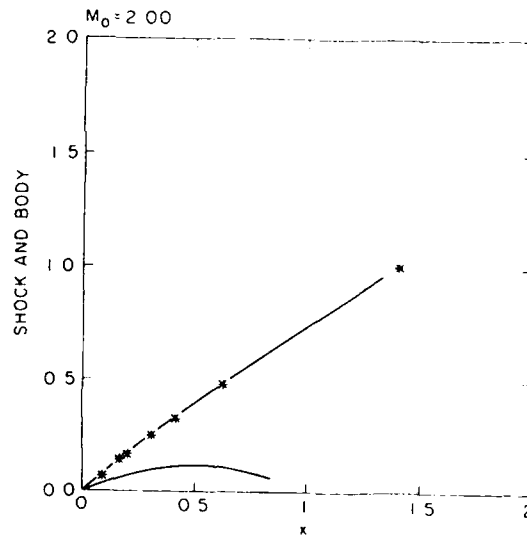


FIG. 4. Body and shock at  $\phi = \pi/4(+)$  and at  $\phi = 3\pi/4(x)$ .

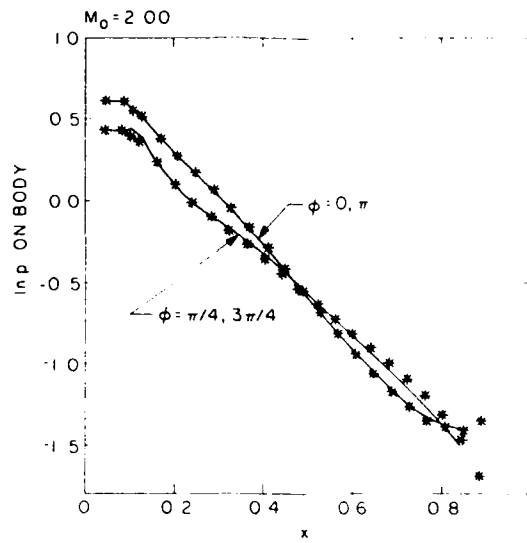


FIG. 5. Pressure distribution on the body. + is at  $\phi = 0$  or  $\pi/4$ ;  $\times$  is at  $\phi = 3\pi/4$  or  $\pi$ .

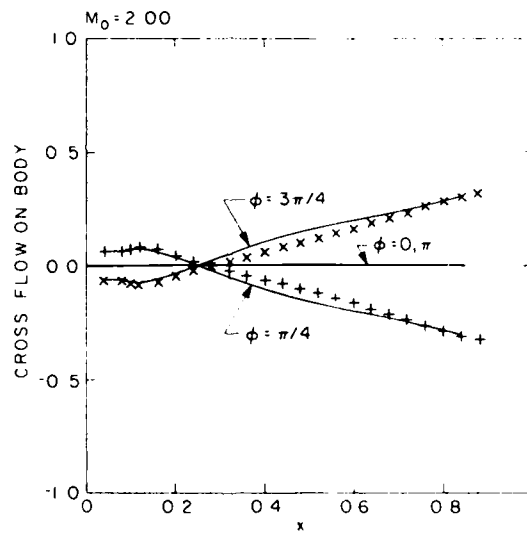


FIG. 6. Cross flow, normalized to  $(u^2 + v^2)^{1/2}$ , on the body

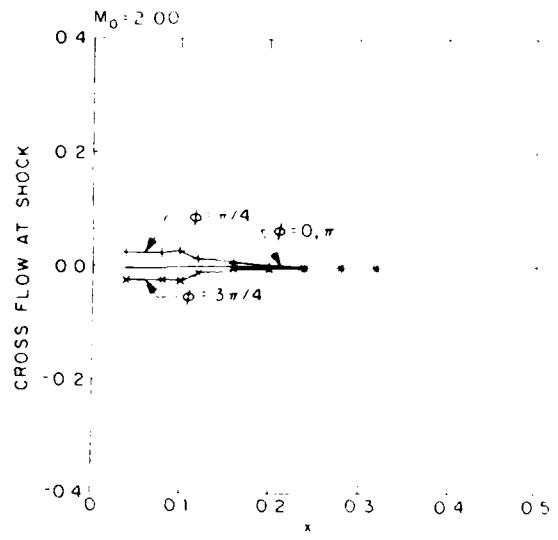


Fig. 7. Cross flow, normalized to  $(u^2 + v^2)^{1/2}$ , at the shock

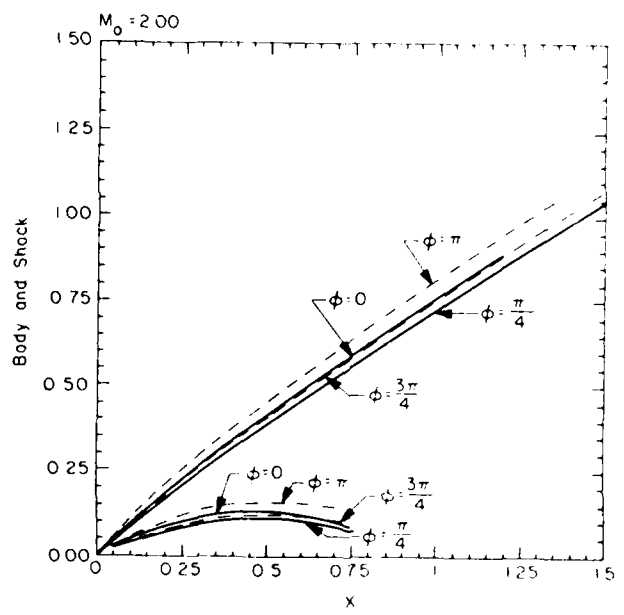


Fig. 8. Body and shock for flow at 2° angle of attack

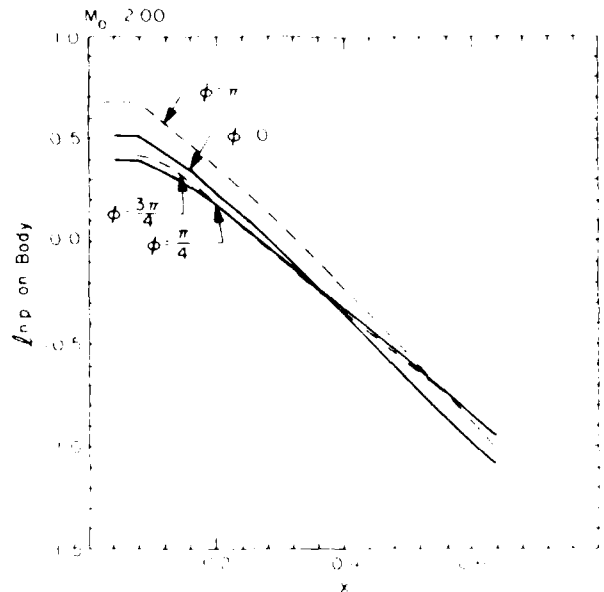


FIG. 9. Pressure distribution on the body for flow at 2 degree angle of attack.

with each pair of + and  $\times$  having the same  $\alpha$  and  $\beta$ . In these two figures, agreement is excellent with respect to both symmetry and the different grid sizes.

For the same flow, the pressure distribution on the body at  $\phi = 0, \pi/4, \pi, 3\pi/4$  is shown in Fig. 5. For  $\phi = 0, \pi$  the agreement is excellent. For  $\phi = \pi/4, 3\pi/4$  the agreement is good with respect to symmetry, but there is a small discrepancy between the coarse and the fine grid calculations. Since the grid size in the  $\zeta$  direction is quite large, about  $\pi/\delta$ , the discrepancy is certainly tolerable.

The cross flow on the body is given in Fig. 6. As the figure shows, the cross flow vanishes in the symmetry plane. At  $\phi = \pi/4, 3\pi/4$ , there is some discrepancy between the coarse and fine grid calculations due to the largeness of the  $\zeta$  grid size. Figure 7 shows that cross flow at the shock. The results are again quite good. Figures 8 and 9 show the same body at two degree angle of attack traveling at  $M_0 = 2$ .

As an indication of the computational speed, we mention that for the whole flow field, the time of a typical calculation is roughly 10 sec on an IBM 3081.

#### APPENDIX A. EQUATIONS IN NONAXISYMMETRIC FLOW

We wish to express the governing equations (1)–(7) in near characteristics form. Since  $\rho = \rho(p, S)$ , using (6) and (7), (1) becomes

$$\mathbf{u} \cdot \nabla p + \gamma p \nabla \cdot \mathbf{u} = 0 \quad (\text{A1})$$

Denote

$$\mathbf{q} = (u, v) \quad \text{and} \quad \nabla_2 = \left( \frac{\partial}{\partial x}, \frac{\partial}{\partial r} \right).$$

Then (2) and (3) become

$$\mathbf{q} \cdot \nabla_2 \mathbf{q} + \frac{1}{\rho} \nabla_2 p = \mathbf{f}, \quad (\text{A2})$$

where

$$\mathbf{f} = -\frac{w}{r} \frac{\partial}{\partial \phi} \mathbf{q} + \left( 0, \frac{w^2}{r} \right).$$

In a constant half-plane with  $\theta$  and  $\mu$  defined by (8) and (9), let  $\mathbf{t}(\theta)$  be the tangent, and  $\mathbf{n}(\theta)$  be the normal on the projected streamline. Denote  $s$  and  $n$  as the arc length and normal coordinate. Then (A1) becomes

$$q \frac{\partial p}{\partial s} + \gamma p \left( \frac{\partial q}{\partial s} + q \frac{\partial \theta}{\partial n} \right) = - \left( \frac{w}{r} \frac{\partial p}{\partial \phi} + \frac{\gamma p v}{r} + \frac{\gamma p}{r} \frac{\partial w}{\partial \phi} \right), \quad (\text{A3})$$

and (A2) becomes

$$q \frac{\partial q}{\partial s} + \frac{1}{\rho} \frac{\partial p}{\partial s} = \frac{-w}{r} \frac{\partial q}{\partial \phi} + \frac{w^2}{r} \sin \theta, \quad (\text{A4})$$

$$q^2 \frac{\partial \theta}{\partial s} + \frac{1}{\rho} \frac{\partial p}{\partial n} = \frac{-wq}{r} \frac{\partial \theta}{\partial \phi} + \frac{w^2}{r} \cos \theta, \quad (\text{A5})$$

Denote  $\sigma = \ln p$  and  $\omega = w/q$ . Rearranging (A3), (A4), and (A5),

$$\begin{aligned} \left( \frac{\partial \theta}{\partial s} \pm \frac{1}{(M_*^2 - 1)^{1/2}} \frac{\partial \theta}{\partial n} \right) \pm \frac{(M_*^2 - 1)^{1/2}}{\gamma M_*^2} \left( \frac{\partial \sigma}{\partial s} \pm \frac{1}{(M_*^2 - 1)^{1/2}} \frac{\partial \sigma}{\partial n} \right) \\ - F_1 \mp \frac{F_2}{(M_*^2 - 1)^{1/2}}, \end{aligned} \quad (\text{A6})$$

where  $F_1 = (\omega^2/r) \cos \theta - (\omega/r) \theta_\phi$ ,

$$F_2 = \frac{1}{r} \omega_\phi + \frac{\omega}{\gamma r} \sigma_\phi + \frac{\sin \theta}{r} (1 + \omega^2).$$

(A6) can then be written as

$$d_s \theta \pm \frac{\sin 2\mu}{2\gamma} d_s \sigma = \frac{F_1 \cos \mu \mp F_2 \sin \mu}{\sin(\theta \pm \mu)} d_s r, \quad (\text{A7})$$

where  $d_s$  is given in (12).

Rewriting (5), we have

$$\begin{aligned} a^2 &= \left(1 + \frac{\gamma-1}{2} (M_0^2 - w^2)\right) \left(1 + \frac{\gamma-1}{2} \frac{1}{\sin^2 \mu}\right) \\ &= \left(1 + \frac{\gamma-1}{2} M_0^2\right) \left(1 + \frac{\gamma-1}{2} \frac{1+w^2}{\sin^2 \mu}\right). \end{aligned} \quad (\text{A8})$$

Combining (6), (A8), and  $\rho = \gamma p/a^2$ , we then obtain (13). Rearranging (A8), we get

$$w^2 = \omega^2 \left(1 + \frac{\gamma-1}{2} M_0^2\right) \left(\sin^2 \mu + \frac{\gamma-1}{2} (1 + \omega^2)\right).$$

Now define

$$W = \ln \left(1 + \frac{\gamma-1}{2} (M_0^2 - w^2)\right). \quad (\text{A9})$$

Since the derivative of the Prandtl function is

$$P'(\mu) = \cos^2 \mu \left(\frac{\gamma-1}{2} + \sin^2 \mu\right),$$

using (13), (A7) becomes (11) with

$$G_1 = \omega \left(\omega - \frac{\theta_\phi}{\cos \theta}\right), \quad (\text{A10})$$

$$G_2 = \tan \mu \left(\omega^2 \tan \theta + \frac{\omega_\phi + (\omega/\gamma) \sigma_\phi}{\cos \theta}\right). \quad (\text{A11})$$

Next, we wish to express the entropy equation (7) in a form useful to us. (7) can be written as

$$(\mathbf{q} \cdot \nabla_s) S + \frac{w}{r} \frac{\partial S}{\partial \phi} = 0.$$

In the natural coordinates  $s$  and  $n$ , this becomes

$$q \frac{\partial S}{\partial s} = \frac{w}{r} \frac{\partial S}{\partial \phi}. \quad (\text{A12})$$

If we define  $(\alpha, \beta, \zeta)$  by (14) and use the fact that  $s$  is the arc length, we get

$$\frac{\partial}{\partial s} = \frac{1}{(x_\mu^2 + r_\mu^2)^{1/2}} \frac{\partial}{\partial \beta} = \frac{1}{x_\mu (1 + \tan^2 \theta)^{1/2}} \frac{\partial}{\partial \beta} = \frac{\cos \theta}{x_\mu} \frac{\partial}{\partial \beta}. \quad (\text{A13})$$

(A12) then becomes (21).

Now we give a similar treatment for the  $\phi$  momentum equation (4). This can be written as

$$(\mathbf{q} \cdot \nabla_2) w + \frac{\gamma p}{\rho} \frac{1}{\gamma r p} \frac{\partial p}{\partial \phi} = \frac{-w}{r} \frac{\partial w}{\partial \phi} - \frac{r w}{r}$$

In natural coordinates, this becomes

$$q \frac{\partial q \omega}{\partial s} + \frac{a^2}{\gamma r} \frac{\partial \sigma}{\partial \phi} = \frac{-q \omega}{r} \frac{\partial q \omega}{\partial \phi} - q^2 \frac{\omega \sin \phi}{r}$$

Using (A4) and (A13), this then becomes (22).

APPENDIX B. COORDINATE TRANSFORMATION

For  $x = x(\alpha, \beta, \zeta)$ ,  $r = r(\alpha, \beta, \zeta)$ ,  $\phi = \phi(\alpha, \beta, \zeta)$ , using the chain rule we obtain

$$\begin{pmatrix} x_\alpha & x_\beta & x_\zeta \\ r_\alpha & r_\beta & r_\zeta \\ \phi_\alpha & \phi_\beta & \phi_\zeta \end{pmatrix} \begin{pmatrix} \alpha & \beta & \zeta \\ \alpha_\phi & \beta_\phi & \zeta_\phi \end{pmatrix} = I$$

Since  $\phi = \zeta$ , and  $\phi_\alpha = \phi_\beta = 0$ ,  $\phi_\zeta = 1$ ,

$$\begin{pmatrix} \alpha & \beta & \zeta \\ \alpha_\phi & \beta_\phi & \zeta_\phi \end{pmatrix} = \frac{1}{D} \begin{pmatrix} r_\beta & -x_\beta & 0 \\ -r_\alpha & x_\alpha & 0 \\ 0 & 0 & D \end{pmatrix} \begin{pmatrix} 1 & 0 & -x_\zeta \\ 0 & 1 & -r_\zeta \\ 0 & 0 & 1 \end{pmatrix}$$

where

$$D = x_\alpha r_\beta - r_\alpha x_\beta = (\tan \theta - \tan(\theta + \mu)) x_\alpha x_\beta$$

Then

$$\begin{aligned} \frac{\partial}{\partial x} &= \alpha_\phi \frac{\partial}{\partial \alpha} + \beta_\phi \frac{\partial}{\partial \beta} = \frac{1}{D} \left( r_\beta \frac{\partial}{\partial \alpha} - r_\alpha \frac{\partial}{\partial \beta} \right), \\ \frac{\partial}{\partial r} &= \alpha_r \frac{\partial}{\partial \alpha} + \beta_r \frac{\partial}{\partial \beta} = \frac{1}{D} \left( -x_\beta \frac{\partial}{\partial \alpha} + x_\alpha \frac{\partial}{\partial \beta} \right), \\ \frac{\partial}{\partial \phi} &= \alpha_\phi \frac{\partial}{\partial \alpha} + \beta_\phi \frac{\partial}{\partial \beta} + \zeta_\phi \frac{\partial}{\partial \zeta} \\ &= \frac{(r_\beta x_\alpha + x_\beta r_\alpha)(\partial/\partial \alpha) + (r_\alpha x_\beta - x_\alpha r_\beta)(\partial/\partial \beta)}{D} + \frac{\partial}{\partial \zeta} \\ &= \frac{(r_\beta - \tan \theta x_\alpha) x_\beta (\partial/\partial \alpha) + (\tan(\theta + \mu) x_\alpha - r_\alpha) x_\alpha (\partial/\partial \beta)}{D} + \frac{\partial}{\partial \zeta} \end{aligned}$$

## REFERENCES

1. M. HOLT, *Numerical Methods in Fluid Dynamics*, 2nd ed (Springer Verlag, New York, 1984).
2. R. PIVRELLI AND T. TAYLOR, *Computational Methods for Fluid Flow* (Springer Verlag, New York, 1983).
3. R. RICHMYER AND K. MORTON, *Difference Method for Initial Value Problem*, 2nd ed (Wiley, New York, 1967).
4. M. CUSI AND J. HOFFMAN, *AIJA J.* **10**, 1452 (1972).
5. F. MARCONI, M. SALAS, AND L. YAIGER, NASA CR 2675, 1976 (unpublished).
6. G. MORELLI, B. GROSSMAN, AND F. MARCONI, *AIJA Paper* 72 (1972).
7. K. BABINSKO, G. VOSKRESENSKII, A. LYUBIMOV, AND V. RUSANOV, NASA TTF 380, 1968, (unpublished).
8. C. FERRARI, *J. Aero Sci.* **16**, 411 (1949).
9. R. SAUER, *Numerische Mathematik* **5**, 55 (1963).
10. A. FERRI, *General Theory of High Speed Aerodynamics*, VI (Princeton Univ. Press, Princeton, N.J., 1954).
11. G. MORELLI, *AIJA J.* **1**, 2192 (1963).
12. J. RAKICH, NASA TN D 5341, 1969, (unpublished).
13. I. LEWIS AND I. SIROVICH, *J. Fluid Mech.* **112**, 265 (1981).
14. J. FONG AND I. SIROVICH, *AIJA J.* (May 1986).
15. M. LILPMANN AND A. ROSHKO, *Elements of Gasdynamics* (Wiley, New York, 1957), p. 85.

# Exact and Approximate Gas Dynamics Using the Tangent Gas

PRABIR K. DARIPA\*

*Division of Engineering, Brown University, Providence, Rhode Island 02912*

AND

LAWRENCE SIROVICH

*Division of Applied Mathematics, Brown University, Providence, Rhode Island 02912*

Received November 13, 1984; revised March 1, 1985

Steady, inviscid, irrotational flow of a perfect gas in two dimensions is considered in the tangent gas approximation. A fast and accurate method of solution is proposed and solved numerically. Comparison of tangent gas and exact flows are presented. Tangent gas solutions when used as the first step in the iterative solution of the exact flowfield are shown to give substantial reduction in computational time. © 1986 Academic Press, Inc.

## 1. INTRODUCTION

The computation of steady flow past an airfoil is crucial to the determination of aerodynamic characteristics such as lift, drag and moment coefficients. In many instances potential theory suffices. Neglecting viscosity it is exact for shockless flow and is a satisfactory approximation for transonic flow with weak shocks. For two dimensions the calculations are usually carried out in a conformally mapped plane, an approach used by Sells [1], Garabedian and Korn [2], and Jameson [3]. Similar techniques have been used for multi-element airfoils [4, 5] and nacelles [6]. Three dimensional potential theory has been treated by Caughey [7].

Since the equations are nonlinear, the potential equation is usually solved iteratively. In some instances the potential equation does not admit unique solutions [8-10] and in addition becomes a poor approximation for increasingly strong shock strengths. As a result more recent investigations treat the full Euler equations. Finite difference and finite volume methods have been successfully implemented by Jameson [11] and Lerat and Sides' [12]. Because of slow rates of convergence considerable effort has been directed towards accelerating these methods [13]. Convergence rates depend on factors such as the grid, initial guess, time stepping scheme and method of solution.

\* Present address: Courant Institute of Mathematical Sciences, 251 Mercer Street, New York, N.Y. 10012.

In this paper we present a set of flow dependent grid systems and initial flowfield guesses which substantially improve convergence rates when applied to the Euler equations for flows past an airfoil. These are based on solution of the tangent gas equations introduced by Chaplygin [14] and further developed by von Kármán and Tsien [15, 16].

Woods [17], who extensively studied these equations, proposed certain iterative methods for solving both the analysis and design problems for flows past an airfoil. The methods developed in this paper are substantially different and offer a method for a fast and accurate solution to a problem. (We have also addressed the inverse problem and presented an exact method for its solution [18].)

As will be seen the tangent gas solution lies close to the Euler solution even for high subcritical flows. This is used as a basis for iterative solution of Euler equation for flows past an airfoil by means of FLO52S (written by A. Jameson, E. Turkel and M. Salas). The grid used is the natural one generated by the tangent gas equations and the starting guess is the tangent gas solution. As will be seen this results in substantial computational reduction even for supercritical flows.

## 2. BASIC EQUATIONS

Consider steady, inviscid, irrotational flow of a perfect gas in two dimensions, then in the usual notation

$$\nabla \cdot (\bar{\rho} \bar{q}) = 0, \quad \nabla \times \bar{q} = 0, \quad p/\rho^\gamma = 1. \quad (1)$$

The variables are normalized by their free stream values and linear dimensions by an appropriate lengthscale.

The stream function  $\psi$  and potential  $\phi$  are introduced in the usual way

$$\bar{\rho} \bar{q} = c \nabla \times (\psi \mathbf{k}), \quad \bar{q} = \nabla \phi, \quad (2)$$

where  $\mathbf{k}$  denotes a vector perpendicular to the plane of motion. The constant  $c$  has been introduced for later purposes.

If  $s$  and  $n$  are local distances along streamlines and potential lines, respectively, (2) can be written as

$$ds + i dn = \frac{1}{q} \left( d\phi + i \frac{c}{\rho} d\psi \right). \quad (3)$$

If equations can be derived that map the space of  $\phi, \psi$  on to the space of the velocity magnitude and direction  $(q, \theta)$ , then one can take advantage of the fact that the tangent of the flow direction,  $\tan \theta$ , is the same as the slope of the airfoil surface where  $\psi = 0$ . Then if  $q$  vs.  $\theta$  can be found corresponding to  $\psi = 0$  on  $\phi, \psi$

plane, the state of flow on the airfoil surface will be known. Toward this end, we write Eq. (3) alternatively as

$$dz = dx + i dy = \frac{c^m}{q} \left( d\phi + i \frac{c}{\rho} d\psi \right), \quad (4)$$

where  $x, y$  are cartesian coordinates and  $\theta$  flow direction angle. With  $q$  and  $\theta$  as independent variables, it is easy to derive from (4)

$$\phi_\theta = \frac{q}{\rho} c \psi_q, \quad \phi_q = -\frac{1-M^2}{\rho q} c \psi_\theta. \quad (5)$$

If dependent and independent variables are interchanged and the Prandtl Meyer function

$$v = \int_1^q \sqrt{|1-M^2|} \frac{dq}{q} \quad (6)$$

is introduced in place of  $q$ , then

$$\theta_\psi + \frac{1}{K(v)} v_\psi = 0, \quad \theta_v \pm K(v) v_\theta = 0. \quad (7)$$

The  $\pm$  sign refers to subsonic and supersonic conditions, respectively and

$$K(v) = \beta \frac{c}{\rho(q(M))}, \quad \beta^2 \quad (8)$$

where

$$\beta^2 = |1-M^2|. \quad (9)$$

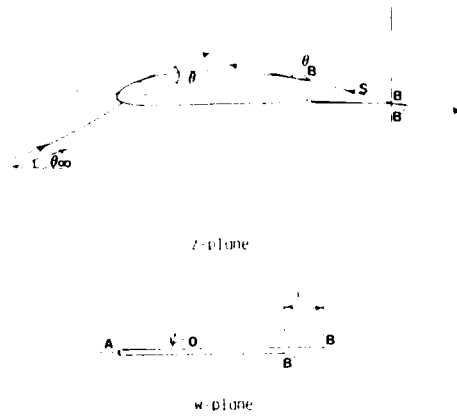
Typical physical  $z (= x + iy)$  and potential  $w (= \phi + i\psi)$  planes are shown in Fig. 1. The airfoil maps into a slit in the  $w$ -plane. The gap  $BB'$  in the potential plane corresponds to  $\Gamma$ , where circulation about the airfoil is  $-\Gamma$ .

The system (7) should be solved subject to the density speed relation obtained from (1) and Bernoulli's relation

$$\frac{q^2}{2} + \frac{1}{\gamma M^2} \int \frac{dp}{\rho} = \text{constant}. \quad (10)$$

### 3. TANGENT GAS APPROXIMATION

Equations (7) are nonlinear and are therefore difficult to solve. A good approximation to those equations under certain conditions can be obtained by

FIG. 1. Airfoil in physical  $z$ -plane and potential  $w$ -plane.

introducing the so-called "tangent gas approximation" [17], in which the isentropic relation between  $p$  and  $\rho$  given in Eq. (1) is replaced by a tangent to the curve of  $p$  vs.  $1/\rho$ . This approximation is then given by

$$(p-1) = \gamma \left( 1 - \frac{1}{\rho} \right). \quad (11)$$

From (10) we obtain

$$\rho = \beta / \beta_{\infty}. \quad (12)$$

With the constant  $c$  in (8) taken as

$$c = 1/\beta_{\infty}, \quad (13)$$

we obtain from (8)

$$K(v) = 1. \quad (14)$$

Then for subsonic flow (7) becomes the Cauchy Riemann equations

$$\theta_{\phi} - v_{\psi} = 0, \quad \theta_{\psi} + v_{\phi} = 0. \quad (15)$$

Equations (15) are exact for the tangent gas and also for incompressible flow ( $M=0$ ). In addition, it will be seen that it can be a very good approximation to the original equations. In the above formulation the tangency point has been taken to the freestream

$$p_{\infty} = 1, \quad \rho_{\infty} = 1. \quad (16)$$

With this selection of tangency point the following relations hold for the tangent gas [17]

$$q = \sinh v^* \operatorname{cosech}(v^* - v), \quad \beta = \tanh(v^* - v), \quad c_p = \frac{2}{1 - \beta} \coth v, \quad (17)$$

where the constant  $v^*$  is given by

$$v^* = \ln \left( \frac{M_\infty}{1 - \beta_\infty} \right). \quad (18)$$

From (6) it is seen that  $v_r = 0$  and at stagnation points (denoted by zero subscript)

$$v_0 = -\alpha, \quad c_{p,0} = \frac{2}{1 + \beta_\infty} \quad (19)$$

#### 4. SOLUTION PROCEDURE

It follows from (15) that

$$\tau = -v + i\theta \quad (20)$$

is an analytic function of  $w$ . It will be useful to map the  $w (= \phi + i\psi)$  plane onto the plane of a new variable  $\sigma = |\sigma| e^{i\alpha}$  such that the body in the  $w$ -plane which is a slit (a part of the line  $\psi = 0$ ) maps onto the unit circle  $\sigma = e^{i\alpha}$ ;  $0 \leq \alpha \leq 2\pi$  and the rest of the  $w$ -plane maps onto the exterior of the unit circle. This is accomplished by

$$w = a(\sigma e^{-i\alpha_0} + \sigma^{-1} e^{i\alpha_0}) + i2a \sin \alpha_0 \ln(\sigma e^{-i\alpha_0}) \quad (21)$$

which allows for angle of attack and circulation about an airfoil surface, to be related to  $|\sigma| = 1$ . Circulation  $-\Gamma$  is related to the constant  $a$  by

$$\Gamma = 4\pi a \sin \alpha_0. \quad (22)$$

Here constants  $a$  and  $\alpha_0$  are as yet unknowns.

From (21) one obtains

$$\frac{dw}{d\sigma} = -ae^{i\alpha_0}(1 - \sigma^{-1})(e^{-i\alpha_0} - \sigma^{-1}). \quad (23)$$

On the body  $\sigma = e^{i\alpha}$ ;  $0 \leq \alpha \leq 2\pi$ ,  $\phi$  and  $\psi$  are given by

$$\phi(\alpha) = 2a[\cos(\alpha - \alpha_0) - (\alpha - \alpha_0) \sin \alpha_0], \quad \psi(\alpha) = 0. \quad (24)$$

$\alpha$ , in (23) is given by

$$\alpha_s = \pi + 2\alpha_0. \quad (25)$$

Thus the rear and front stagnation points map into  $\sigma = 1$  and  $\sigma = e^{i\alpha}$ , respectively.

Since  $\tau$  is an analytic function of  $\sigma$ , a convenient representation of  $\tau(\sigma)$  is given by (see also Ref. [19])

$$\exp(\tau(\sigma)) = (1 - \sigma^{-1})^{-\delta} (e^{-i\alpha} - \sigma^{-1})^{-1} \exp\left(\sum_{n=0}^{\infty} c_n \sigma^{-n}\right), \quad (26)$$

where  $\delta = \theta_t/\pi$ ,  $\theta_t$  the trailing edge angle. The complex constants  $c_n$  are represented by,

$$c_n = A_n + iB_n. \quad (27)$$

Note that (26) contains the Kutta condition. Two Schwarz Christoffel factors appear in (26) because of the discontinuity in  $\theta$  at the two stagnation points.

From (26) the relationship between upstream flow direction  $\theta_\infty$  and  $\alpha_0$  is given by

$$\theta_\infty = B_0 + \pi + 2\alpha_0. \quad (28)$$

The free stream condition is given by

$$A_0 = 0. \quad (29)$$

On the unit circle, (26) reduces to

$$\exp(\tau(e^{i\alpha})) = G(\alpha) e^{m(\alpha)} \exp\left(\sum_{n=0}^{\infty} c_n e^{-in\alpha}\right), \quad (30)$$

where

$$G(\alpha) = \left|2 \sin \frac{\alpha}{2}\right|^{-\delta} |2(\sin \alpha_0 + \sin(\alpha - \alpha_0))|^{-1}, \quad (31)$$

$$\eta(\alpha) = \frac{1}{2}(1 - \delta)(\pi - \alpha) + \left(\alpha + \frac{\pi}{2}\right) - \pi U(\alpha - \alpha_0) + \alpha_0. \quad (32)$$

$U(\alpha - \alpha_0)$  in (32) is the unit step function. The tangent angle  $\theta_B$  of the body is related to  $\theta$  by

$$\theta(\alpha) = \theta_B(\alpha) - \pi - \pi U(\alpha - \alpha_0). \quad (33)$$

Separation of (30) into real and imaginary parts leads to

$$\tilde{v}(\alpha) = \sum_{n=0}^{\infty} (A_n \cos n\alpha + B_n \sin n\alpha) \quad (34)$$

$$\tilde{\theta}(\alpha) = \sum_{n=0}^{\infty} (B_n \cos n\alpha - A_n \sin n\alpha) + \pi + \alpha_0 \quad (35)$$

where

$$\bar{v}(\alpha) = -v(\alpha) - \ln G(\alpha), \quad (36)$$

and

$$\bar{\theta}(\alpha) = \theta_B(\alpha) - \frac{1}{2} (1 - \delta)(\pi - \alpha) - \left( \alpha + \frac{\pi}{2} \right). \quad (37)$$

The closure condition of the airfoil is related to the leading terms of the series by (Appendix A).

$$A_1 = (1 - \delta) - (1 - \beta_r) 2 \sin^2 \alpha_0, \quad (38)$$

$$B_1 = (1 - \beta_r) \sin 2\alpha_0. \quad (39)$$

### 5. ANALYSIS (DIRECT) PROBLEM

Here the flow past an airfoil is sought. An iterative method of solution similar to the one for incompressible flow (15) is found to converge with good accuracy. The method of solution goes as follows.

An initial estimate of arclength as a function of circle angle,  $s(\alpha)$ , (e.g., of a flat plate in incompressible flow) is made. From the given contour  $\theta_B(s)$ ,  $\theta_B(\alpha)$  is estimated and  $\bar{\theta}(\alpha)$  is calculated from (37).  $\alpha_0$  is obtained from (28). After the closure conditions (38) and (39) are imposed, a new form of  $\bar{\theta}(\alpha)$  is generated and then its conjugate  $\bar{v}(\alpha)$  is obtained from (34).  $v(\alpha)$  is then obtained from (36) and speed  $q(\alpha)$  is obtained from (17). The updated value of  $s(\alpha)$  is now obtained from  $q(\alpha)$  using the relation

$$\begin{aligned} s(\alpha) &= \int_0^\alpha \frac{1}{q} \frac{|d\phi|}{d\alpha} d\alpha \\ &= 2a \int_0^\alpha \frac{|\sin \alpha_0 + \sin(\alpha - \alpha_0)|}{q} d\alpha, \end{aligned} \quad (40)$$

where the constant  $a$  is now given by

$$s(2\pi) = l. \quad (41)$$

The above procedure is repeated until convergence is obtained. The criterion for convergence was taken to be that maximum difference in arc-length between successive iterations be  $O(10^{-6})$ . Typically the number of iterations required was no more than eight and the computation time was roughly one second on an IBM 3081 with 128 points taken on the unit circle. The actual numerical calculation is facilitated through the use of the fast fourier transform (FFT) and the fact that (34) and (35) are conjugate fourier series. The fourier constants,  $c_n$ , are also obtained easily during FFT which are used for generating grids.

## 6. GRID GENERATION

The physical plane is related to the circle plane through [17]

$$dz = \frac{1}{2\beta_x} \left\{ (1 + \beta_x) e^{\tau} \frac{dw}{d\sigma} d\sigma - (1 - \beta_x) e^{-\tau} \overline{\frac{dw}{d\sigma}} d\sigma \right\} \quad (42)$$

Here an overbar denotes complex conjugate. Note that for incompressible flow  $z$  is an analytic function of  $\sigma$ , as it should be.

From (21) and (26) it is easily seen that

$$e^{\tau} \frac{dw}{d\sigma} = -ae^{-i\alpha_0} (1 - \sigma^{-1})^{1-\delta} \exp\left(\sum_{n=0}^{\infty} c_n \sigma^{-n}\right), \quad (43)$$

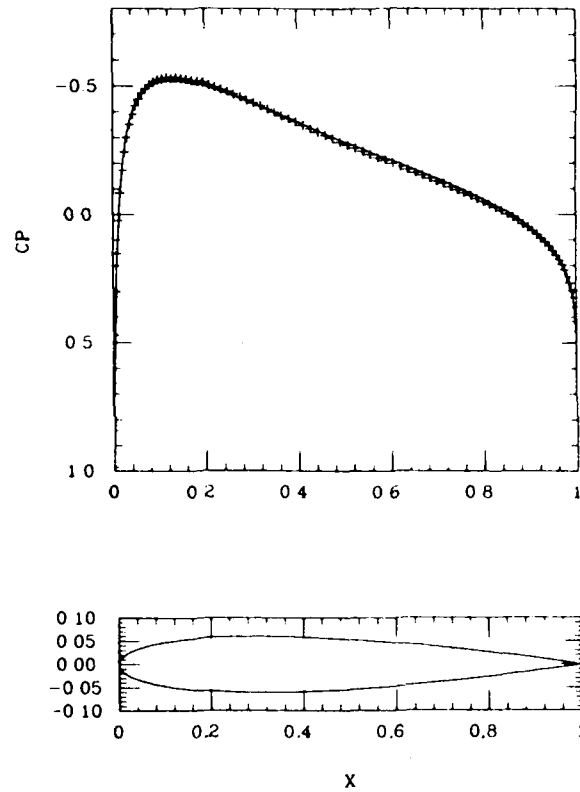


FIG. 2. Comparison of tangent gas solution and Euler solution over NACA 0012 Airfoil at Mach = 0.6 and angle of attack = 0.0. —, tangent gas solution; + + +, Euler solution.

and

$$e^{-\tau} \frac{dw}{d\sigma} = -ae^{i\alpha_0}(1-\sigma^{-1})^{1+\delta}(e^{i\alpha_1}-\sigma^{-1})^2 \exp\left(-\sum_{n=0}^{\infty} c_n \sigma^{-n}\right). \quad (44)$$

Equations (42), (43) and (44) are used to map the circle plane into physical plane and the flowfield variables are obtained from (26), (17), and (18).

Observe that the grid generated is flow dependent. Since the mapping from  $\sigma$  plane to  $z$ -plane is not conformal except when  $M=0$ , the grid generated in physical plane is not in general orthogonal. The grid produced by this method appears to be more natural than the incompressible conformal grid.

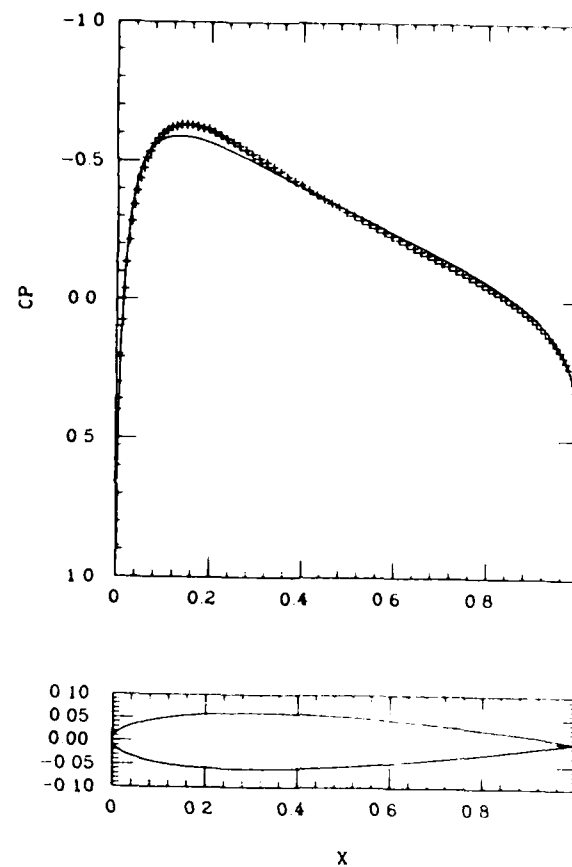


FIG. 3. Comparison of tangent gas solution and Euler solution over NACA 0012 Airfoil at Mach 0.7 and angle of attack = 0.0. —, tangent gas solution; + + +, Euler solution.

## 7. RESULTS

Figures 2-5 compare the tangent gas solution with the converged Euler solution (as calculated by FLO52S). The tangent gas solution is seen to be remarkably accurate even at the near critical case depicted in Fig. 3 and the slightly critical case shown in Fig. 4. Even when a clear shock is present as in Fig. 5, the tangent gas solution only fails in a relatively small neighborhood of the shock.

Figures 6 and 7 indicate for two typical cases the number of iterative cycles to achieve a convergence criterion. The criterion used is the enthalpy error introduced by Jameson [20]. In each figure we indicate the number iterations required to reach the indicated criterion. The first column of each figure refers to use of the tangent gas grid and the tangent gas solution as a starting flow. The second column

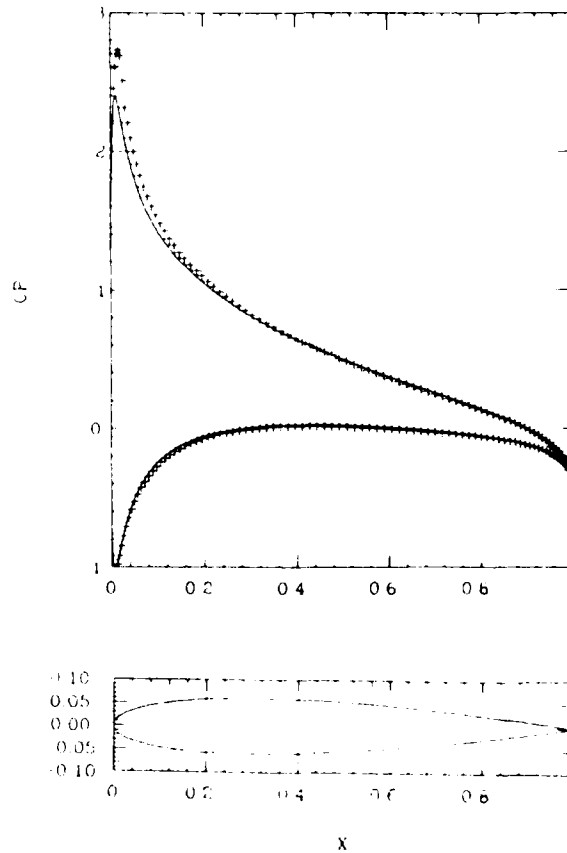


FIG. 4. Comparison of tangent gas solution and Euler solution over NACA 0012 Airfoil at Mach = 0.50 and angle of attack = 5.0 degrees. —, tangent gas solution, + + +, Euler solution.

gives the analogous values using the conventional grid, viz., that generated by conformal mapping and a uniform flowfield as the starting guess. (Little change in convergence was observed if incompressible flow was taken as the initial guess.) As is seen the reduction in cycles is substantial. In this same vein if the convergence criterion is reduced by a factor of 10 the comparison becomes more dramatic the tangent gas approach leads to a 10-fold reduction in cycles over the usual approach.

In order to distinguish whether the grid or the tangent gas approximation was more significant in speeding convergence, we also ran the programs using the tangent gas grid with a uniform first guess. Although some improvement resulted, the clear implication from this was that the tangent gas solution as a first guess was the most important factor.

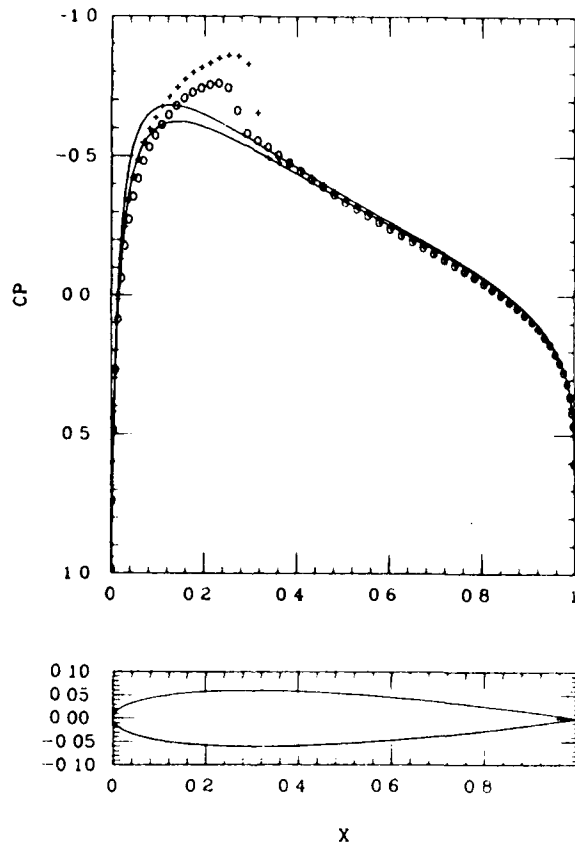


FIG. 5. Comparison of tangent gas solution and Euler solution over NACA 0012 Airfoil at Mach = 0.758 and angle of attack = 0.14 degrees. —, tangent gas solution; (+, o) Euler solution; +, upper surface; o, lower surface.

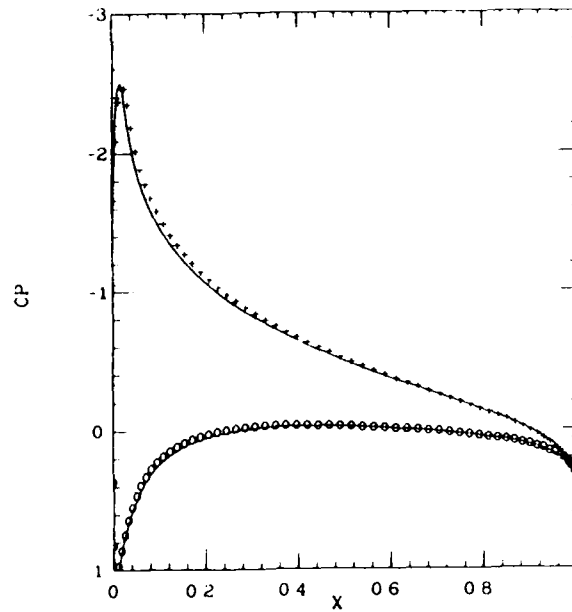


FIG. 6. Euler solution (FLO52S) for near critical flow past an NACA 0012 Airfoil at Mach 0.50 and angle of attack = 5.0 degrees. (+, O): grid, 64\*32; grid type, tangent; initial guess, tangent; number of cycles, 344. (—): grid, 64\*32; grid type, conformal; initial guess, uniform; number of cycles 913. Average error in enthalpy, 0.1385E-03. +, upper surface; O, lower surface.

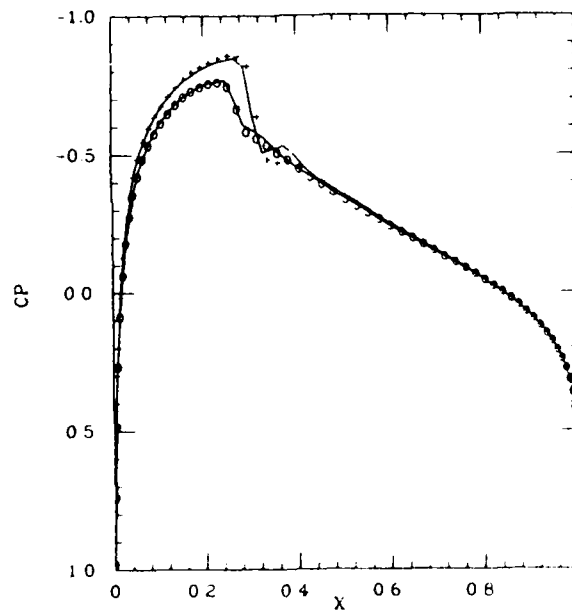


FIG. 7. Euler solution (FLO52S) for supercritical flow past an NACA 0012 Airfoil at Mach 0.758 and angle of attack = 0.14 degrees. (+, O): grid, 64\*32; grid type, tangent; initial guess, tangent; number of cycles, 381. (---): grid, 64\*32; grid type, conformal; initial guess, uniform; number of cycles, 715. Average error in enthalpy, 0.2454E-03. +, upper surface; O, lower surface.

## APPENDIX A: CLOSURE CONDITIONS

If  $C$  is a closed contour around an airfoil, the the closure condition is

$$\oint_C dz = 0. \quad (\text{A1})$$

Hence from (42) we obtain (see also Ref. [17])

$$(1 + \beta_x) \oint_C e^\tau \frac{dw}{d\sigma} d\sigma = (1 - \beta_x) \overline{\oint_C e^{-\tau} \frac{dw}{d\sigma} d\sigma}. \quad (\text{A2})$$

From (43) and (44) it follows

$$e^\tau \frac{dw}{d\sigma} = -ae^{i(\beta_0 + \alpha_0)} \left[ 1 + \frac{K_1}{\sigma} + O(\sigma^{-2}) \right] \quad (\text{A3})$$

$$e^{-\tau} \frac{dw}{d\sigma} = +ae^{i(\alpha_0 - \beta_0)} \left[ -e^{-2i\alpha_0} + \frac{K_2}{\sigma} + O(\sigma^{-2}) \right] \quad (\text{A4})$$

where

$$K_1 = c_1 + \delta - 1, \quad K_2 = (1 + \delta + c_1) e^{-2i\alpha_0} + 2e^{-i\alpha_0}. \quad (\text{A5})$$

Use of residue theorem, (A3) and (A4) reduces (A2) to

$$(1 + \beta_x) e^{i\alpha_0} K_1 = (1 - \beta_x) e^{-i\alpha_0} \bar{K}_2. \quad (\text{A6})$$

Equating real and imaginary parts we obtain

$$(A_1 + \delta - 1) \cos \alpha_0 = B_1 \sin \alpha_0, \quad (A_1 + \delta + 1 - 2\beta_x) \sin \alpha_0 = B_1 \cos \alpha_0. \quad (\text{A7})$$

From (A7) we obtain

$$A_1 = (1 - \delta) - (1 - \beta_x) 2 \sin^2 \alpha_0, \quad B_1 = (1 - \beta_x) \sin 2\alpha_0. \quad (\text{A8})$$

For the incompressible case ( $\beta_x = 1$ ) this reduces to

$$A_1 = (1 - \delta), \quad B_1 = 0. \quad (\text{A9})$$

## ACKNOWLEDGMENTS

This research was supported by the National Aeronautics and Space Administration under Grant NSG-1617 and the Air Force Office of Scientific Research under Grant AFOSR-83-0336. The authors would also like to thank the reviewers for helpful criticism.

## REFERENCES

1. C. C. L. SELLS, *Proc. R. Soc. A* **308** (1968), 377-401.
2. P. R. GARABEDIAN AND D. G. KORN, *Comm. Pure Appl. Math.* **24** (1971), 841-851.
3. A. JAMESON, in "Proceedings, AIAA 2nd Computational Fluid Dynamics Conf., Hartford, Connecticut, 1975," pp. 148-161.
4. B. GROSSMAN AND R. E. MELNIK, in "Proceedings, Fifth International Conference on Numerical Methods in Fluid Dynamics," Lecture Notes in Physics Vol. 59, pp. 220-227. Springer-Verlag, Berlin, 1976.
5. D. C. IVES AND J. F. LUITERMOZA, *AIAA J.* **15** (1977), 647-657.
6. B. G. ARLINGER, *AIAA J.* **13** (1975), 1614-1621.
7. D. A. CAUGHY, in "Transonic Shock and Multidimensional Flows: Advances in Scientific Computing" (R. E. Meyers, Ed.), pp. 71-105, Academic Press, New York/London, 1982.
8. J. STEINHOFF AND A. JAMESON, in "Proceedings, AIAA 5th Computational Fluid Dynamics Conference, Palo Alto, Calif., June 1981," pp. 317-353.
9. M. D. SALAS, A. JAMESON, AND R. E. MELNIK, in "Proceedings, AIAA 7th Computational Fluid Dynamics Conference, June 1983," pp. 48-60.
10. P. EMID, J. GOODMAN, AND A. MAJDA, *SIAM J. Sci. Statist. Comput.* **5**, No. 1 (1984).
11. A. JAMESON AND D. A. CAUGHY, in "Proceedings, Third AIAA Conference on Computational Fluid Dynamics, Albuquerque, 1977."
12. A. LERAT AND J. SIDES, in "Numerical Methods for Aeronautical Fluid Dynamics," (P. I. Roe, Ed.), pp. 245-288, 1982.
13. E. TURKEL, "Fast Solutions to the Steady State," ICASE Report No. 84-28, June 1984.
14. S. A. CHAPLYGIN, "On Gas Jets," NASA Technical Memorandum No. 1063 (1944).
15. VON KÄRMÁN, *J. Aero. Sci.* **8** (1941), 337-356.
16. H. S. TSIEN, *J. Aero. Sci.* **6** (1939), 399-407.
17. L. C. WOODS, "The Theory of Subsonic Plane Flow," Cambridge Univ. Press, London-New York, 1961.
18. P. K. DARIPA AND L. SIROVICH, *J. Comput. Phys.* **62** (1986), in press.
19. F. BAUER, P. R. GARABEDIAN, AND D. G. KORN, "Supercritical Wing Sections II," Lecture Notes in Economics and Mathematical Systems Vol. 108, Springer-Verlag, Berlin/New York/Heidelberg, 1975.
20. A. JAMESON, in "Transonic Shock and Multidimensional Flows: Advances in Scientific Computing," (R. E. Meyer, Ed.), pp. 37-70, Academic Press, New York/London, 1982.

# An Inverse Method for Subcritical Flows

PRABIR K. DARIPA\*

*Division of Engineering, Brown University, Providence, Rhode Island 02912*

AND

LAWRENCE SIROVICH

*Division of Applied Mathematics, Brown University, Providence, Rhode Island 02912*

Received December 13, 1984; revised March 29, 1985

The inverse problem in the tangent gas approximation is considered. An exact method for designing airfoils is presented. Constraints on the speed distribution are easily implemented. A simple numerical algorithm which is fast and accurate is presented. Comparison of designed airfoils using the tangent gas method with exact Euler results is found to be excellent for subcritical flows. © 1986 Academic Press, Inc.

## 1. INTRODUCTION

As is well known (see [1]) certain types of pressure distributions achieve aerodynamically desirable features such as delay of transition and boundary layer control. The determination of an unknown airfoil from a specified pressure distribution is known as the inverse problem.

Numerous methods for the two dimensional incompressible case exist [2-5]. Compressible inverse methods are for the most part based on some kind of iterative procedure, relying on either a Dirichlet or Neumann-type boundary condition. In the Dirichlet formulation [6-11] a sequence of boundary value problems for the velocity potential, with wing geometry updated at each step, is solved. The updated condition arises from the normal velocity resulting at each unconverged step. For the Neumann formulation [12-15] a sequence of analysis problems are solved over a corresponding series of geometries. Each geometry is provided by some rational method depending on the error being driven to zero. A complete survey of such methods has been given by Slooff [16].

In this paper we present an exact method for two-dimensional subsonic flow within the limitations of the tangent gas approximation [17-19]. Woods [20] extensively studied these equations and proposed certain iterative methods for solving both the analysis and inverse problems. We presented a substantially different

\* Present address: Courant Institute of Mathematical Sciences, 251 Mercer street, New York, N.Y. 10012.

method for the analysis problem [21]. The inverse method developed here is non-iterative and exact.

As is shown in [21] the tangent gas solution lies very close to the Euler solution even for high subcritical flows. Therefore the design of an airfoil in this regime by our method should be an almost correct airfoil.

In this paper, we have been able to show that the direct Euler solution over the designed airfoil is very close to the input speed distribution. Moreover, the constraints necessitated by upstream condition and closure requirements are very easily incorporated.

## 2. BASIC EQUATIONS

Consider steady two-dimensional flow, then in the usual notation

$$\nabla \cdot (\rho \mathbf{q}) = 0, \quad \nabla \times \mathbf{q} = 0, \quad \rho / \rho_\infty = 1. \quad (1)$$

The variables are normalized by their free stream values and linear dimensions by an appropriate length scale.

The stream function  $\psi$  and potential  $\phi$  are introduced in the usual way

$$\rho \mathbf{q} = c \nabla \times (\psi \mathbf{k}), \quad \mathbf{q} = \nabla \phi, \quad (2)$$

where  $\mathbf{k}$  denotes a vector perpendicular to the plane of motion. The constant  $c$  has been introduced for later purposes.

If  $s$  and  $n$  are local distances along streamlines and potential lines, respectively, (2) can be written as

$$ds + i dn = \frac{1}{q} \left( d\phi + i \frac{c}{\rho} d\psi \right). \quad (3)$$

Alternately, we can write

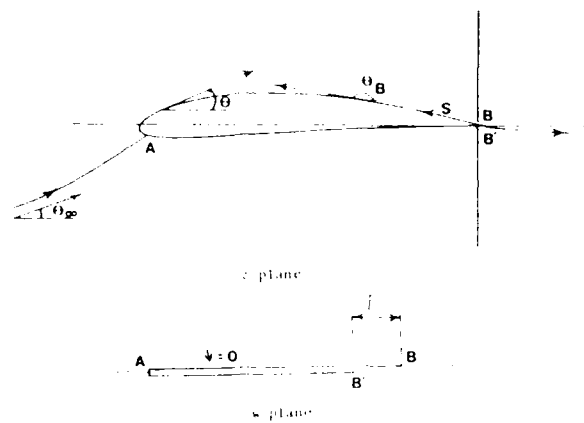
$$dz = dx + i dy = \frac{e^{i\theta}}{q} \left( d\phi + i \frac{c}{\rho} d\psi \right), \quad (4)$$

where  $x$  and  $y$  are cartesian coordinates and  $\theta$  the flow angle. If  $q$  and  $\theta$  are taken as independent variables, then it is easy to derive from (4) that

$$\phi_n = \frac{q}{\rho} c \psi_q, \quad \phi_x = -\frac{1 - M^2}{\rho q} c \psi_\theta. \quad (5)$$

If dependent and independent variables are interchanged and the Prandtl Meyer function

$$v = \int_1^q (1 - M^2)^{1/2} \frac{dq}{q} \quad (6)$$

Fig. 1. Airfoil in physical  $z$ -plane and potential  $w$ -plane

is introduced in place of  $q$ , then

$$\theta_\phi - \frac{1}{K(v)} v_\psi = 0, \quad \theta_\psi \pm K(v) v_\phi = 0. \quad (7)$$

The  $\pm$  sign refers to subsonic and supersonic conditions, respectively, and

$$K(v) = \beta \frac{c}{\rho(q(M))}, \quad (8)$$

where

$$\beta^2 = (1 - M^2)^{-1}. \quad (9)$$

Typical physical  $z (= x + iy)$  and potential  $w (= \phi + i\psi)$  planes are shown in Fig. 1. The airfoil maps into a slit in the  $w$  plane. The gap  $BB'$  in the potential plane corresponds to  $l$ , where circulation about the airfoil is  $-l$ .

The system (7) is augmented by the density speed relation obtained from (1) and Bernoulli's relation

$$\frac{q^2}{2} + \frac{1}{\gamma M^2} \int \frac{dp}{\rho} = \text{constant}. \quad (10)$$

### 3. MAPPINGS

The  $w$ -plane is mapped onto the exterior of the unit circle in the  $\sigma$  plane by

$$w = a(\sigma e^{-i\alpha_0} + \sigma^{-1} e^{i\alpha_0}) + i2a \sin \alpha_0 \ln(\sigma e^{-i\alpha_0}). \quad (11)$$

where circulation  $- \Gamma$  is related to the constant  $a$  by

$$\Gamma = 4\pi a \sin \alpha_0. \quad (12)$$

From (11) one obtains

$$\frac{dw}{d\sigma} = -ae^{-i\alpha_0}(1 - \sigma^{-1})(e^{-i\alpha_0} - \sigma^{-1}). \quad (13)$$

On the body  $\sigma = e^{i\alpha}$  ( $0 \leq \alpha \leq 2\pi$ ),  $\phi$  and  $\psi$  are given by

$$\phi(\alpha) = 2a[\cos(\alpha - \alpha_0) - (\alpha - \alpha_0) \sin \alpha_0], \quad \psi(\alpha) = 0. \quad (14)$$

$\alpha_s$  in (13) is given by

$$\alpha_s = \pi + 2\alpha_0. \quad (15)$$

Thus the rear and front stagnation points map into  $\sigma = 1$  and  $\sigma = e^{i\alpha}$ , respectively.

#### 4. DETERMINATION OF SPEED IN THE CIRCLE PLANE

Equation (2) suggests that speed  $q_s(s)$  on the body is related to the potential function  $\phi$  by

$$q_s(s) ds = |d\phi|, \quad (16)$$

where the subscript  $s$  refers to surface values. Equation (14) reduces (16) to

$$q_s(s) ds = 2a[\sin \alpha_0 + \sin(\alpha - \alpha_0)] d\alpha, \quad 0 \leq \alpha \leq 2\pi, \quad (17)$$

which is simply an ordinary differential equation for  $s(\alpha)$ . To integrate (17), we introduce

$$dQ = d \int_0^\alpha q_s(s') ds', \quad (18)$$

from which,

$$\begin{aligned} \tilde{Q}(\alpha) &= Q(s(\alpha)) \\ &= \begin{cases} 2a[\alpha \sin \alpha_0 + \cos \alpha_0 - \cos(\alpha - \alpha_0)], & 0 \leq \alpha < \alpha_s \\ 2a[2(\alpha_s \sin \alpha_0 + \cos \alpha_0) - \{\alpha \sin \alpha_0 - \cos(\alpha - \alpha_0) - \cos \alpha_0\}], & \alpha_s \leq \alpha \leq 2\pi. \end{cases} \end{aligned} \quad (19)$$

Observe that

$$Q(s = 1) = 8a(\alpha_0 \sin \alpha_0 + \cos \alpha_0), \quad Q(s = s_f) = 2a(\alpha_s \sin \alpha_0 + 2 \cos \alpha_0). \quad (20)$$

$\Gamma$  is related to  $Q(s=1)$  and  $Q(s=s_f)$  by

$$\Gamma = 2Q(s=s_f) - Q(s=1) = 4\pi a \sin \alpha_0. \quad (21)$$

Here  $s_f$  denotes the distance of the front stagnation point from the upsides of the trailing edge.  $Q(s=1)$ ,  $Q(s=s_f)$ , and hence  $\Gamma$  are known from the given surface speed distribution  $q_s(s)$ .

From (20) and (21)

$$\frac{Q(s=1)}{\Gamma} = \frac{2}{\pi} (\alpha_0 + \cot \alpha_0). \quad (22)$$

After (22) is solved for  $\alpha_0$  we obtain the constant  $a$  from (21). Next  $\tilde{Q}(x)$  is computed from (19) and  $s(x)$  is obtained by inverting (18)

$$s(x) = Q^{-1}(\tilde{Q}(x)) \quad (23)$$

and  $\tilde{q}_s(x) = q_s(s(x))$  is obtained from (17).

Thus far our deliberations are exact. Ideally system (7) should now be solved to determine the body shape. For the tangent gas approximation considered next the problem can be solved by an exact method similar to the one in the incompressible case [4].

#### 5. TANGENT GAS APPROXIMATION

The tangent gas approximation is given by (see [21])

$$(\rho - 1) = \gamma \left( 1 - \frac{1}{\rho} \right). \quad (24)$$

From (10) we obtain

$$\rho = \frac{\beta}{\beta_a}, \quad (25)$$

where the subscript  $a$  denotes a suitable reference point. With the constant  $c$  in (8) taken as

$$c = V\beta_a, \quad (26)$$

we obtain from (8)

$$K(v) = 1. \quad (27)$$

Then for subsonic flow the system (7) becomes the Cauchy Riemann equations

$$u_\phi - v_\psi = 0, \quad u_\psi + v_\phi = 0. \quad (28)$$

Equations (28) are exact for both the tangent gas and also for incompressible flow ( $M=0$ ). Henceforth, we take the tangency point  $(p_a, 1/\rho_a)$  to be the free stream,

$$p_a = p_\infty = 1, \quad \rho_a = \rho_\infty = 1. \quad (29)$$

With this selection the following relations hold [21]

$$q = \sinh v^* \operatorname{cosech}(v^* - v), \quad \beta = \tanh(v^* - v), \quad c_p = \frac{2}{1 - \beta_\infty \coth v}, \quad (30)$$

where the constant  $v^*$  is given by

$$v^* = \ln \left( \frac{M_\infty}{1 - \beta_\infty} \right). \quad (31)$$

From (6) it is seen that  $v_x = 0$  and at a stagnation point (denoted by zero subscript)

$$v_0 = -\infty, \quad c_{p,0} = \frac{2}{1 + \beta_\infty}. \quad (32)$$

It follows from (28) that

$$\tau = -v + i\theta \quad (33)$$

is an analytic function of  $w$  and hence of  $\sigma$ . A convenient representation of  $\tau(\sigma)$  is given by (see also [8]),

$$\exp(\tau(\sigma)) = (1 - \sigma^{-1})^{-\delta} (e^{i\alpha} - \sigma^{-1})^{-1} \exp \left( \sum_{n=0}^{\infty} c_n \sigma^{-n} \right), \quad (34)$$

where  $\delta = \theta_i/\pi$ ,  $\theta_i$  the trailing edge angle. The complex constants  $c_n$  are denoted by

$$c_n = A_n + iB_n. \quad (35)$$

Note that (34) contains the Kutta condition. Two Schwarz-Christoffel factors appear in (33) because of the discontinuity in  $\theta$  at the two stagnation points. On the unit circle, (33) reduces to

$$\exp(\tau(e^{i\alpha})) = G(\alpha) e^{i\theta(\alpha)} \exp \left( \sum_{n=0}^{\infty} c_n e^{-in\alpha} \right), \quad (36)$$

where

$$G(\alpha) = \left| 2 \sin \frac{\alpha}{2} \right|^{-\delta} |2(\sin \alpha_0 + \sin(\alpha - \alpha_0))|^{-1}, \quad (37)$$

$$\eta(\alpha) = \frac{1}{2} (1 - \delta)(\pi - \alpha) + \left( \alpha + \frac{\pi}{2} \right) - \pi U(\alpha - \alpha_0) + \alpha_0. \quad (38)$$

$U(\alpha - \alpha_s)$  in (38) is the unit step function. The tangent angle  $\theta_B$  at the body is related to  $\theta$  by

$$\theta(\alpha) = \theta_B(\alpha) - \pi - \pi U(\alpha - \alpha_s). \quad (39)$$

Separation of (36) into real and imaginary parts leads to

$$\tilde{v}(\alpha) = \sum_{n=0}^{\infty} (A_n \cos n\alpha + B_n \sin n\alpha) \quad (40)$$

and

$$\tilde{\theta}(\alpha) = \sum_{n=0}^{\infty} (B_n \cos n\alpha - A_n \sin n\alpha) + \pi + \alpha_0 \quad (41)$$

where

$$\tilde{v}(\alpha) = -v(\alpha) - \ln G(\alpha) \quad (42)$$

and

$$\tilde{\theta}(\alpha) = \theta_B(\alpha) - \frac{1}{2} (1 - \delta)(\pi - \alpha) - \left( \alpha + \frac{\pi}{2} \right). \quad (43)$$

Notice from (34) the upstream flow direction  $\theta_x$  is related to  $B_0$  by

$$\theta_x = B_0 + \pi + 2\alpha_0. \quad (44)$$

where  $B_0$  is given by

$$B_0 = \frac{1}{2\pi} \int_0^{2\pi} \tilde{\theta}(\alpha) d\alpha - \pi - \alpha_0. \quad (45)$$

The free stream condition ( $q_x = 1$ ) is given by

$$A_0 = 0. \quad (46)$$

The condition for closure of the airfoil is related to the leading terms of the series (40) and (41) by (see [21])

$$A_1 = (1 - \delta) - (1 - \beta_x) 2 \sin^2 \alpha_0, \quad (47)$$

$$B_1 = (1 - \beta_x) \sin 2\alpha_0. \quad (48)$$

## 6. BEHAVIOUR AT STAGNATION POINTS

It is both interesting and useful to study the behavior of speed at the stagnation points. From (30) and (42) we obtain

$$q_x \sim \frac{2\beta_x}{1 + \beta_x} \frac{e^{-\tilde{v}_x}}{G} \quad \text{for } q_x \sim 0. \quad (49)$$

From (37)

$$\frac{1}{G(\alpha)} \sim \begin{cases} \alpha^\delta (2 \cos \alpha_0) & \text{for } \alpha \sim 0 \\ |\alpha_s - \alpha| (2 \cos \alpha_0)^\delta & \text{for } \alpha \sim \alpha_s. \end{cases} \quad (50)$$

From (49) and (50)

$$\tilde{q}_s \sim \begin{cases} K_1 \alpha^\delta & \text{for } \alpha \sim 0 \\ K_2 |\alpha_s - \alpha| & \text{for } \alpha \sim \alpha_s, \end{cases} \quad (51)$$

where

$$K_1 = \frac{2\beta_{\alpha_0}}{1 + \beta_{\alpha_0}} e^{-\tilde{v}_s(\alpha=0)} (2 \cos \alpha_0), \quad K_2 = \frac{2\beta_{\alpha_s}}{1 + \beta_{\alpha_s}} e^{-\tilde{v}_s(\alpha=\alpha_s)} (2 \cos \alpha_0)^\delta. \quad (52)$$

If  $\alpha_1$  and  $\alpha_2$  are close to  $\alpha \sim 0$ , then from (51) we obtain

$$\delta \sim \frac{\ln(\tilde{q}_s(\alpha_2)/\tilde{q}_s(\alpha_1))}{\ln(\alpha_2/\alpha_1)}. \quad (53)$$

From (51), (52), and (53) we obtain

$$\tilde{v}_s(\alpha=0) \sim -\ln \left( \frac{\tilde{q}_s(\alpha_1)}{\alpha_1^\delta} \frac{1 + \beta_{\alpha_0}}{2\beta_{\alpha_0}} (2 \cos \alpha_0)^{-1} \right) \quad (54)$$

and

$$\tilde{v}_s(\alpha=\alpha_s) \sim -\ln \left( \frac{\tilde{q}_s(\alpha_s)}{|\alpha_s - \alpha_s|} \frac{1 + \beta_{\alpha_s}}{2\beta_{\alpha_s}} (2 \cos \alpha_0)^\delta \right), \quad (55)$$

where  $\alpha_s$  is close to  $\alpha$ , and  $\alpha_1$  is close to zero.

## 7. METHOD OF SOLUTION

The speed distribution  $q_s(s)$  is usually given at a finite number of points  $s_j$ ,  $j = 0, 1, 2, \dots$ , in the interval  $0 \leq s \leq 1$ . From this the integral in Eq. (18) can be evaluated to obtain  $Q(s_j)$  as a function of  $q_s(s_j)$ . Next the circulation  $\Gamma$  is computed from the relation

$$\Gamma = 2Q(s = s_j) - Q(s = 1).$$

Equation (22) is then solved to obtain  $\alpha_0$ . The second equation of (20) is next used to calculate the value of the constant  $a$ . In general  $\alpha_0$  and  $a$  so obtained do not satisfy the first equation of (20) exactly because  $\alpha_0$  is calculated numerically. If

$$Q(s=1) - Q(s=s_j) = \int_{s_j}^1 q_s ds$$

differs slightly from  $Q(s=s_j) - 4\pi a \sin \alpha_0$  (see Eq. (21)), the speed  $q_1(s)$  is modified by a constant factor over the interval  $s_j < s < 1$  to adjust the above integral to this value.

The values of  $\tilde{Q}(\alpha_j)$  at  $N$  (a power of 2) equally spaced points on the unit circle,  $\alpha_j = 2\pi j/N$ ,  $j=0, 1, \dots, N$ , are calculated using Eq. (19). The value of speed  $\tilde{q}_1(\alpha_j)$  at the grid points  $\alpha_j$  are now easily obtained by interpolation since  $q_1(s)$  is already known as a function of  $Q(s_j)$ .

The approximate value of the trailing edge angle  $\delta$  is obtained from Eq. (53).  $\tilde{v}_1(\alpha)$  is then obtained from Eqs. (42), (37), and (30) and its value at a stagnation point is calculated from (54) and (55). If  $\tilde{v}_1(\alpha)$  satisfies the constraints (46), (47), and (48) then the conjugate function  $\tilde{\theta}(\alpha)$  is calculated from (41) using the fast Fourier transform. In case  $\tilde{v}_1(\alpha)$  does not satisfy the constraints, the prescribed speed distribution must be modified. This is discussed in the next section.

The value of the constant  $B_0$  in (41) which is also needed to calculate  $\tilde{\theta}(\alpha)$  is obtained from (44) by setting the free stream direction  $\theta_\infty$  to zero. The tangent angle  $\theta_H$  at the body is now obtained from  $\tilde{\theta}(\alpha)$  using the relation (43). The body coordinates are then calculated from

$$x(\alpha) = \int_0^\alpha \frac{ds}{dx} \cos \theta_H(\alpha) d\alpha, \quad (56a)$$

$$y(\alpha) = \int_0^\alpha \frac{ds}{dx} \sin \theta_H(\alpha) d\alpha, \quad (56b)$$

where  $ds/d\alpha$  is given by

$$\frac{ds}{d\alpha} = 2a \frac{|\sin \alpha_0 + \sin(\alpha - \alpha_0)|}{\tilde{q}_1(\alpha)}. \quad (57)$$

The value of (57) at a stagnation point ( $\alpha = 0$ ,  $\alpha = \alpha_1$ ) is given by (see Eq. (51))

$$\frac{ds}{d\alpha} = \begin{cases} 2a \frac{\cos \alpha_0}{K_1} \alpha^{1-\delta} & \text{for } \alpha = 0 \\ 2a \frac{\cos \alpha_0}{K_2} & \text{for } \alpha = \alpha_1. \end{cases} \quad (58)$$

Instead of calculating  $\delta$  from Eq. (53) as was done above, one can prescribe  $\delta$  because the constraints (46), (47), and (48) depend on  $\delta$ . Modification of the speed distribution subject to these constraints will automatically satisfy the Eq. (53) because this equation is valid if the speed distribution is consistent with those constraints. In either case if  $\tilde{v}_1(\alpha)$  obtained from a given speed distribution does not satisfy the constraints then the prescribed speed distribution must be modified according to the method discussed in the next section.

Even though the above method is exact theoretically, there are numerical sources of error. These errors depend on the kind of interpolation and integration scheme,

the number of data points, the number of grid points, the evaluation of  $\alpha_0$  from (22) and the use of the approximate expressions (53), (54), and (55) to calculate trailing edge angle  $\delta$ ,  $\bar{v}_s(\alpha = 0)$ , and  $\bar{v}_s(\alpha = \alpha_s)$ , respectively.

In view of the simplicity of the procedure no attempt was made to incorporate highly accurate computations. Simpson's rule with evenly spaced grid points and trapezoidal rule with unevenly spaced data points were used for integration. The interpolation scheme used was linear. The speed  $q_s(s)$  was prescribed at 129 unevenly spaced data points on  $0 \leq s \leq 1$  and the number of grid points on the unit circle was taken to be 128.  $\alpha_0$  was obtained within an accuracy of  $10^{-6}$  by solving Eq. (22) by regular falsi method and the trailing edge angle  $\delta$  used was calculated by using the approximate relation (55).

The program was run on an IBM 3081 in single precision and the computation time was about a half second in most cases.

### 8. MODIFICATION OF SPEED DISTRIBUTION

Constraints (46), (47), and (48) must be satisfied by the prescribed speed distribution to find a closed body solution. Therefore in general any arbitrary speed distribution must be modified subject to these constraints. These constraints can be written in terms of surface values  $\bar{v}_s(\alpha)$  given by

$$\frac{1}{\pi} \int_0^{2\pi} \bar{v}_s(\alpha) g_j(\alpha) d\alpha = P_j, \quad j = 1, 2, 3, \quad (59)$$

where  $g_j(\alpha)$  and  $P_j$  are given by (see (46), (47), and (48))

$$g_j(\alpha) = \begin{cases} 1, & j = 1 \\ \cos \alpha, & j = 2 \\ \sin \alpha, & j = 3 \end{cases} \quad (60)$$

and

$$P_j = \begin{cases} 0, & j = 1 \\ (1 - \delta) - (1 - \beta_s) 2 \sin^2 \alpha_0, & j = 2 \\ (1 - \beta_s) \sin 2\alpha_0, & j = 3. \end{cases} \quad (61)$$

Linearity of (28) implies the following form of modification of prescribed values  $\bar{v}_s(\alpha)$  (see [4])

$$\bar{v}_s(\alpha) = \bar{v}_s(\alpha) + \sum_{k=1}^3 \gamma_k J_k(\alpha), \quad (62)$$

where  $\gamma_k$ ,  $k = 1, 2, 3$ , are constants to be determined and  $f_k(\alpha)$ ,  $k = 1, 2, 3$ , are suitable correction terms. The correction terms can be set to zero outside a specified interval  $(\alpha_1, \alpha_2)$  leaving speed distribution same as the prescribed one outside this interval. This is extremely useful when designing an airfoil where in general no modification of speed distribution over the suction side is desired. The speed distribution can be modified in various ways depending on the choice of functions  $f_k(\alpha)$ ,  $k = 1, 2, 3$ , and the correction interval  $(\alpha_1, \alpha_2)$ .

Substituting (62) in (59) one obtains

$$\sum_{k=1}^3 \gamma_k a_{jk} = b_j, \quad j = 1, 2, 3, \quad (63)$$

where

$$a_{jk} = \int_0^{2\pi} f_k(\alpha) g_j(\alpha) d\alpha = \int_{\alpha_1}^{\alpha_2} f_k(\alpha) g_j(\alpha) d\alpha, \quad (64)$$

$$b_j = \pi P_j - \int_0^{2\pi} \tilde{v}_0(\alpha) g_j(\alpha) d\alpha = \pi P_j - \int_{\alpha_1}^{\alpha_2} \tilde{v}_0(\alpha) g_j(\alpha) d\alpha. \quad (65)$$

Constants  $\gamma_k$ ,  $k = 1, 2, 3$ , are obtained by inverting (63) and the corrected  $\tilde{v}_1(\alpha)$  is then obtained from (62). The corrected speed distribution is then obtained from (42) and (30) and the body is found from (55).

The matrix  $a_{jk}$  in (65) must be positive definite to be able to invert (63) which restricts the choice of  $f_k(\alpha)$ ,  $\alpha_1$ , and  $\alpha_2$ . These should be carefully selected so that the correction to a prescribed speed distribution is minimum. This can be done in the same spirit as in Strand [22] and Arlinger [4].

For our purpose we choose  $\alpha_1 = 0$ ,  $\alpha_2 = 2\pi$  and  $f_k(\alpha) = g_k(\alpha)$ ,  $k = 1, 2, 3$ . This modifies the speed distribution over the whole interval. In this case (63) gives

$$\gamma_1 = \frac{b_1}{2\pi}, \quad \gamma_2 = \frac{b_2}{\pi}, \quad \text{and} \quad \gamma_3 = \frac{b_3}{\pi} \quad (66)$$

and hence (62) becomes

$$\tilde{v}_1(\alpha) = \tilde{v}_0(\alpha) + \frac{1}{2\pi} (b_1 + 2b_2 \cos \alpha + 2b_3 \sin \alpha). \quad (67)$$

## 9. RESULTS

A basic test of the inverse method is the recovery of a known airfoil from its pressure distribution. Figures 2 and 3 provide a verification of the method within the tangent gas approximation. Here a pressure distribution is computed in tangent gas approximation over a NACA 4412 airfoil (see [21]). Speed distribution is com-

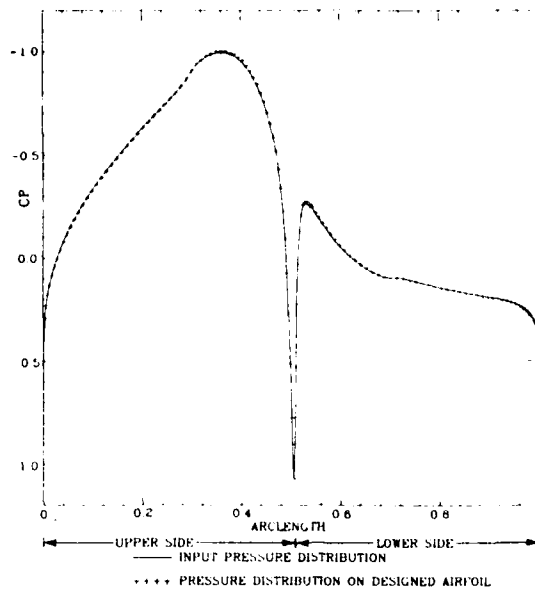


FIG. 2. Comparison of pressure distributions on NACA 4412 airfoil (input) and on designed airfoil from tangent gas solution at free stream Mach number 0.7 and zero angle of attack.

puted from this pressure distribution using Eqs. (30). Then the airfoil is designed from this speed distribution by the method discussed in Section 7. In Fig. 2 we show the pressure distribution over a NACA 4412 airfoil as calculated by the tangent gas and compare it with the pressure over the designed airfoil. The error is less than  $O(10^{-3})$ . Figure 3 compares the given airfoil with the designed airfoil. The error is less than  $O(10^{-4})$ . (The origin of these errors is numerical and was discussed in Section 7.)

Figure 4 shows a pressure distribution which did not satisfy the constraints (46), (47), and (48). The pressure distribution which results from the correction according to (67) is shown in the same figure. The resulting body along with its design and analysis pressure is shown in Fig. 5.

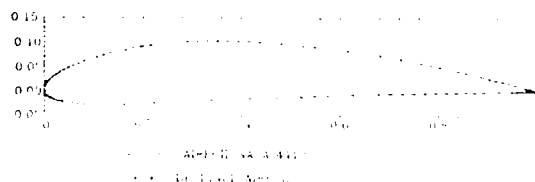


FIG. 3. Comparison of NACA4412 airfoil and the airfoil designed by tangent gas approximation from input pressure distribution of Fig. 2.

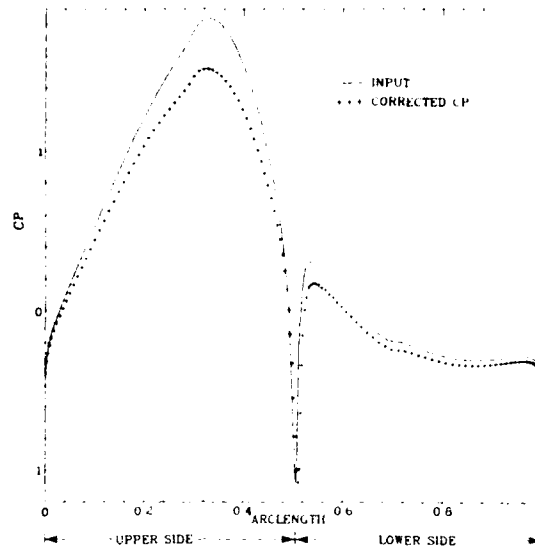


FIG. 4. Target and corrected pressure distribution.

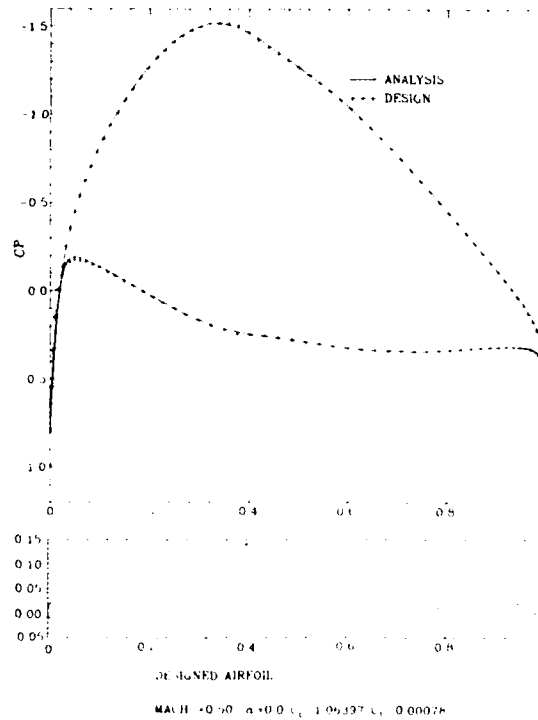


FIG. 5. Designed airfoil from input pressure distribution of Fig. 4 and pressure distribution on designed airfoil from design and direct analysis by tangent gas method.

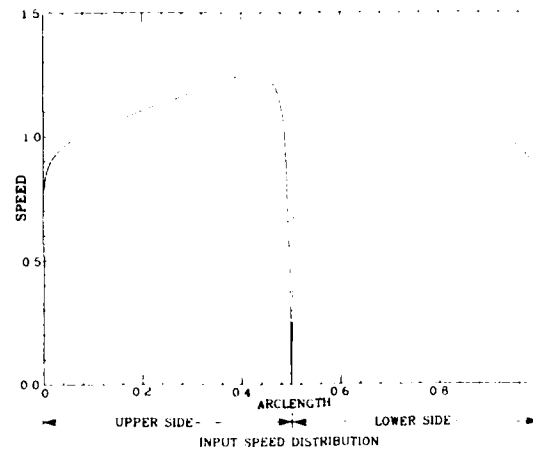


FIG. 6. Speed distribution on NACA0012 airfoil from Euler solution (FLO52S) at  $M_\infty = 0.6$  and  $x = 0.0$ .

Next, we wish to evaluate the usefulness of the tangent gas method by comparing its results with comparable results gotten from the exact Euler equations. For this purpose we use FLO52S written by A. Jameson, M. Salas, and E. Turkel. The pressure distribution obtained from the Euler code is used to compute the speed distribution according to the relation

$$q^2 = \left( \frac{\rho_0/\rho_0 - p/\rho}{\rho_0/\rho_0 - 1} \right) \quad (68)$$

which is the same for the tangent gas and ideal gas. The subscript 0 refers to the stagnation point values (normalized by free stream values) as mentioned in Section 5. The  $\rho_0/\rho_0$  in (68) is given by the ideal gas relations (see [23])

$$\rho_0/\rho_0 = \left( 1 + \frac{\gamma-1}{2} M_\infty^2 \right). \quad (69)$$

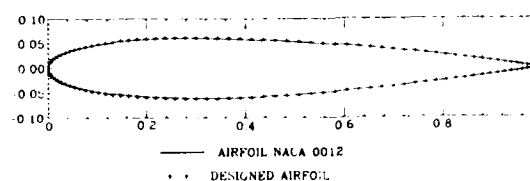


FIG. 7. Comparison of NACA0012 and the airfoil designed by tangent gas approximation from speed distribution of Fig. 6.

This speed distribution is used to design the airfoil by the method mentioned before. Figure 6 shows the speed distribution on a NACA0012 airfoil as calculated from the Euler equations at free stream Mach number 0.6 and zero angle of attack. Figure 7 compares the NACA0012 airfoil and the designed airfoil in the tangent gas approximation. It is seen that the airfoil is almost exactly recovered along with the zero angle of attack. The pointwise error is less than 3% and this only occurs in a small neighborhood of the leading edge. Figure 8 compares the Euler pressure with the pressure over the designed airfoil. Again the comparison is excellent except near the leading edge where the error in  $C_p$  is  $O(10^{-2})$ . It is to be emphasized that this error occurs as a result of using the tangent gas approximation and is in no way numerical. We believe on the basis of this discussion that this recommends the use of the method presented here for airfoil design especially since it is computationally very efficient.

In the next example we push the method beyond its limits by considering a supercritical case. We show in Fig. 9 the Euler speed distribution over a NACA0012 airfoil at free stream Mach number 0.5 and angle of attack  $5^\circ$ . Figure 10 shows that we recover the correct angle of attack and the airfoil except over a small region

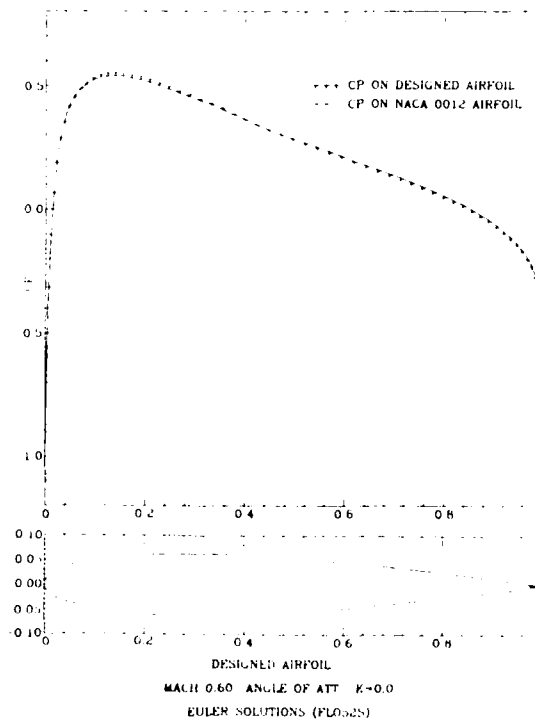


FIG. 8. Comparison of Euler pressure distributions over NACA0012 airfoil and the airfoil designed from speed distribution of Fig. 6 at  $M_\infty = 0.6$  and  $\alpha = 0.0$ .

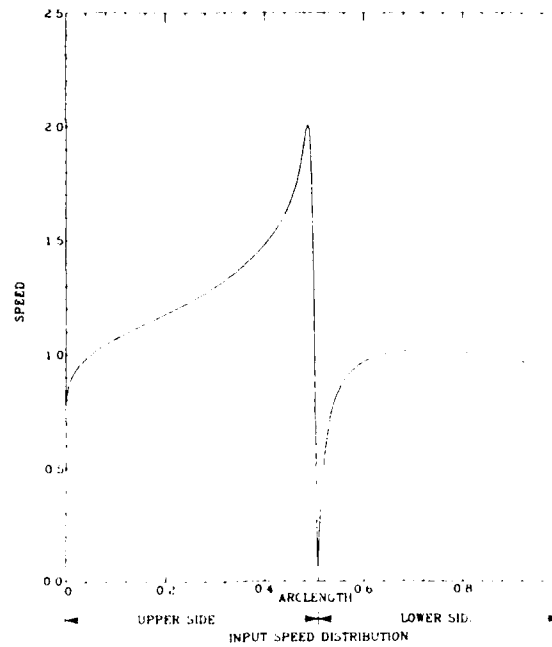


FIG. 9. Speed distribution on NACA0012 airfoil from Euler solution (FLO52S) at  $M_\infty = 0.5$  and  $x = 5$ .

near the nose where the error is within 2%, and where the flow is actually supercritical. Again the error is nonnumerical and gives a measure of the deviation of the tangent gas approximation from the exact Euler result. In Fig. 11 we compare the Euler solution over the NACA0012 airfoil and designed airfoil. Note that the agreement near the leading edge is not as good as elsewhere because the designed airfoil suffers maximum deviation from the NACA0012 airfoil near the leading edge.

Finally a useful application of our approximate method is to provide a starting airfoil in a design procedure in which the Euler equations are used directly to give the corrected pressure distribution. At successive stages the pressure distribution is

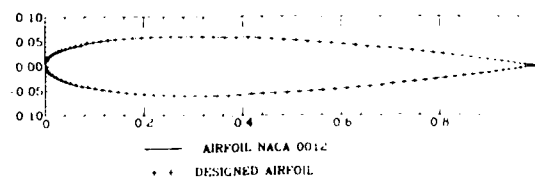


FIG. 10. Comparison of NACA0012 and the airfoil designed by tangent gas approximation from speed distribution of Fig. 9.

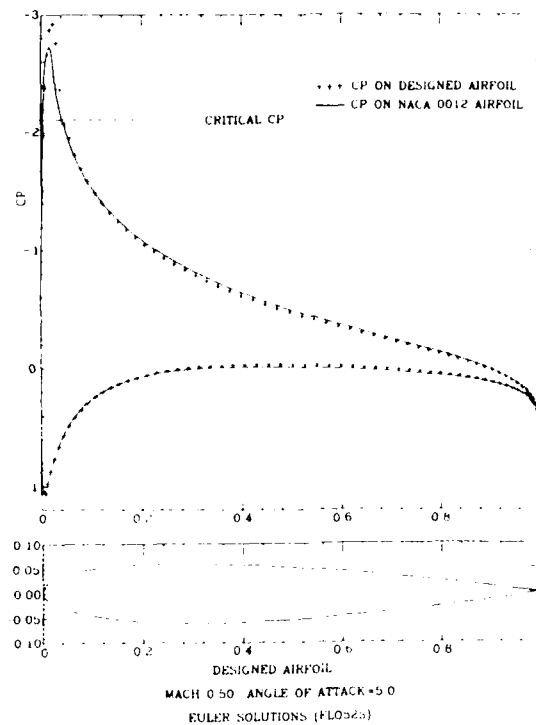


FIG. 11. Comparison of Euler pressure distributions over NACA0012 airfoil and the airfoil designed from speed distribution of Fig 9 at  $M_\infty = 0.5$  and  $\alpha = 5^\circ$ .

modified to meet the design criteria and the inverse method reapplied and so forth. The interactive iteration should go quite quickly for subcritical flows. However, the value of such a procedure remains uncertain for supercritical flows.

#### ACKNOWLEDGMENTS

This research was supported by the National Aeronautics and Space Administration under Grant NSG-1617 and the Air Force Office of Scientific Research under Grant AFOSR-83-0336. The authors would also like to thank the reviewers for helpful criticism.

#### REFERENCES

1. B. S. STRATFORD, *J. Fluid Mech.* **5** (1959), 1.
2. S. GOLDSTEIN, "A Theory of Aerofoils of Small Thickness. Part III. Approximate Designs of Symmetrical Aerofoils for Specified Pressure Distributions," Aeronautical Research Committee, London, Report, No. ARC 6225, October 1942.

3. M. J. LIGHTHILL, "A New Method of Two-Dimensional Design," Aeronautical Research Committee, London, R & M 2112, 1945.
4. B. ARLINGER, "An Exact Method of Two-Dimensional Airfoil Design," *SAAB*, TN67, 1970.
5. F. T. JOHNSON, "A General Panel Method for the Analysis and Design of Arbitrary Configurations in Incompressible Flows," NASA CR 3079, May 1980.
6. G. VOLPE, "The Inverse Design of Closed Airfoils in Transonic Flow," AIAA Paper, No. 83-0504, 1983.
7. T. L. TRANEN, "A Rapid Computer Aided Transonic Airfoil Design Method," AIAA Paper, No. 74-501, 1974.
8. F. BAUER, P. GARABEDIAN, AND D. KORN, "Supercritical Wing Sections II," Springer Verlag, Berlin, 1975.
9. B. ARLINGER AND W. SCHMIDT, "Design and Analysis of Slat Systems in Transonic Flow," ICAS Paper, 1978.
10. L. A. CARLSON, *J. Aircraft* **13** (1976), 356.
11. P. A. HENNE, "An Inverse Transonic Wing Design Method," AIAA Paper, No. 80-0330, 1980.
12. J. M. J. FRAY AND J. W. SLOOF, "A Constrained Inverse Method for the Aerodynamic Design of Thick Wings with Given Pressure Distribution in Subsonic Flow," AGARD CP., No. 285, Paper 16, 1980.
13. W. H. DAVIS, JR., "Technique for Developing Design Tools from the Analysis Methods of Computational Aerodynamics," AIAA Paper, No. 79-1529, 1979.
14. G. B. MCFADDEN, "An Artificial viscosity method for the design of Supercritical Airfoils," Ph.D. thesis, New York Univ., New York, 1979.
15. P. GARABEDIAN AND G. MCFADDEN, in "Proceedings of Symposium on Transonic, Shock and Multi-dimensional Flows," pp. 1-16, University of Wisconsin, Madison, 1981; Academic Press, New York, 1982.
16. J. W. SLOOF, in "Proceedings on ICIDES," pp. 1-68, Univ. of Texas, Austin, 1984.
17. VON KÄRMÁN, *J. Aeronaut. Sci.* **8** (1941), 337.
18. H. S. TSJEN, *J. Aeronaut. Sci.* **6** (1939), 399.
19. S. A. CHAPLYGIN, "On Gas Jets," NASA Technical Memorandum, No. 1063, 1944.
20. L. C. WOODS, "The Theory of Subsonic Plane Flow," Cambridge Univ. Press, London, 1961.
21. P. K. DARIPA AND L. SIROVICH, *J. Comput. Phys.*, in press.
22. T. STRAND, *J. Aircraft* **10** (1973), 651.
23. H. W. LIEPMANN AND A. ROSHKO, "Elements of Gas Dynamics," Wiley, New York, 1957.

## A FAST APPROACH TO DESIGNING AIRFOILS FROM GIVEN PRESSURE DISTRIBUTION IN COMPRESSIBLE FLOWS

Prabir Daripa<sup>\*,†</sup>

Courant Institute of Mathematical Sciences  
New York University  
New York, NY 10012

### Abstract

A new inverse method for aerodynamic design of airfoils is presented for subcritical flows. The pressure distribution in this method can be prescribed in a natural way, i.e., as a function of arclength of the as yet unknown body. This inverse problem is shown to be mathematically equivalent to solving only one nonlinear boundary value problem subject to known Dirichlet data on the boundary. The solution to this problem determines the airfoil, free stream Mach number  $M_\infty$  and the upstream flow direction  $\theta_\infty$ . The existence of a solution to a given pressure distribution is discussed. The method is easy to implement and extremely efficient. We present a series of results for which comparisons are made with the known airfoils.

### 1. Introduction

The objective of this paper is to present a new method for solving inverse problems in the context of aerodynamics. By the inverse problem we mean the problem of finding a profile associated with a given pressure distribution.

Interest in inverse problems arises from design considerations of airfoils. There are two different numerical approaches of airfoil design, one based on the analysis of flow over a known profile and other based on the inverse methods. The idea behind the analysis approach is to determine the airfoil that meets some design criteria through the analysis of flows over a series of airfoils. The approach based on the inverse method offers the flexibility of tailoring the pressure distribution that controls many of the important flow features such as

boundary layer separation, wave drag and lift. Success with this method in designing cost efficient airfoils has made this approach useful in airfoil design.

The mathematical theory behind solving the inverse problem is somewhat more difficult than the corresponding analysis problem for the following reasons: a) difficulty with formulation of proper differential equations; b) lack of existence of a solution for arbitrarily prescribed pressure data; c) the difficulty in imposing closure constraints (a specified gap at the trailing edge of the designed airfoil). For incompressible flows the theory of harmonic functions<sup>1,2</sup> makes the above issues easily tractable due to the linearity of the problem. Here the existence and the closure constraints can easily be established. The specified pressure distribution can be modified a priori to satisfy these constraints. Most of the solution techniques for this case have been based on analytic function theory.<sup>3-9</sup> The tangent gas approximation makes the inverse problem for subsonic flows similar to the incompressible case.<sup>10,11</sup>

Nonlinearity in compressible flows makes this problem difficult. Most of the inverse methods rely on either a Dirichlet or Neumann formulation depending on the choice of the dependent variable<sup>12-18</sup> and usually involves solving a series of nonlinear elliptic problems. An excellent account of these methods can be found in Sloof.<sup>19</sup> Formulation of the closure constraints and the existence of a solution for such flows, similar to the case of incompressible flows, may prove useful in developing new numerical techniques. The constraint necessitated by the existence of a solution in the subsonic case was established in Daripa.<sup>20</sup> It is shown there that because of the nonlinearity of the constraint, the existence of a solution can not be established a priori from the prescribed pressure distribution. However it suggests that the correct formulation of the problem must have at least one free

<sup>\*</sup> Research Scientist  
Member AIAA

<sup>†</sup> Permanent address: Assistant Professor  
Department of Mathematics, Texas A.M. University  
College Station, TX 77843

parameter to make the problem solvable in general. This free parameter will be determined by the solution. Such an attempt has been made in two dimensions<sup>12</sup> for transonic flows.

The case of transonic flow is more difficult than the other cases owing to the mixed elliptic-hyperbolic nature of the transonic flow equations. The mathematically elegant method of complex characteristics, was successfully used by Garabedian<sup>21-24</sup> to generate supercritical airfoils. In this method the boundary is unknown and iteration on the boundary is used to generate the airfoil. There are also cost effective methods based on the fictitious gas concept to generate supercritical airfoils.<sup>25</sup> An excellent review on the design of supercritical airfoils and wings can be found in Sobieczky.<sup>26</sup>

We discuss our method in this paper for subsonic flows only. In our formulation, the equations of motion are cast into one boundary value problem in the potential plane. To avoid dealing with the infinite potential plane, we map our potential plane into the interior of a unit circle and solve our equations there. To render the problem solvable we choose the Mach number distribution, computed from the prescribed pressure distribution, as the boundary data. By doing this we have at our disposal the free stream Mach number as free parameter which is determined as part of the solution of the boundary value problem. The solution also determines the shape of a profile. This free stream Mach number and the input Mach number distribution together determine the pressure distribution over the designed profile. In general the prescribed and computed pressure distributions will not be same except in cases where there exists a solution to the prescribed pressure distributions.

Our method requires solving only one nonlinear boundary value problem as opposed to solving a sequence of such problems. In addition a profile is always generated by our method. The designed airfoil however may have a gap at the trailing edge. To be able to design an airfoil with any prescribed gap we need to do further work that is currently in progress. An obvious approach is to use this method in some iterative mode.

## II. Problem Formulation

The equations of motion are

$$\nabla \cdot (\rho \bar{q}) = 0, \quad \nabla \times \bar{q} = 0, \quad p = \rho \gamma \quad (1a,b,c)$$

The variables are normalized by their sonic values and linear dimensions by some appropriate linear dimension. Here  $p$  is the pressure,  $\rho$  is the density and  $q$  is the speed. These equations imply the existence of a stream function  $\psi$  and a potential  $\phi$  given by

$$\rho \bar{q} = \nabla \times (\psi \bar{K}), \quad \bar{q} = \nabla \phi, \quad (2a,b)$$

where  $\bar{K}$  denotes a unit vector perpendicular to the plane of the motion. The above equations can alternatively be put in the form

$$\theta_{\delta} - (K(M))^{-1} \nu_{\psi} = 0; \quad \theta_{\psi} + (K(M)) \nu_{\delta} = 0 \quad (3a,b)$$

Here  $K$  and  $\nu$  are functions of Mach number  $M$  only<sup>27</sup> and  $\theta$  is the flow direction.  $\nu$  is known as the Prandtl-Meyer function. The body maps onto a slit in the potential ( $w = \phi + i\psi$ ) plane as shown in Fig. 1.

Differentiation and elimination reduces the system (3a,b) of first order partial differential equations (PDEs) to an equivalent second order PDE in  $\nu$  only.

$$(K^{-1}(M) \nu_{\psi})_{\psi} + (K(M) \nu_{\delta})_{\delta} = 0. \quad (4)$$

A little algebra shows that this equation can alternatively be written in the form<sup>27</sup>

$$\nabla^2_{\delta, \psi} \nu = (1 - K^2) \nu_{\delta \delta} + f(M) \nu_{\psi}^2 - K^2 f(M) \nu_{\delta}^2 \quad (5)$$

where  $f(M)$  is a function of Mach number.<sup>27</sup>

The appropriate boundary condition is seen to be (see Fig. 1)

$$M = M(\phi) \quad \begin{cases} \text{for } \psi = 0^-, & 0 \leq \phi \leq \phi_B \\ \text{for } \psi = 0^+, & 0 \leq \phi \leq \phi_B \end{cases} \quad (6)$$

where  $(\phi, \psi) = (\phi_A = 0, 0)$  corresponds to the front stagnation point and  $(\phi, \psi) = (\phi_B, 0)$  and  $(\phi, \psi) = (\phi_B, 0)$  correspond to the upper and lower side of the rear stagnation point respectively (see Fig. 1). Bernoulli's law gives  $q = q(C_p)$  and  $M = M(C_p)$ <sup>28,29</sup> that are used to determine  $q(s)$  and  $M(s)$  from the input pressure distribution  $C_p(s); 0 \leq s \leq 1$ . Here  $s$  parametrizes the arclength. The equation (2b) implies

$$\phi = \int |q(s) ds| \quad (7)$$

which together with known  $q(s)$  and  $M(s), 0 \leq s \leq 1$  determines the boundary condition (6) and the boundary (the slit) in the potential plane.

The solution of the boundary value problem (5) and (6) determines  $v_0$  on the slit that is subsequently used in (3a) to compute  $\theta_0$  on the slit. Integrating this and using (7) determine the flow angle as a function of arclength on the body and hence the profile is known.

To avoid dealing with infinity in the  $(\phi - \psi)$  plane we map this plane into the interior of a unit circle such that the body maps onto the unit circle. We carry out our calculations in this circle plane.<sup>27</sup>

The solution of this boundary value problem also determines the upstream Mach number. Pressure on the designed body can be computed using the computed  $M_\infty$  and the input Mach number distribution. The flow direction at infinity with respect to the body can be calculated by integrating either (3a) or (3b) from the slit to infinity in the potential plane. This integration process becomes much easier in the mapped circle plane. See Daripa<sup>27</sup> for details.

### III. Method of Solution

As mentioned earlier, the boundary and the boundary data in the potential plane and hence in the mapped circle plane are known from the input pressure distribution. The equation (5) is solved numerically inside the unit circle subject to the known Dirichlet data. In solving equation (5) numerically, a general linear Helmholtz equation solver<sup>30</sup> is used iteratively. An initial guess of the flowfield inside the unit circle determines the right hand side of equation (5) within the unit circle. The solver then updates the values of  $v$  inside the unit circle by solving the linear Poisson equation and the process is repeated until a given convergence criterion is met.

The solution is considered to have converged if the difference in the maximum value of Prandtl-Meyer function  $v$  inside the unit circle between two successive iterations is less than  $5 \times 10^{-6}$ . We never needed more than six iterations in any of our calculations when the initial guess was taken to be that of uniform flowfield. The solution values of  $v$  inside the unit circle are then used to compute the estimate of the normal derivative on the unit circle. This estimate is then used to compute the body angle through the use of equation (3a) and the mapping function. Similarly the flow direction at infinity is calculated by integrating equation (3a) along an appropriate ray in the circle plane. The solution of the nonlinear elliptic equation (5) also determines the upstream Mach number

### IV. Results

To validate our method we present a series of results which recovers a known airfoil from its pressure distribution. We generate pressure distributions over a series of closed airfoils at a given free stream Mach number  $M_\infty$  and angle of attack  $\theta_\infty$  by using an Euler code (flo52s written by A. Jameson, E. Turkel and M. Salas). This pressure distribution is then used in our method to generate the airfoil. Numerical sources of error in practice may introduce some error and so we monitor the following as a measure of accuracy of our method:  $E(M) = |M_\infty - M_\infty^c|$ ,  $E(\theta_\infty) = |\theta_\infty - \theta_\infty^c|$ ,  $E(\theta_B) = \max |\theta_B(s_i) - \theta_B^c(s_i)|$ ,  $y_{gap} = |y(s=0) - y(s=1)|$  and  $x_{gap} = |x(s=0) - x(s=1)|$ , where  $x_{gap}$  and  $y_{gap}$  (normalized by chord length) measure the gap at the trailing edge of the airfoil and  $\theta_B$  refers to the body angle. In the above a superscript refers to the computed value. Here we present a few results for cases where the trailing edge is not a stagnation point. The case with rear stagnation point has been excluded here because some difficulties was encountered in removing the singularity at the trailing edge.<sup>27</sup> This case will be taken up in future.

Fig. 2 shows the Euler pressure distribution over a 12% thick Kutta airfoil at  $M_\infty = 0.5$  and angle of attack  $= 2.0$  degrees. The application of the above method then generates the body and also gives the computed values of the free stream Mach number,  $M_\infty^c$ , and the angle of attack,  $\theta_\infty^c$ . The number of iterations (see § III) required to converge to the solution using the linear elliptic solver were only five in this case. In Fig. 3 we compare the designed airfoil with the exact airfoil and find that the agreement is excellent. We find the computed free stream Mach number  $M_\infty^c = 0.50005$  and the angle of attack  $\theta_\infty^c = 2.05$  degrees. The values of the error diagnostics in this case are  $E(M) = 0.00005$ ,  $E(\theta_\infty) = 0.00087$ ,  $E(\theta_B) = 0.009$ ,  $x_{gap} = 0.00043$  and  $y_{gap} = 0.00010$ . The gap at the trailing edge is within 0.01% of the thickness of the airfoil which is negligibly small. A more important quantity is the body angle which is likely to suffer maximum error near the leading edge since the body angle is a rapidly varying function of arclength there. Fig. 4 compares the computed and exact values of body angle as a function of arclength. Fig. 5 compares the same in the leading edge region. Here again we find the error in the body angle is 0.0005.

everywhere except near the leading edge where it is maximum and is given by  $E(\theta_B) = 0.009$ . In general closure can not be expected unless explicitly imposed either by some iterative or exact method. (We will report on the design of closed airfoil in the near future.) The source of these errors is numerical as has been discussed before.

Next we show a more vigorous test case for generating an airfoil from an arbitrary pressure distribution. Such an arbitrary pressure distribution (solid line) is shown in Fig. 6. The asymmetric pressure distribution in Fig. 6 is a minor variation of the pressure distribution in Fig. 2 and as we shall see there is no airfoil corresponding to this input pressure distribution. The resulting airfoil designed with our inverse method is shown in Fig. 7. This airfoil has a finite gap at the trailing edge. We find the computed Mach number  $M_\infty = 0.5504$  and angle of attack  $\theta_\infty = 2$  degrees. The pressure distribution on the designed airfoil obtained by our inverse code at this Mach number and angle of attack is also shown in Fig. 6 (+ sign) which is different from the input pressure distribution (solid line). This is due to the fact that there is no airfoil associated with this input pressure distribution. In order to have a specified gap at the trailing edge, this method can be used in an iterative mode.

#### V. Discussions and Conclusions

We have developed a fast approach to solve inverse problem for subcritical flows. We have shown that solution of the inverse problem requires solving only one nonlinear boundary value problem in an appropriate plane. Mach number distribution is used as the boundary values which are in turn used to generate the airfoil. This approach leaves the upstream Mach number as a free parameter which is also determined by the solution.

The numerical sources of error may introduce a gap at the trailing edge even in cases where ideally there should be no gap. Therefore it is necessary to incorporate some kind of closure procedure in our present formulation. It is my contention that this method can easily be extended to deal with the design of a supercritical airfoil in an efficient manner. However such an attempt has not yet been made.

#### Acknowledgment

It is a pleasure to thank Prof. Lawrence Sirovich, Prof. James Glimm and Prof. Paul Garabedian for their comments and suggestions. This work was supported by National Aeronautics and Space Administration under Grant NSG-1617 and the Air Force Office of Scientific Research under Grant AFOSR-83-0336 at Brown University and by the Applied Mathematical Sciences subprogram of the Office of Energy Research, U. S. Department of Energy, under Contract No. DE-AC02-76ER03007 at New York University.

#### References

- <sup>1</sup> Lighthill, M. J., "A new method of two dimensional aerodynamic design," *ARC, R&M 2712*, April 1945.
- <sup>2</sup> Arlinger, B., "An exact method of two-dimensional airfoil design," *SAAB TN67*, 1970.
- <sup>3</sup> Glauert, H., *Aerofoil and Airscrew Theory*, Cambridge University Press, 1926.
- <sup>4</sup> Goldstein, S., "A Theory of Aerofoils of Small Thickness," *Aeronautical Research Committee*, London, Oct. 1942.
- <sup>5</sup> Halsey, N. D., "Methods for the Design and Analysis of Jet-Flapped Airfoils," *AIAA Paper No. 74-188*, Feb. 1974.
- <sup>6</sup> Johnson, F. T., "A general panel method for the analysis and design of arbitrary configurations in incompressible flows," *NASA CR*, vol. 3079, May 1980.
- <sup>7</sup> Johnson, F. T. and Rubbert, P. E., "Advanced Panel-Type Influence Coefficient Methods Applied to Subsonic Flows," *AIAA Paper 75-50*, Jan. 1975.
- <sup>8</sup> Langley, M. J., "Numerical methods for two-dimensional and axisymmetric flows," *ARA memo 143*, 1973.
- <sup>9</sup> Strand, T., "Exact Method of Designing Airfoils with Given Velocity Distribution in Incompressible Flow," *J. Aircraft*, vol. 10, pp. 651-659, 1973.
- <sup>10</sup> Daripa, P. and Sirovich, L., "An Inverse Method for Subcritical Flows," *J. Comp. Phys.*, vol. 63, No. 2, April, 1986.
- <sup>11</sup> Woods, I. C., *The Theory of Subsonic Plane Flow*, Cambridge University Press, 1961.

<sup>12</sup> Volpe, G., "The inverse design of closed airfoils in transonic flow," *AIAA Paper No. 83-0504*, 1983.

<sup>13</sup> Volpe, G. and Melnik, R.E., "The Role of Constraints in the Inverse Design Problem for Transonic Airfoils," *AIAA Paper 81-1233*, 1981.

<sup>14</sup> Tranen, T.L., "A rapid computer aided transonic airfoil design method," *AIAA Paper No. 74-501*, 1974.

<sup>15</sup> Carlson, L.A., "The inverse transonic flow calculations using experimental pressure distributions," *AIAA*, vol. 12, no. 4, pp. 571-572, April 1974.

<sup>16</sup> Davis, W.H. Jr., "Technique for developing design tools from the analysis methods of computational aerodynamics," *AIAA Paper No. 79-1529*, 1979.

<sup>17</sup> Hicks, R.M., Vanderplaats, G.N., Murman, E.M., and King, R.R., "Airfoil Section Drag Reduction at Transonic Speeds by Numerical Optimization," *NASA TMX-73097*, February 1976.

<sup>18</sup> McFadden, G.B., *An artificial viscosity method for the design of supercritical airfoils*, Ph.D. Thesis, N.Y. University, New York, 1979.

<sup>19</sup> Sloof, J.W., "A Survey of Computational Methods for Subsonic and Transonic Aerodynamics Design," *Proceedings on ICIDES, University of Texas*, pp. 1-68, Austin, 1984.

<sup>20</sup> Daripa, P., "A Nonlinear Integral Theory For Inverse Problems," *In Preparation*.

<sup>21</sup> Garabedian, P. and Korn, D., "Numerical design of transonic airfoils," in *Numerical Solution of Partial Differential Equation*, vol. 2, p. 253, Academic Press, New York, 1971.

<sup>22</sup> Bauer, F., Garabedian, P.R., and Korn, D., *Supercritical Wing Sections III, Lecture Notes in Economics and Mathematical Systems*, 150, Springer Verlag, New York, 1977.

<sup>23</sup> Garabedian, P. and McFadden, G., "Computational Fluid Dynamics of Airfoils and Wings," *Transonic, Shock and Multidimensional Flows: Advances in Scientific Computing*, Academic Press, Edited by R.E. Meyer, 1982.

<sup>24</sup> Sanz, J., "A well posed boundary value problem in transonic gas dynamics," *Comm Pure Appl. Math.*, vol. 31, pp. 671-679, 1978.

<sup>25</sup> Sobieczky, H., "Related analytical, analog and numerical methods in transonic airfoil design," *AIAA Paper 79-1556*, 1979.

<sup>26</sup> Hassan, A.A., Sobieczky, H., and Seebass, A.R., "Subsonic Airfoils with a Given Pressure Distribution," *AIAA Journal*, vol. 22, no. 9, 1984.

<sup>27</sup> Daripa, P., "An Exact Inverse Method For Supercritical Flows," *Quart Appl Math.* To appear.

<sup>28</sup> Liepmann, H.W. and Roshko, A., *Elements of Gas Dynamics*, John Wiley and Sons, Inc., 1957.

<sup>29</sup> Daripa, P., *The Direct and Inverse Problems in Gas Dynamics*, Ph.D. Thesis, Brown University, Providence, R.I., 1985.

<sup>30</sup> Swartztrauber, P. and Sweet, R., "Efficient Fortran Subprograms For The Solution of Elliptic Equations," *NCAR TN/A-109*, p. 138, July, 1975.

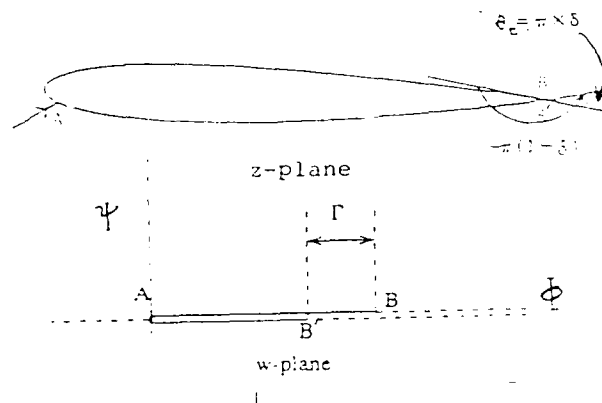


Fig. 1 Airfoil in the physical  $z$ -plane and potential  $w$ -plane.

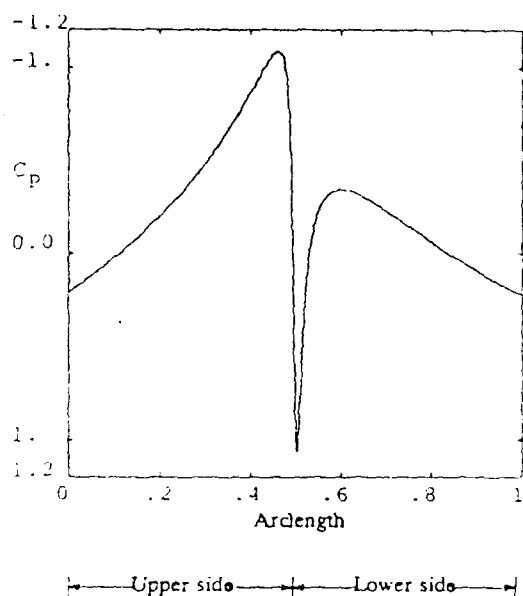


Fig. 2 Pressure distribution over a 12% thick Kutta airfoil from Euler solution (flo52s) at  $M_\infty = 0.5$  and  $\alpha = 2^\circ$  degrees.

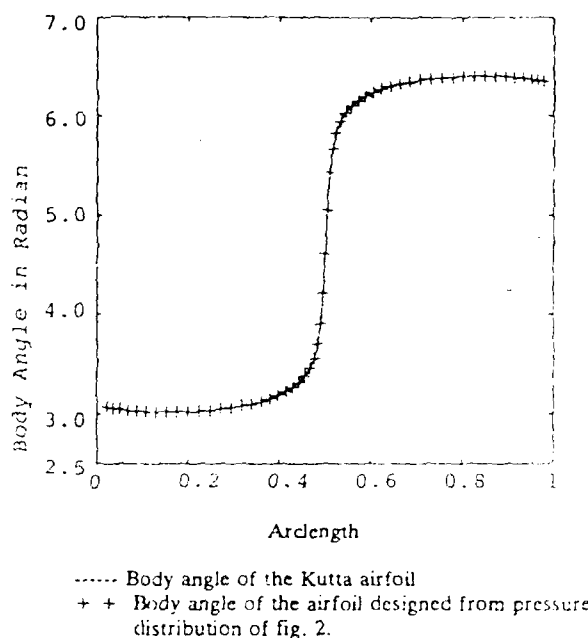


Fig. 4 Comparison of the body angle of the designed airfoil and of the Kutta airfoil as a function of arclength of the airfoil. The input pressure distribution of the designed airfoil is shown in Fig. 2.

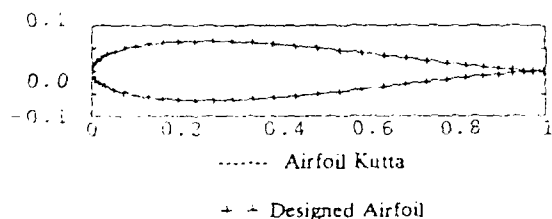


Fig. 3 Comparison of the 12% thick Kutta airfoil and the airfoil designed from the Euler pressure distribution of Fig. 2.

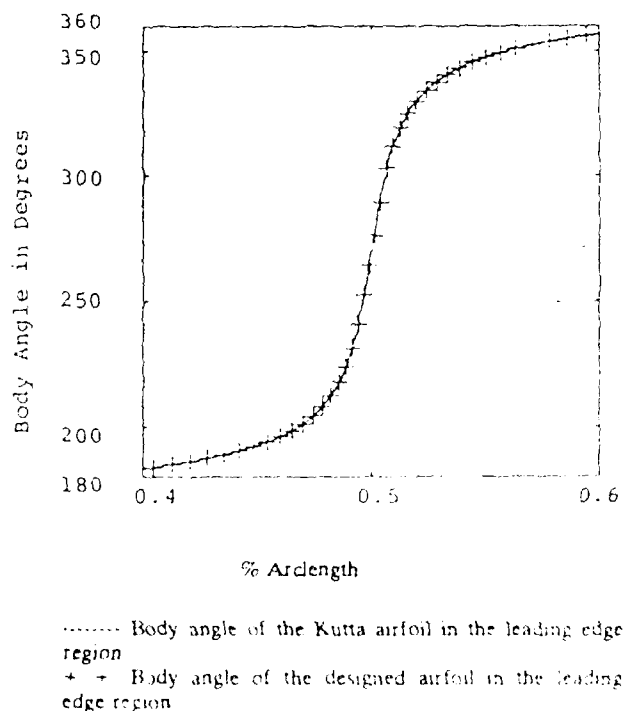


Fig. 5 Comparison of the body angle of the designed airfoil and of the Kutta airfoil as a function of arclength of the airfoil in the leading edge region. The input pressure distribution of the designed airfoil is shown in Fig. 2.

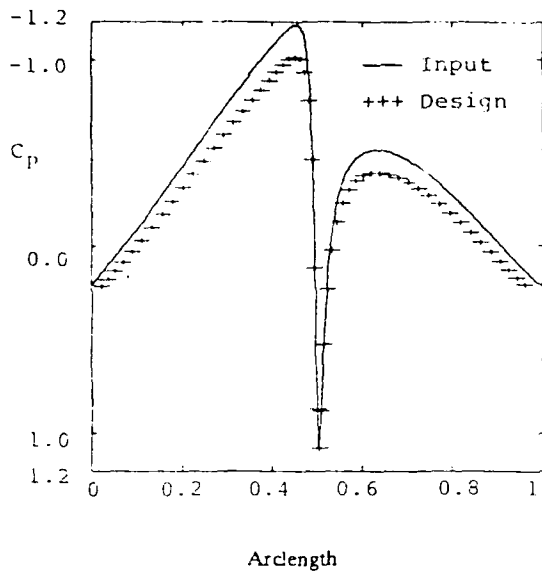
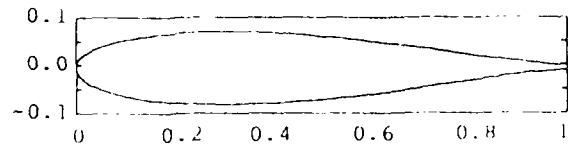


Fig. 6 Target and design pressure distributions



Mach = 0.5504 AOA = 0.0

Fig. 7 Designed airfoil from input pressure distribution of Fig. 6. The airfoil is open at the trailing edge.

END  
DATE  
FILMED  
JAN  
1988